Molecular Mechanisms Underlying the Pathogenesis of Leigh Syndrome French Canadian

Shamisa Honarmand

Department of Human Genetics

Faculty of Medicine

McGill University

Montreal, Quebec, Canada

October 2018

A thesis submitted to McGill University in partial fulfillment of the requirements of the degree of Doctor of Philosophy

I dedicate this thesis to my mom, Molouk, and deceased dad, Esmaeil, who guided me to where I am today.

Abstract

Functional mitochondria are required for cellular fitness and for generating ATP through oxidative phosphorylation (OXPHOS) pathway. Impaired mitochondrial function is associated with neurodegenerative disorders such as Leigh Syndrome French Canadian (LSFC), an early-onset autosomal recessive disease common in a small northern region of Quebec, Saguenay Lac Saint Jean. The causative gene is located on chromosome 2 and encodes Leucine Rich Pentatricopeptide Repeat containing protein (LRPPRC), a Pentatricopeptide Repeat (PPR) protein localized in mitochondria. The exact function of LRPPRC remains to be elucidated, but *in vivo* studies have revealed that LRPPRC forms a complex with Steroid Receptor RNA activator stem loop interacting RNA binding protein (SLIRP), and this complex is required for mitochondrial mRNA stability. Biochemically, an LSFC subject carrying the founder missense mutation in LRPPRC (p. A354V) demonstrated a very heterogenous phenotype in different tissues.

The work presented in this thesis first elaborates the impact of LRPPRC deficiency on mitochondrial function in liver-specific LRPPRC knock-out mice. We showed that the loss of LRPPRC caused a generalized growth delay and typical histological features of mitochondrial hepatopathy. At the molecular level, LRPPRC deficiency caused destabilization of a number of polyadenylated mitochondrial mRNAs and a severe complex IV and complex V (ATP synthase) assembly defect. The impact of LRPPRC deficiency was not limited to OXPHOS, but also included the impairment of long-chain fatty acid oxidation, a striking dysregulation of the mitochondrial permeability transition pore, and an alteration of trans-membrane H_2O_2 diffusion, which could result from the ATP synthase assembly defect and changes in the lipid composition of mitochondrial membranes.

Secondly, we showed that the poly A tail length of a selected number of mitochondrial mRNAs varies in human tissues. We further established the role of LRPPRC in polyadenylation of mt-mRNAs in LSFC subject tissues, and we concluded that LRPPRC is involved in polyadenylation and stabilization of a subset of mitochondrial mRNAs in a tissue-specific manner. To further investigate the pathogenic mechanism of LRPPRC in LSFC, we generated HEK293 cell lines expressing FLAG-BirA tagged wild-type (wt) and LRPPRC variants (p. A354V and p. Y172C) and tested whether the pathogenic variants altered the LRPPRC interactome using BioID, a proximity labeling technique. Pathogenic amino acid substitutions in LRPPRC shortened the half-life of the protein, which accumulated in distinct foci in the HEK cells. Although the tagged proteins were properly localized in the mitochondrial matrix and formed a complex with SLIRP, the BioID analysis showed that the pathogenic variants specifically interacted with caseinolytic peptidase B protein homologue (CLPB), a mitochondrial AAA ATPase chaperonin that localizes to the mitochondrial intermembrane space. These findings suggest that missense mutations in *LRPPRC* result in the production of unstable proteins that require the activity of a refoldase to properly target the mitochondrial matrix, providing an explanation for the reduced steady-state levels of LRPPRC in LSFC patient tissues.

Résumé

Des mitochondries pleinement fonctionnelles sont essentielles au maintien de la physiologie cellulaire, notamment grâce à la génération d'ATP par la voie de la phosphorylation oxydative. Une dysfonction mitochondriale peut être à l'origine de certaines maladies neurodégénératives telles que le syndrome de Leigh franco-canadien (LSFC), un trouble précoce autosomique récessif répandu dans une région du nord du Québec, le Saguenay Lac-Saint-Jean. Le gène responsable, situé sur le chromosome 2, code pour la protéine mitochondriale LRPPRC, riche en leucine et motif pentatricopeptide (PPR). La fonction exacte de LRPPRC reste à être élucidée. Cependant, des études *in vivo* révèlent que LRPPRC forme un complexe avec la protéine de liaison à l'ARN SLIRP, et que ce complexe est nécessaire à la stabilité de l'ARNm mitochondrial. Il est intéressant de constater qu'il existe une forte hétérogénéité du déficit mitochondrial selon les tissus, c'est ce que nous avons observé chez un patient porteur de la mutation *de novo* (p. A354V).

Cette thèse porte sur l'étude de la fonction mitochondriale chez des souris invalidées pour le gène *LRPPRC* au niveau hépatique. Nous avons démontré que la perte de LRPPRC entraîne un retard de croissance généralisé et des caractéristiques histologiques typiques d'une l'hépato-pathie mitochondriale. Au niveau moléculaire, l'absence LRPPRC entraîne la déstabilisation d'un certain nombre d'ARNm mitochondriaux polyadénylés et un défaut d'assemblage des complexes IV et V de la chaine respiratoire. On observe également une altération de l'oxydation des acides gras à longue chaîne, une dérégulation de la perméabilité mitochondriale et une altération de la diffusion transmembranaire de H_2O_2. Ceci pouvant être due à un défaut d'assemblage du complexe V et/ou des modifications de la composition lipidique des membranes mitochondriales. Deuxièmement, nous avons montré que la longueur des extensions de polyA de certains ARNm mitochondriaux varie dans les tissus humains et que LRPPRC joue un rôle

important dans leur stabilisation. Afin d'étudier les mécanismes physiopathologiques en jeu dans le LSFC et les partenaires fonctionnels de LRPPRC, nous avons généré des lignées cellulaires HEK293 sur-exprimant les formes sauvage ou mutées (p. A354V et p. Y172C) de LRPPRC, en fusion avec l'enzyme biotin ligase BirA. Tout d'abord, les variantes pathogènes de LRPPRC ont une demi-vie réduite et s'accumulent sous forme de *foci* au sein des mitochondries. Ils sont correctement localisés dans la matrice mitochondriale et forment un complexe avec SLIRP. Cependant, l'analyse de leurs partenaires en BioID montre que les variantes interagissent spécifiquement avec la protéine CLPB, une chaperonne mitochondriale AAA ATPase localisée dans l'espace inter-membranaire mitochondrial. Ces résultats suggèrent donc que des mutations faux-sens dans LRPPRC entraînent la production de protéines instables nécessitant l'activité d'une chaperonne pour les cibler correctement dans la matrice mitochondriale, expliquant les niveaux réduits de protéine LRPPRC dans les tissus des patients LSFC.

Table of contents

List of Abbreviations

2-D: two dimensional

ADP: adenosin diphosphate

AFG3L2: ATPase family gene 3

ATP: adenosin triphosphate

ATP 6 & 8: subunits of the complex V of oxidative phosphorylation

BN: blue native

bp: base pair

cDNA: complementary DNA

CNS: central nervous system

COX: cytochrome *c* oxidase

CsCl: cesium chloride

CTD: c-terminal domain

CTP: cytidine triphosphate

Cyt *b*: subunit of complex III of the oxidative phosphorylation

Cyt *c*: cytochrome *c*

D-loop: displacement loop of the mitochondrial DNA

DDM: n-dodecyl β-D-maltopyranoside

DMEM: Dulbecco′s modified Eagle′s medium

DNA: deoxyribonucleic acid

EDTA: ethylenediaminetetraacetic acid

EM: electron microscopy

ETC: electron transport chain

$FADH_2$: Flavin adenine dinucleotide, reduced form

F0: hydrophobic region of complex V

F1: hydrophilic region of complex V

GDP: Guanosine diphosphate

GTP: Guanosine triphosphate

GRSF1: G-rich sequence factor 1

H-strand: heavy strand

HEPES: 4-(2-hydoxyethyl)-1-piperazineethanesulfonic acid

HMG: high mobility group

HSP: heavy strand promoter

IF: initiation factor

IM: inner membrane

IMM: inner mitochondrial membrane

IMS: inner membrane space

IP: immunoprecipitation

Kb: kilo base

KDa: kilodalton

LRPPRC: leucine rich penta tricopeptide repeat protein

LS: Leigh syndrome

LSFC: Leigh syndrome French Canadian

L-strand: light strand

LSP: light strand promoter

MnSOD: manganese superoxide dismutase

MRG: mitochondrial RNA granule

mRNA: messenger ribonucleic acid

mtDNA: mitochondrial deoxyribonucleic acid

mt-mRNA: mitochondrial messenger ribonucleic acid

mtEFG: mitochondrial elongation factor G

mtEFTs: mitochondrial elongation factor Ts

mtEFTu: mitochondrial elongation factor Tu

mtIF: mitochondrial initiation factor

mtRF: mitochondrial releasing factor

mtRRF: mitochondrial ribosomal recycling factor

mtSSB: mitochondrial single stranded binding protein

mtSSU: small subunit of mitochondrial ribosome

mtLSU: large subunit of mitochondrial ribosome

mtTFA: mitochondrial transcription factor A

mtTFB: mitochondrial transcription factor B

mTERF: mitochondrial transcription termination factor

NADH: nicotinamide adenine dinucleotide, reduced form

ND: subunits of complex I of the oxidative phosphorylation

NTD: n-terminal domain

O_H: heavy strand origin of replication

O_L: light strand origin of replication

OSCP: subunit of complex V

OXPHOS: oxidative phosphorylation

PAGE: poly acrylamide gel electrophoresis

PBS: phosphate buffered saline

PCR: polymerase chain reaction

PMSF: phenylmethyl sulfonyl fluoride

POLGA: DNA polymerase gamma A

POLγ: DNA polymerase gamma

POLRMT: mitochondrial RNA polymerase

PPR: pentatricopeptide repeat protein

PTC: peptidyl transferase center

qRT-PCR: quantitative reverese transcriptase PCR

RF: releasing factor

RITOLS: RNA incorporation during mitochondrial DNA replication

RNA: ribonucleic acid

RNAi: RNA interference

RRF: ribosomal recycling factor

rRNA: ribosomal ribonucleic acid

RT-PCR: reverse transcription PCR

SDM: strand displacement mechanism

SDS: sodium dodecyl sulfate

SLIRP: steroid receptor RNA activator interacting RNA binding protein

siRNA: small interfering RNA

SSBP1: single stranded DNA binding protein 1

ssDNA: single stranded DNA

SYM: slow moving replication fork

TCA: trichloroacetic acid

TFAM: mitochondrial transcription factor A

tRNA: transfer ribonucleic acid

UTR: untranslated region

List of Figures

List of tables

Acknowledgments

I have had a great opportunity of working with remarkable people during my graduate studies at the University of McGill. I begin by thanking my supervisor Prof. Eric Shoubridge for his patience, generosity, and immense knowledge. His guidance helped in all the times of research and writing of this thesis. I am grateful to you for the many positive outlook, mentorship, and continuous support in my research that gave me confidence. I would also like to thank the members of my advisory committee Dr. Gregory Brown and Dr. Bernard Brais for their encouragement, criticism, and helpful advice.

I thank my fellow lab mates for stimulating discussions and for all the fun we have had in the last seven years. In particular, I am grateful to Hana Antonicka for sharing her expertise so willingly and most importantly for performing some parts of my experiments while I was in maternity leave. To Kathleen Daigneault, thank you for the practical help you so cheerfully provided. To Alexandre Janer, thanks for teaching me the immunoprecipitation experiment and being always there in times of need. Thank you, Isabella, for your great friendship and providing helpful insights, Mari Aaltonen for teaching me the Proteinase K experiment and for being a good friend, Woranontee Weraarpachai for your collaboration and friendship. I am also grateful to Archita Rajasekharan, and Jana Schuettpelz who lately joined our group. I would like to thank the past members of Shoubridge lab Tamiko, Florin, Tim, Reetta, Isabelle, Steven, Neil, Vincent, and Olga for providing me with a fantastic lab training and insightful discussions. I am grateful to work with highly skilled scientists like you.

And to François, thank you for being there on a daily base. Your encouragement, wisdom, endless kindness and support keeps me positive and help me to be a better person. Without your hard work the completion of this thesis would not be possible. To our darling Léonie for being such a good little baby that made it possible for me to complete the path I

started. I am indebted to my sister and friend, Shahrnoush who sponsored me to immigrate to Canada and have always supported me with anything she has when things got especially tough. My deep appreciation goes out to my family in Iran and in Vancouver for their support from far and skyping me all the weekends.

I am thankful to Dr. Yan Burelle and the members of his laboratory specially Alexanne Cuillerier, for their collaboration on the LSFC mouse project.

I would like to thank the scientists in rare neurological research group for journal clubs, lunch time chats, and for providing an amazing collaborative research unit.

I am grateful to the department of human genetics Dr. Eric Shoubridge and Dr. Aimée Ryan for making the department a scientifically rich and a fun place to be. To Ross MacKay, Rimi Joshi, and Cadnas Springer for making administrative tasks stress free.

I gratefully acknowledge my friends and colleagues I worked with in HGSS. Andreanne, Gaby, Vicki, Heather, Karine, Emma, Renata, Lundi, Jean, Amanda, Sean, John, Aziz, Fiona, Hamid, Pat, Mihaela, and Alison. I am so pleased to have friends like you. A very special thanks to my friends Alison Brebner, Neda Parinejad, and Andréanne Morin who have been constantly supporting me throughout this journey.

Last but not the least, I would like to thank CIHR as this research was supported by a grant from CIHR to Dr. Eric Alan Shoubridge.

Contribution of Authors

This thesis is comprised of eight chapters. The results chapters include three to five, which comprise one co-author publication and two first-author manuscripts in preparation.

Chapter 3 is a manuscript published in 2017 in Human Molecular Genetics, 26 (16): 3186- 3201 by Cuillerier A, Honarmand S, Cadete VJJ, Ruiz M, Forest A, Deschênes S, Beauchamp C; LSFC Consortium, Charron G, Rioux JD, Des Rosiers C, Shoubridge EA, Burelle Y. Figures 1 to 7 were designed and executed by Shamisa Honarmand under the supervision of Dr. Eric A. Shoubridge. Figures 8 to 13 were designed and executed by Cuillerier A, Cadete VJJ, Ruiz M, Forest A, Deschênes S, Beauchamp C, Charron G, Rioux JD, Des Rosiers C, and Burelle Y.

Chapter 4 is a manuscript to be submitted for publication by Shamisa Honarmand and Eric A. Shoubridge. All the experiments in Chapter 4 are executed and designed by Shamisa Honarmand under the supervision of Dr. Eric A. Shoubridge.

Chapter 5 is a manuscript to be submitted for publication by Shamisa Honarmand, Hana Antonicka, and Eric A. Shoubridge. All three authors are responsible for the design of the experiments. Shamisa Honarmand executed the experiments presented in this chapter with the exception of Figure 1 C, Figure 9, and Figure 13 B-C that were performed by Hana Antonicka.

Chapter 1 Introduction

1.1. OXPHOS

Oxidative phosphorylation is the process by which mitochondria generate aerobic energy in the form of ATP. The OXPHOS system comprises five large enzyme complexes located in the inner mitochondrial membrane and is involved in transferring electrons derived from NADH or FADH2 through electron transport chain (ETC). The ETC includes complex I (NADH: ubiquinone oxidoreductase), complex II (succinate: ubiquinone oxidoreductase), complex III (ubiquinol: cytochrome *c* oxidoreductase), complex IV (cytochrome *c* oxidase). Upon oxidizing NADH or FADH2, electrons are transferred to ubiquinone (ubiquinol), a lipid soluble electron carrier located in the mitochondrial inner membrane, by complex I, composed of 38 nuclear- and 7 mitochondrial-encoded subunits, and complex II, exclusively nuclear encoded subunits. From ubiquinol electrons are then carried to cyt *c* through complex III, which is composed of 1 mitochondrial and 10 nuclear encoded subunits. Complex IV subsequently catalyzes the oxidation of cytochrome *c* and transfers electrons to molecular oxygen to produce water.

The energy released from this procedure is used to translocate protons (4 protons through complex I and III, respectively, and 2 protons by complex IV) from the mitochondrial matrix into the inter membrane space [1]. This creates a proton gradient which is dissipated in a controlled way to phosphorylate ADP by ATP synthase (complex V) to produce ATP. Complex V consists of an insoluble F0 and hydrophilic F1 regions embedded in the inner mitochondrial membrane (IMM). The F0 consists identical c subunits and subunit a that catalyzes the transfer of electrons to mitochondrial intermembrane membrane space (IMS). Other subunits of F0 including subunit b, f, d, 8, F6, and OSCP aid the catalytic F1 to connect to IMM. The F1 consists of a catalytic head $(\alpha\beta)3$ subunits in addition to $\gamma\delta\varepsilon$ central subunits which are involved in synthesizing and releasing ATP [2].

1.2. Human mitochondrial genome

The human mitochondrial genome is a circular, double stranded 16,569 bp DNA with no introns that is maternally inherited. mtDNA copy number varies in different cell lines, and most animal cells have 1000-5000 copies of mtDNA per cell [3]. The mechanisms by which mtDNA copy number is regulated are not completely understood, but it was shown that POLGA plays a key role in mtDNA maintenance early in development [77]. Depending on the energy demand, the copy number of mtDNA is increased during later stages of development, for example, high-energy consuming tissues such as brain and muscle harbour significant changes in mtDNA copy number [78]. In healthy individuals, mitochondrial DNA is not mutated, and only wild-type DNA molecules are present, a condition called homoplasmy. Heteroplasmy occurs when a mixture of wild-type and mutant mtDNA is present in the cell. Once the level of mutant mtDNAs passes a certain threshold, the person develops a mitochondrial disease in which the severity of the illness correlates with the relative proportion of the mutant mtDNA. This threshold varies depending on the type of mutations or tissues [4]. mtDNA contains 37 genes that encode 13 protein coding genes (OXPHOS subunits), 2 rRNAs (12S and 16S), and 22 tRNAs. The remaining mitochondrial proteins including OXPHOS or proteins involved in other aspects of mitochondrial function are encoded by nuclear DNA, synthesized in cytoplasm and targeted to mitochondria [5].

1.2.1. Mitochondrial DNA structure and organization

Mitochondrial DNA is packaged into a compact DNA-protein structure called the nucleoid. There are about 2 to 10 nucleoids per mitochondrion [6], and frequently one copy of mtDNA per nucleoid [7]. The components of nucleoid have been studied for several years by using different purification methods; however, the exact role of each factor in modulating the

structure of mitochondrial genome remains unknown. Studies on Hella cells implicates several factors modulating the structure of nucleoid [8]. Amongst all protein, TFAM and SSBP1 are the core components of nucleoid structure and have been shown to play a role in mtDNA maintenance and transcription. The crystal structure of TFAM, a 24 KDa protein, has been determined by [20], and it is shown that TFAM imposes a U-turn bend in mtDNA. SSBP1 interacts with single stranded mitochondrial DNA and is required for mitochondrial replication, recombination and repair. Tiranti *et al.* 1995 found that SSBP1 forms a heterotetramer to stabilize the single stranded DNA at the D-loop during replication in order to prevent the formation of secondary structure and facilitating the interaction of gamma DNA polymerase [80]. Mitochondrial DNA consists of a heavy strand (H) rich in guanine and a light strand (L) rich in cytosine. Heavy and light refers to the buoyant density of mtDNA strands in an alkaline CsCl gradient. Most of the genes are encoded by the H strand except ND6 and 8 tRNAs which are coded on the light strand. Another characteristic feature of mtDNA, apart from having no introns, is the presence of a single noncoding region called D-loop. The D-loop is a triple-stranded part of mtDNA with an approximate size of 1 kb containing the origin of replication and the promoters for the H- and L-strand required for mitochondrial transcription [9]. While only one promoter exists for L-strand, there are several controversial studies debating on the presence of one or two promoters for H-strand [20, 81, 82].

1.2.2. Mitochondrial DNA replication

Several proteins and enzymes are necessary for mtDNA replication including mitochondrial DNA polymerase γ [10], Twinkle DNA helicase [11] , mitochondrial RNA polymerase, single-stranded DNA binding protein, RNase H1 [12], DNA ligase III [13], and topoisomerases. Several mechanisms have been proposed for mtDNA replication. The first one

was proposed in 1973 by Kasamatsu *et al*, and it is known as strand-displacement mechanism or SDM [14]. In this article, mouse mtDNA was isolated by CsCl density centrifugation and was imaged by electron microscopy (EM). This model suggests that the synthesis of mtDNA leading strand begins at O_H, the origin of replication at D-loop, and advances around the molecule, approximately two thirds of the way around the genome, where the O_L is exposed and the synthesis of the second strand starts.

A second model is known as RNA incorporation during mtDNA replication (RITOLS). In 2002 Yang *et al.* [15] showed that highly purified mtDNA on second dimension gel yielded slow-moving replication forks (SMY) that are undigested by restriction enzymes that specifically cut ssDNA or dsDNA. However, Yasukawa *et al.* 2006 [16] suggested that SMY is digested by RNaseH, an enzyme that only digests RNA molecules hybridized to DNA. The RITOLS model proposes that mitochondrial DNA replication initiates at one of the two sites, O_H or O_L, followed by the synthesis of leading strand DNA and the incorporation of newly synthesized RNA into the lagging strand. These segments of RNAs are later replaced or converted to DNA. A third model is known as coupled leading and lagging strand DNA synthesis elaborated in 2000 [17] where the authors analyzed purified mouse mtDNA by two dimensional agarose gel and suggest two classes of replication intermediates: one sensitive to single strand nuclear digestion and the other one resistant to the digestion. In this model, DNA synthesis initiates in a noncoding region containing cytb, ND5, and ND6 with simultaneously bidirectional synthesis of the leading and lagging strands [17].

1.2.3. Mitochondrial DNA transcription

Mitochondrial transcription is driven from light and heavy strand promoters (LSP and HSP1). LSP is responsible for the transcription of genes encoded on the light strand (cytb, ND5,

and ND6), HSP1 promotes the transcription initiation of the genes encoded in heavy strand including 12 mRNAs, 2 rRNAs, and 14 tRNAs [18].

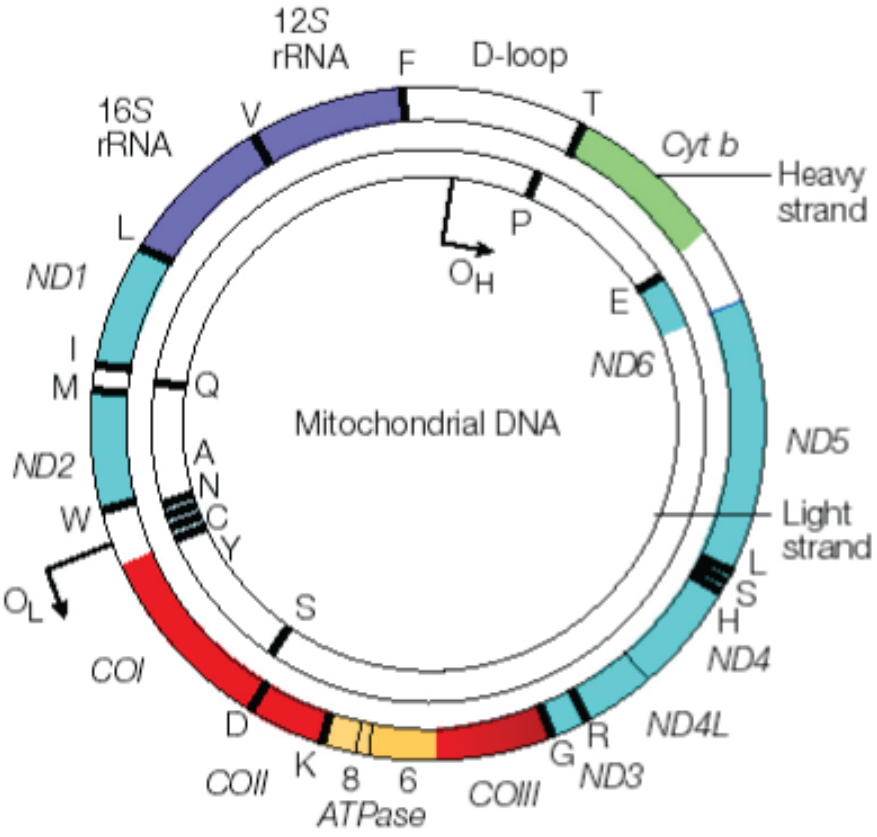
12S
rRNA
F
D-loop
T
16S
rRNA
V
Cyt b
Heavy
strand
L
P
ND1
O
H
E
I
ND6
M
Q
Mitochondrial DNA
ND5
A
ND2
N
C
W
Y
Light
strand
L
S
O
L
S
H
ND4
COI
D
ND4L
R
G
K
8
6
ND3
COII
COIII
ATPase

Figure 1.1. Schematic view of circular double-stranded human mtDNA. The 37 mitochondrial genes encoded in both H- and L-strand. The 22 tRNA genes are depicted by the single letter code for the amino acid. ND indicates NADH dehydrogenase genes coding the subunits of complex I (ND1-6, ND4L) and is shown in blue; cyt b of complex III is shown in green; COX, cytochrome c oxidase genes (COXI-III) are shown in red; ATPase 6 and 8 coding the subunits of ATP synthase are shown in yellow; and 12S/16S indicates ribosomal RNA genes. The figure is from Taylor R.W *et al.* 2005 [79].

Transcription at mitochondrial promoters requires three proteins including mitochondrial transcription factor A (TFAM), mitochondrial transcription factor B2 (TFB2M), and mitochondrial RNA polymerase (POLRMT) [18, 24, 25, 83]. TFAM is a DNA binding protein and a member of the high mobility group (HMG) proteins defined by the HMG DNA binding domain. TFAM consists of a matrix targeting sequence (42 amino acids), two HMG domains (HMG1, and HMG2) linked by 37 amino acids, and a 30 amino acid C-terminal domain (CTD) [20]. TFAM binds DNA molecule, which is mapped to positions 12 to 35 upstream of HSP1 and LSP, and simultaneously interacts with TFB2M to assist loading POLRMT on transcription start sites [20]. POLRMT is a 139 KDa protein consisting of an N-terminal extension containing a PPR domain, an N-terminal domain (NTD), and a C-terminal domain (CTD) that binds to DNA and has catalytic activity [21]. POLRMT can only initiate transcription of mitochondrial double stranded DNA in the presence of TFAM and TFB2M. TFB2M is a 45 KDa protein consisting of a priming substrate-interacting domain, a promoter-interacting domain, an S-adenosylmethionine-dependent methyltransferase-like domain, and a POLRMT- interacting domain [22]. TEFM is a newly discovered protein involving in the elongation stage of mitochondrial transcription, and it consists of a helix-hairpin-helix domain, and an RNaseH-like fold domain [24].

Similar to nuclear transcription, the stages through which mitochondrial genome is transcribed consists of initiation, elongation, and termination. At the initiation stage, TFAM binds to HMG site upstream of the HSP1 and LSP promoters and induces a sharp bend in mtDNA [20]. POLRMT is, then, recruited by interacting with the TFAM C-terminal end, facilitating the interaction of TFB2M and consequently promoting promoter melting and recruitment of the priming site to the catalytic site of POLRMT. Next, TFB2M is dissociated

from the initiation complex and the elongation stage starts. At this stage, mitochondrial transcription elongation factor (TEFM) interacts with POLRMT along with helicase to increase the processivity of POLRMT. Transcription is terminated by MTERF1 most likely through interference with transcription elongation machinery. Although the exact mechanism remains poorly understood, it is suggested that MTERF1 unwinds mtDNA at the termination site and makes a strong interaction with DNA to facilitate the termination of transcription [23, 24].

Transcription of mtDNA occurs at two promoter sites: HSP2 located in the H-strand and LSP located in the L-strand. Transcripts produced from HSP2 is a polycistronic RNA molecule containing 12 mRNAs, 14 tRNAs, and the two ribosomal RNAs. The transcript generated from the only promoter of light strand contains 1 mRNA and 8 tRNAs [24, 25].

The long polycistronic transcripts need to be further processed and cleaved by appropriate enzymes in order to generate mRNAs, rRNAs, and tRNAs. According to the tRNA punctuation model, tRNA molecules form cloverleaf structures that are recognized by the processing enzymes RNAase P and Z, which cleave tRNAs at the 5’ and 3’ ends, respectively, releasing the appropriate mature RNAs [26]. The limitation of this model is evident for explaining the processing of those mtRNAs that are not flanked by tRNAs. Recently, it has been suggested that the RNA processing occurs in RNA granules in mitochondria. These RNA foci contain nascent mRNAs, RNAase P, and G rich sequence factor1 (GRSF1). It is demonstrated that FASTKD5 is involved in processing mt-mRNAs that are not flanked by tRNAs [27].

The family of FASTK (Fas-activated serine/threonine kinase) proteins were first found to interact with T cell intracellular antigen (TCI) [152]. TCI is an RNA binding protein that interacts with premature RNA in cytoplasm. FASTK was initially reported with a kinase activity, but this protein does not contain any kinase domain [152]. The members of FASTK protein are localized in mitochondrial matrix, and they all have mitochondrial targeting sequence at the N-

terminus and interact with RNA. Knowing that only 50% of FASTK are localized in mitochondria [151], still the protein plays an essential role in the stability of ND6 mRNA, which is the only L-strand encoded mitochondrial mRNA and lack tRNA at the 3′ end. In fact, FASTK stabilizes ND6 transcript by interacting to the 3′ end and protecting it from degradation by Suv3p-PNPase complex [151]. FASKD1 is shown to interact and regulate the level of ND3 mRNA through an unknown mechanism [153]. FASTKD2 interacts with 16s rRNA and ND6 mRNA. As the depletion of FSTKD2 leads to decrease in the expression of 16s rRNA and ND6 mRNA in addition to reduction of all OXPHOS complexes activity except complex II suggesting the importance of FASTKD2 in mitochondrial expression and translation [154]. The last FASTK in MRGs is FASTKD5 that is required for the processing of the mitochondrial RNAs that cannot be cleaved by RNase P and RNase Z such as 5′ end-COX I, ATP8/6+ COX III, ND5+ cyt b [147]. Once mitochondrial transcripts are processed and RNA species are released, ATP(CTP): tRNA nucleotidyltransferase then adds CCA trinucleotides to the 3′ ends of tRNAs [28] and mRNAs are polyadenylated by mitochondrial poly A polymerase [29].

1.2.4. Mitochondrial DNA translation

Mitochondrial ribosomes contain two ribosomal RNAs (rRNAs) encoded by mitochondrial DNA and 80 ribosomal proteins (MRPs) encoded by nuclear DNA [24]. All MRPs are synthesized in cytoplasm and transported into mitochondria where they get assembled into mitochondrial small subunit mt-SSU 28S and mitochondrial large subunit mt-LSU 39S together with 12S and 16S rRNAs, respectively [30].

Assembled mitochondrial ribosomes (55S) differ from eukaryotic cytosolic (80S) and prokaryotic (70S) ribosomes in density and the ratio of protein to RNA. Bacterial ribosomes contain high RNA to protein ratio (2:1) [31] whereas mitochondrial ribosomes are rich in

proteins with a reverse ratio [32, 33]. Processed mitochondrial mRNAs are translated on the mitochondrial ribosome. These mRNAs have a unique codon usage that is different from universal cytosolic codons. For example, UGA stop codon is recognized as tryptophan, AUA as methionine, and AGA or AGG codons are not recognized by any mt-tRNAs [30].

The first step in the translation process is to recruit mitochondrial mRNA to mitoribosome. The involvement of two proteins initiation factor 3 (mtIF3) and PPR protein, mS39, in the recruitment of mitochondrial mRNA to the small subunit of mitochondrial ribosome (mt-SSU) has been shown [32]. Once the mitochondrial mRNA loaded, the initiation start-codons AUG, AUA, and AUU are recognized by mt-SSU and the formylated methionyl-tRNA (f-Met-tRNA Met) is recruited to the preassembled ribosome by mt IF2: GTP. The correct interaction between initiation codon to anticodon facilitates the recruitment of mitochondrial large subunit (mt-LSU). Once the mt-LSU interacts with the pre-assembled complex, the monosme is formed, and the elongation step begins.

In this stage, there are a number of mitochondrial elongation factors such as mtEF-Tu and mtEF-Ts known to be involved in the placement of charged mt-tRNA in the monosome. mtEF-Ts interacts with mtEF-Tu: GDP to generate mtEF-Tu: GTP and facilitates the entrance of the charged mt-tRNA to the A site. The correct interaction of codon and anticodon triggers the conformational change of mitoribosme, hydrolyzation of GTP, and release of mtEF-Tu: GDP. Once mtEF-Tu is released, a peptide bond is formed at the peptidyl transferase center (PTC) in the mt-LSU. Next, elongation factor mtEF-G1 interacts with mitoribosome and facilitates the release of deacylated mt-tRNA from the P-site, and the movement of dipeptidyl-tRNA from the A-site in to the P-site. The elongation step ends once stop codon moves to the A-site [32, 33].

The termination stage takes place upon the recognition of the termination codon by mitochondrial release factor 1a (mtRF1a), which seems to recognize the stop codon of all 13

ORFs. mtRF1a is a class I release factor that specifically recognizes the termination codons UAA and UAG and triggers the first step of termination by interacting with mt-mRNA through RNA binding motifs. This interaction leads to a conformational change in mtRF1a and promotes the second step, which is the hydrolysis of the ester bond between mt-tRNA and the final amino acid by a conserved GGQ motif of mtRF1a. Disassembly of the ribosomal subunits, the release of mt-mRNA and deacylated tRNA is catalyzed by two ribosomal release factors mtRRF1 and mtEF-G2 [30].

1.3. Mitochondrial disease

Defects in OXPHOS are linked to multiple cellular impairments and referred to as mitochondrial encephalomyopathies because of the prominent involvement of brain and skeletal muscles [34]. All human cells contain mitochondria except mature red blood cells, and as a result, mitochondrial defects could lead to impairment of ATP production in different cells especially high consuming ATP tissues such as brain, heart, and skeletal muscles. Mitochondria contain on the order of 1200 proteins that have been catalogued in MitoCarta, an inventory of the mammalian mitochondrial proteome [36]. In this list, except 13 proteins encoded by mitochondrial DNA (mtDNA), the remaining are encoded by nuclear DNA (nDNA). The function of these proteins varies from being involved in oxidative phosphorylation and ATP synthesis (about 150 proteins) to OXPHOS assembly factors (37 proteins). The rest are involved in maintenance and expression of mtDNA, protein synthesis, mitochondrial dynamics, mitochondrial metabolism such as pyruvate dehydrogenase, Krebs cycle, ketone bodies, fatty acid oxidation, heme synthesis, urea cycle, and mitochondrial homeostasis such as protein import, protein quality control and Ca^{+2} transport [37]. Mutations in either mitochondrial or nuclear encoded genes described above are associated with mitochondrial diseases.

Involvement of both mitochondrial and nuclear genome and the presence of a wide variety of symptoms make mitochondrial disease difficult to diagnose and to treat. In addition, the mode of inheritance of mitochondrial diseases varies from maternal to autosomal recessive, autosomal dominant, X-linked, and *de novo*. The fact that the mitochondrial disease could manifest itself in early life or old age is another aspect that complicates therapeutic interventions [38, 39]. More than two hundred pathogenic point mutations in mitochondrial- and nuclear-encoded genes have been reported to date leading to mitochondrial diseases [40, 84]. These mutations result a broad range of neurological symptoms including developmental regression,

seizures, brain lesions, failure to thrive, altered mental states, altered consciousness, spasticity, dystonia, ataxia, abnormal postures, respiratory abnormalities, neonatal lactic acidosis, liver hemosiderosis, abnormal muscle and eye movements, hearing loss, and twisted hair shafts [35].

Besides trying to develop treatments for mitochondrial diseases, it is possible to prevent the disease occurrence by genetic counseling and using advanced diagnostic methods in families with mitochondrial disease background. One preventive method for women carrying mitochondrial DNA mutation is known as mitochondrial donation in which nucleus of a woman with mtDNA mutation is transferred to an enucleated oocyte in order to generate a healthy fertilized egg *in vitro* [39]. This manipulation can be performed before fertilization using metaphase II oocytes (polar body or maternal spindle transfer) or instantly after fertilization using pronuclear stage zygotes (pronuclear transfer) [39]. This method was applied on animals [41, 42] and human, and the first child derived from oocyte nuclear transfer was born in 2016 [43]. Despite the recent advances in the diagnosis of mitochondrial diseases, the exact pathogenic mechanisms associated with most genetic mutations remain poorly understood. There are some examples of *in vivo* studies where the authors describe mouse models to better address this issue. The first model was described in 1995 by Li *et al* in which they investigated manganese superoxide dismutase knock-out mice [44]. Yet, there is no patient reported with MnSOD mutations but the significance of MnSOD as cancer biomarker has been established [85]. Since then, about 50 nuclear genes involving in mitochondrial function and mitochondrial disease have been studied [45-48]. For instance, mouse models for mitochondrial disease gene involving in RNA metabolism LRPPRC have provided valuable information relating to our understanding of the disease gene function [45]. Mutations in LRPPRC are associated with a pediatric mitochondrial disease, Leigh Syndrome French Canadian (LSFC). Specific disruption of LRPPRC in mouse heart leads to severe COX deficiency, an abnormal sub-assembly of

complex V corresponding to the F1 portion, while the activities of other OXPHOS complexes appear to be normal, and decrease in the length of mitochondrial mRNA poly A tail [75], suggesting a role for LRPPRC in post-transcriptional handling of mitochondrial mRNAs. Apart from LRPPRC, there have been many other genes involved in mitochondrial RNA metabolism modeled in mice but not all of them are linked to mitochondrial diseases. These genes include Dars2 [86], Tfam [87], Polrmt [88], Ptcd2 [89], Tfb1m [90], Suv3 [91], Nsun4 [92], and Slirp [72].

1.3.1. Leigh syndrome (LS)

LS is one of the most frequent presentations of mitochondrial disease in infants, and mutations in more than 75 mitochondrial and nuclear genes have been reported to cause LS. These genes are involved in different aspects of mitochondrial energy metabolism including structural OXPHOS subunits and assembly factors, biosynthesis of ubiquinone, and the pyruvate dehydrogenase complex [51, 52]. Table 1.1 suggests the genes in which mutations lead to LS and describes the biochemical deficiency. LS was initially described by a British neuropsychiatrist, Denis Archibald Leigh [49] and characterized by neurological deterioration associated with the brain stem and basal ganglia, particularly in the putamen region. Necrotic lesions also occur in other CNS regions such as cerebellum, thalamus, and the spinal cord; however, but the exact mechanism by which neurodegeneration occurs remains poorly understood. The symptoms include developmental deficiencies and failure to thrive in early life usually around two years old, but some rare cases present the disease at older age [50].

Biochemical deficiency	**Genes**
Pyruvate dehydrogenase	*PDHA1*[a], *PDHB*, *PDHX*, *DLAT*, *DLD*, *LIPT1*, *LIAS*, *TPK1*, *SLC19A3*, *SLC25A19*
Complex I	*MTND1*[b], *MTND2*[b], *MTND3*[b], *MTND4*[b], *MTND5*[b], *MTND6*[b], *NDUFV1*, *NDUFV2*, *NDUFS1*, *NDUFS2*, *NDUFS3*, *NDUFS4*, *NDUFS7*, *NDUFS8*, *NDUFA1*[a], *NDUFA2*, *NDUFA9*, *NDUFA10*, *NDUFA11*, *NDUFA12*, *NDUFB8*, *NDUFAF5*, *NDUFAF6*, *FOXRED1*
Complex II	*SDHA*, *SDHAF1*
Coenzyme Q10	*PDSS2*
Complex III	*UQCRQ*, *BCS1L*, *TTC19*
Complex IV	*MTCO3*[b], *NDUFA4*, *SURF1*, *COX10*, *COX15*, *SCO2*, *PET100*, *LRPPRC*, *TACO1*, *ETHE1*, *SLC25A46*
Complex V	*MTATP6*[b]
Combined OXPHOS defects- pathway affected	
Mitochondrial DNA maintenance	*FBXL4*, *POLG*, *SUCLA2*, *SUCLG1*
Mitochondrial DNA translation	ΔmtDNA[c], *MTTI*[b], *MTTK*[b], *MTTL1*[b], *MTTV*[b], *MTTW*[b], *MTFMT*, *GTPBP3*, *TRMU*, *EARS2*, *FARS2*, *IARS2*, *NARS2*, *GFM1*, *GFM2*, *TSFM*, *C12orf65*, *PNPT1*, *MRPS34*
Disease genes that cause secondary impairment	

of mitochondrial energy generation	
OXPHOS±PDH_C	*HIBCH*, *ECHS1*, *SERAC1*, *AIFM1*[a]
Biotinidase	*BTD*

Table 1.1. The table depicts the genes associated with LS. a X-linked inheritance, b Maternal inheritance, c Sporadic inheritance. OXPHOS=oxidative phosphorylation; PDHc=pyruvate dehydrogenase complex; ΔmtDNA= mt DNA deletion. The table is from Lake *et al*, 2016 [52] and is updated using PubMed.

1.3.2. Leigh Syndrome French Canadian (LSFC)

A variant of LS called Leigh Syndrome French Canadian (LSFC) occurs at relatively high frequency in the Saguenay-Lac St-Jean region of Quebec, owing to a founder effect [53]. LSFC is an autosomal recessive, neurodegenerative disorder with onset in infancy that is characterized by delayed psychomotor development, mental retardation, mild dysmorphic facial features, hypotonia, ataxia, lesions in the brain stem and basal ganglia, and microvesicular steatosis in the liver [53]. Most patients show lack of facial and limb movement, unexpressive faces, prominent forehead, and upturned nose. The patients are frequently diagnosed during fatal metabolic crises, and mortality occurs as a result of acidosis and coma. This disorder in the Quebec founder population is biochemically characterized by a tissue-specific decrease in COX activity in the brain and liver and moderate or normal COX activity in the heart, kidneys, skeletal muscles, and skin fibroblasts [53, 54].

The gene responsible for LSFC was identified in 2003 and codes for leucine-rich pentatricopeptide (PPR) repeat motif-containing protein (LRPPRC) [55]. But, the exact role of LRPPRC in the development of this disease is poorly understood. Based on a cohort study in Saguenay Lac Saint Jean region, most LSFC patients harbor a homozygous point mutation, C-to-T, at nucleotide position 1119 of the LRPPRC gene, which changes alanine at position 354 to valine (A354V); a single patient is compound heterozygous for this mutation and a nonsense codon [56]. Mutations in LRPPRC gene are not limited to French Canadian population. In fact, there are a few reported cases in England of Caucasian or middle eastern origin who carry novel pathogenic mutations [57, 58]. The mutations include substitution of a single amino acid, microdeletion, frameshift, or mutations altering the splice site. Severe lactic acidosis, neurological deterioration including motor difficulties (hypotonia, dystonia or ataxia), dysphagia, strabismus and seizures in addition to complex IV deficiency are some common clinical features

observed in both French Canadian and UK patients. However, a number of patients from England manifest cardiomyopathy, a phenotype that is not prominent in the French-Canadian population [57, 58].

Pathogenic variants	Clinical phenotypes
p. Arg1276_Lys1300del	Episodes of lactic acidosis, hypoglycaemia, developmental delay, mild hirsutism and a broad nasal bridge
p. [Glu497*], p. [Gly1050Argfs*4]	Seizures, severe encephalopathy, central hypopnoea, profound hypotonia, persistent metabolic acidosis
p. (Val 866 del)	Lactic acidosis, hypotonia, hypospadias, mild hypertrophic cardiomyopathy, dystonia, respiratory failure
p. (Lys 909 del)	Developmental delay, muscular hypotonia, truncal ataxia, arterial hypertension and left ventricular hypertrophy
p. Arg1044Cys, p. Arg1144Cys, p. Ala1360Thr	Mild intermittent metabolic acidosis, generalized dystonia, intermittent eye contact and minimal vocalization
p. Ala354Val, p. Cys1277Xdel8	Developmental delay, hypotonia, weakness and paucity of facial expression, truncal ataxia, lactic acidosis
p. Tyr172Cys	Developmental delay, hypotonia, infantile spasms, lactic acidosis

Table 1.2. Pathogenic variants in LRPPRC reported in cases of LSFC.

Abbreviations: del, deletion; fs, frame shift; X, nonsense mutation.

1.4 PPR proteins and LRPPRC

PPR proteins contain 35-amino acid repeats and impact various aspects of RNA metabolism, such as processing, stability, editing, splicing, and translation initiation in organelles (mitochondria or chloroplasts) [59]. PPRs belong to the alpha solenoid family of proteins containing short helical repeats that interact either with protein ligands or nucleic acids [60]. One well characterized PPR protein is maize PPR10 containing 19 PPR motifs, binds to its target RNA sequence via a combinatorial amino acid code. Using a gel mobility shift assay, it was shown that there is a strong interaction between specific amino acids of PPR10 and particular nucleic acids of target RNA molecule that allows them to bind specifically [61]. A study done by Small *et al*, indicates that PPR repeats fold into a pair of antiparallel alpha helices based on a weak sequence similarity to tetratricopeptide repeats (TPRs) [62]. The crystal structure of PPR proteins further establishes the previous prediction [63]. In contrast to TPRs, PPR proteins are present in all eukaryotes whereas TPRs have been observed in prokaryotes as well. Thus, it appears that PPRs are derived from TPRs very early in eukaryotic evolution and are localized or predicted to be present in mitochondria or chloroplasts.

PPRs are ubiquitously expressed in eukaryotes with mitochondrial genomes and absent in prokaryotes except pathogenic bacteria or symbionts, which could have been due to horizontal gene transfer from their eukaryotic hosts [64]. The large expansion of PPRs in land plants could be probably explained by various adaptive drivers in chloroplast such as repairing the mutations occur in chloroplast genome due to asexual reproduction [167], editing the chloroplast RNAs [168], or regulating the organelle gene expression [169]. Despite the presence of the large number of PPR proteins in chloroplasts, their molecular function is not redundant; each protein has a specific function in organellar RNA metabolism [64].

In contrast to the large number of PPR proteins reported in land plants (more than 400

members), only seven mammalian PPR proteins have been identified to date, and all of them localize to mitochondria [65, and 59]. Mitochondrial RNA polymerase (POLRMT) is one of the mammalians PPR proteins, which contains two PPR motifs at the N-terminus. POLRMT is a single subunit protein essential for the transcription of mtDNA. Other members include PTCD1 [66], which is involved in the stabilization of 16S rRNA and the assembly of mitochondrial ribosome [67]. PTCD2, which regulates cytb RNA processing; PTCD3, which is found to be associated with 12s rRNA and small subunits of mitochondrial ribosome in humans; MRPP3, which is one of the three essential components of mitochondrial RNase P that processes the 5′ ends of mitochondrial tRNAs; and MRPS27 that contains six PPR domains and interacts with 12s rRNA and small subunits of mitochondrial ribosomes [59]. LRPPRC, a 130-KDa protein, is predicted to contain nearly 30 pentatricopeptide repeat (PPR) motifs [68]. On the basis of *in vitro* assays, LRPPRC binds to single-stranded nucleic acids with a preference for polypyrimidine sequences [68].

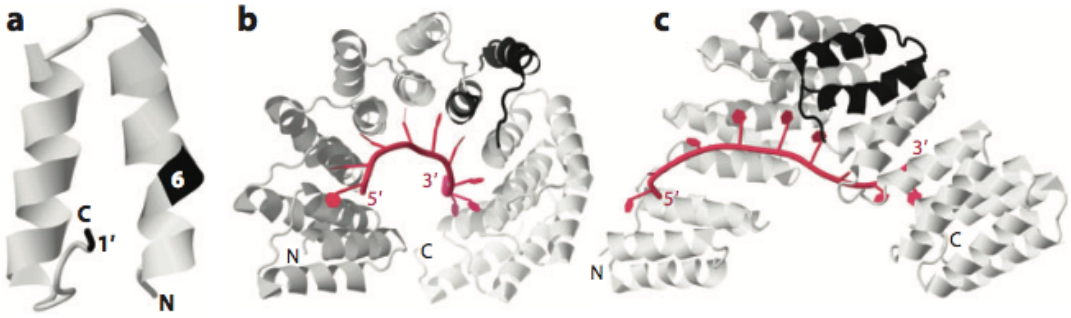
a
6
C
1′
N
b
5′
3′
N
C
c
3′
5′
N
C

Figure 1.2. Schematic view of the structure of a PPR protein and a model suggesting the interaction of PPRs to their RNA target; a) A PPR motif from Arabidopsis RNaseP (PRORP1), b) a model of 10 PPR repeats bound to 9 nucleotides at poly(U) RNA, and c) The side view of the same model to show the interaction of the bases with the edges of PPR repeats Barkan *et al* [64].

1.4.1. LRPPRC protein and its mitochondrial partner

LRPPRC forms a stable complex with the stem-loop interacting RNA binding protein (SLIRP) that is primarily localized in mitochondria [69]. This interaction was initially established using immunoprecipitation and blue native polyacrylamide gel electrophoresis (BN-PAGE) assays [69]. SLIRP, a 12-KDa protein, contains a single RNA recognition motif (RRM) and was initially thought to be associated with transactivation of nuclear hormone receptors [70]. However, a subcellular fractionation experiment proposed a role for SLIRP in mitochondria [70], and using immunofluorescence Sasarman *et al*., 2010 suggests that LRPPRC is exclusively localized in mitochondria [69].

Until now, many analyses have been applied to scrutinize the mitochondrial function(s) of SLIRP. For example, it has been suggested that reducing the levels of either LRPPRC or SLIRP using siRNA transfection causes a marked reduction in the levels of mitochondrial mRNAs such as COX1, COX2, and COX3, but it does not affect the levels of tRNAs and rRNAs [69]. Knock down experiments in human control fibroblasts also suggest that LRPPRC and SLIRP form an interdependent complex [71]. Reduction in the steady-state levels of SLIRP causes a significant decrease in the steady-state level of LRPPRC and of COX subunits such as COX1 and COX2 [71], the phenotype that is observed in LSFC patient fibroblasts in which the level of LRPPRC is reduced to 30% of control [69]. A recent study regarding the *in vivo* function of SLIRP suggests that SLIRP knock-out mice, in contrast to LRPPRC knock-out mice, have a normal life span [72]. Despite of reduction in the steady-state levels of mitochondrial mRNAs in SLIRP knock-out mice, mRNA polyadenylation status is not affected. Perhaps, the residual LRPPRC is sufficient to maintain normal polyA tail length. These results indicate a specific role for the LRPPRC/SLIRP complex in the posttranscriptional handling of mRNAs.

1.4.2. LRPPRC function

At the cellular level, analysis of the LSFC patients' fibroblasts demonstrates a specific defect in COX activity and assembly, a decrease in the synthesis of all three mitochondrial COX subunits, and a global reduction in the steady-state levels of all mitochondrial mRNAs except ND3 and ND6 [69]. This finding is in good agreement with the quantitative RT-PCR (qRT-PCR) analysis of mitochondrial mRNAs in LSFC cell line models that show a significant decrease of all mitochondrial mRNAs [73]. In addition, investigation of the LSFC myoblasts and myotubes in our lab demonstrated similar defects to those previously identified in fibroblasts: 1) Defects in the steady-state levels of SLIRP and LRPPRC, and 2) defects in the translation pattern of the mitochondrial proteins particularly COX1 and COX2. However, unlike the LSFC fibroblasts, a combined deficiency of OXPHOS complexes IV and I is observed in these cell lines [71].

A recent study in our lab revealed some biochemical features of the LSFC disease in various tissues. Analysis of the assembled OXPHOS complexes suggested a combined deficiency of complexes IV and I in the skeletal muscle and a severe or mild deficiency of complex IV in the liver and heart, respectively. These results manifest a correlation between the clinical phenotype of the disease and the severity of the defect that is observed in the assembly of the OXPHOS complexes especially complex IV. Surprisingly, the clinical phenotype of the LSFC disease is not explained by analyzing the steady-state levels of mitochondrial mRNAs in the liver, heart, and skeletal muscles isolated from an LSFC patient because the most severe reduction in the steady-state levels of mitochondrial mRNAs is not observed in the liver, which is a severely affected tissue in the LSFC disease [71]. Investigation of the LRPPRC complex using BN-PAGE demonstrated that LRPPRC is present in a complex of ~250 KDa in the liver, skeletal muscle, and fibroblasts in human control samples. However, this complex is not visualized in the heart tissue. In addition, it is hypothesized that the solubility of LRPPRC and

SLIRP are likely altered in the LSFC tissues. Using DDM detergent to extract proteins from the LSFC liver and heart, LRPPRC and SLIRP were predominantly found in the insoluble fraction. Using alkaline carbonate to investigate whether the protein is associated with the mitochondrial membrane, these proteins were equally abundant in the soluble and insoluble fractions. These results were obtained by tissue characterization of a limited number of individuals owing to the lack of human tissue samples [71]. In conclusion, the authors suggested that the LRPPRC/SLIRP complex is partially associated with the mitochondrial membrane despite lacking predicted transmembrane domain in these proteins, and that the detergent solubility of LRPPRC and SLIRP is decreased in tissues of the LSFC patient [71]. Another study suggests that the LRPPRC/SLIRP complex stabilizes mRNAs by promoting mitochondrial mRNA polyadenylation and suppressing mRNA degradation, but the exact mechanism by which LRPPRC affects these processes remains unknown. Human mitochondrial mRNA poly A tail length is regulated by mitochondria-specific poly (A) polymerase (MTPAP), which mediates mRNA polyadenylation, and polynucleotide phosphorylase (PNPase), which mediates mRNA degradation [74]. The polyadenylation profile of mitochondrial mRNAs upon knock down of LRPPRC and SLIRP in Hela cells suggests a specific reduction in the poly A tail length of mRNAs such as COX1, COX3, ND2, ND3, ND5, and CYTB [74]. Further analysis of polyadenylation status of mitochondrial mRNAs in heart-specific LRPPRC knock-out mice demonstrated a marked reduction in the length of poly A tail in all mitochondrial mRNAs except ND6, which does not contain a terminal poly A tail. This tissue-specific disruption of LRPPRC causes severe COX deficiency and an abnormal sub-assembly of complex V corresponding to the F1 portion, while the activities of other OXPHOS complexes appear to be normal [75].

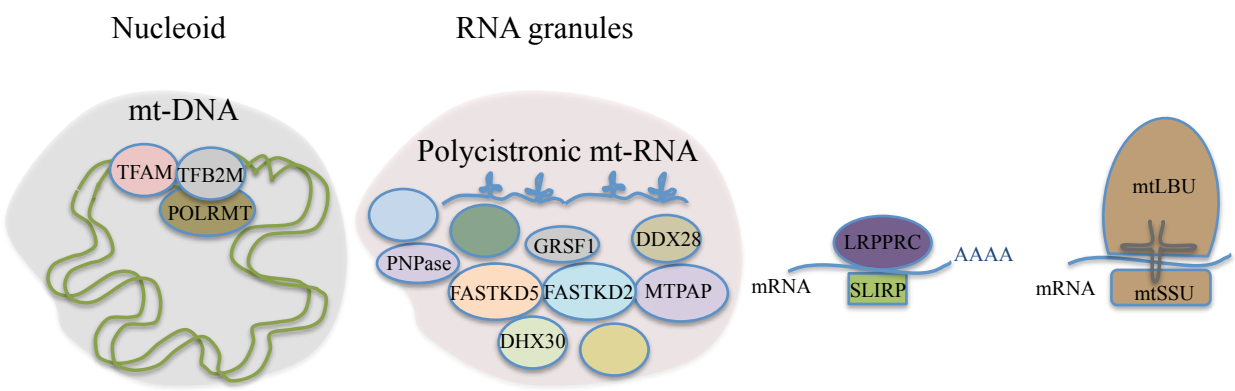
Nucleoid
RNA granules
mt-DNA
TFAM
TFB2M
POLRMT
Polycistronic mt-RNA
PNPase
GRSF1
DDX28
FASTKD5
FASTKD2
MTPAP
DHX30
mRNA
LRPPRC
SLIRP
AAAA
mRNA
mtLBU
mtSSU
Transcription
Processing
Modification
Polyadenylation
Degradation
Stability
Translation

Figure 1.3. Schematic view of a hypothetical model for LRPPRC function. This model suggests that mt-DNA is transcribed as precursor polycistronic RNA in nucleoid. mt-RNA processing of the large polycistronic transcript occurs in RNA granules. Once mt-mRNA released, LRPPRC forms a stable complex with SLIRP and binds to mt-mRNA coding sequences. This complex seems to promote mt-mRNA stability through polyadenylation; however, the exact mechanism through which LRPPRC functions as such remains unclear. mt-mRNAs are translated by mitochondrial ribosomal machinery, large (mtLSU) and small (mtSSU) subunits.

1.5. Hypothesis and objectives

Over the past decades, the field has made significant progress in the study of the clinical features, the underlying genetic cause, and the pathogenesis of LSFC disease. In 2003, a homozygous mutation in *LRPPRC* was found to be the causative factor [55]. Genealogical studies suggested that the corresponding gene was introduced to French Canadian population by early Europeans settlers of 18th century. Regarding the pathogenesis of LSFC, Sasarman *et al* [69] showed that the mutant LRPPRC protein was normally targeted to mitochondria but the steady-state levels of the protein was reduced [69]. From these observations three main questions arose as to; 1) why are the steady-state levels of the mutant protein low (is it a problem of protein synthesis or turnover) 2) what are the interacting partners of the mutant LRPPRC and 3) could the defect be rescued by over-expressing LRPPRC. To answer these questions; I generated several cell line models and over-expressed wild type and mutant LRPPRC in order to: 1) measure the half-life, 2) investigate the interacting partners, 3) rescue the biochemical defects observed in the LSFC subject fibroblasts.

Investigation of patient tissues or cell lines provided some valuable information regarding the biochemical phenotype of the disease [71]. Generally, two major phenotypes were reported; 1) a severe complex IV deficiency, 2) defect in the levels of most mt-mRNAs; however, the exact mechanism by which LRPPRC deficiency leads to such phenotype remains unclear. Logically, the protein should be involved in stabilizing mitochondrial mRNAs, yet little is known about the factors modulating this process. To address this, we developed a conditional LRPPRC knock-out model to investigate the impact of LRPPRC deficiency on mitochondrial function. In summary, the aim of this thesis was to investigate the function of LRPPRC and the pathogenesis of the protein containing pathogenic amino acid substitutions in LSFC disease. This thesis is presented in a traditional format, separated in eight chapters. In chapter 3, I

investigated the liver-specific LRPPRC knock-out mice and demonstrated the impact of LRPPRC deficiency on mitochondrial function. In chapter 4, using total RNA isolated from three tissues (skeletal muscle, heart, and liver) of an LSFC patient, I amplified the 3′ end of some mt-mRNAs (COX1, COX2, ND3) and showed that the poly A tail length is reduced. In chapter 5, I measured the protein half-life of wild type and mutant LRPPRC and suggested that p. A354V and p. Y172C mutations in LRPPRC make the protein unstable. Using BioID [76], I found caseinolytic peptidase B homolog CLPB, a member of the AAA+ protein family, as an interacting partner of mutant LRPPRC and showed that over-expressing CLPB increases the stability of the mutant LRPPRC.

1.6. Preface

Deficiency of cytochrome *c* oxidase leads to early-onset fatal diseases in most cases and is one of the causes of Leigh syndrome, the prominent cause of Saguenay-Lac-St-Jean form of Leigh syndrome (LSFC), fatal infantile COX deficiency, cardiomyopathy, myopathy and a reversible COX deficiency in muscle [93, 94]. In chapter 3 of this thesis, we describe the results of investigating LSFC mouse model. We hypothesized that depletion of LRPPRC in mouse liver may provide some insights toward the mechanisms underlying the disease pathogenesis. To examine this, we generated a liver-specific Lrpprc knock-out mouse. Our findings implicate that loss of LRPPRC triggers a multi-faceted phenotypic remodelling including OXPHOS impairment, mitochondrial ultrastructure abnormalities, impaired lipid metabolism, dysregulation of the permeability transition pore, and changes in ROS dynamics, thus highlighting the complex pathogenesis of OXPHOS disorders. LSFC fibroblasts recapitulated several alterations in mitochondrial function including mitochondrial fragmentation, a decrease mitochondrial membrane potential, and reduced ADP-stimulated respiration [95]. Consistent with these findings, a case-control prospective metabolic profiling study in LSFC patients revealed a metabolic signature of disrupted oxidative phosphorylation, which include markers reflecting changes in NAD^+ lipid and amine metabolism [96]. In chapter 4, the role of LRPPRC in mitochondrial gene expression is investigated. Gene expression is widely regulated by RNA binding proteins (RBPs) at the post-transcriptional level. Knowing that human mitochondrial genome encodes ribosomal RNAs (rRNAs), messenger RNAs (mRNAs), and tRNAs that are transcribed into a polycistronic RNA, the presence of post-transcriptional regulations is an asset for efficient processing. Based on the tRNA punctuation model [26], mt-mRNAs should be synthesized in equal copy numbers, but in fact, the half-life of mt-mRNAs differs extensively, which subsequently results in variable steady-state levels [74]. The factors modulating the post-

transcriptional handling of mt-mRNAs, thus, play an essential role for regulating their steady-state levels. Two mitochondrial mRNA binding proteins including GRSF1 [27] and LRPPRC [69, 71] have been functionally characterized. GRSF1 is shown to interact preferentially with one mRNA and two long noncoding RNAs transcribed from the light strand of mitochondrial DNA through GRSF1 consensus binding motifs [27]. LRPPRC in a complex with SLIRP is demonstrated to interact with RNA precursors before maturation, and mt-mRNAs are co-immunoprecipitated by this complex but with a different frequency [74]. Recent studies implicate the role of LRPPRC in the maintenance of mt-mRNA poly A tail length [74-75]. Investigation of the heart-specific LRPPRC knock out mice properly demonstrate the impact of LRPPRC deficiency on poly A tail length of most mt-mRNAs. As such, the majority of mt-mRNAs lose their poly A tail and consequently become less stable. ND6 is the only mt-mRNA with unchanged steady-state level or poly A tail length in the absence of LRPPRC in the mouse heart, due to the fact that this mRNA lacks poly A tail [75]. It is yet unclear how LRPPRC regulates the tail length of mt-mRNA poly A, as no data have ever suggested the interaction of mitochondrial poly A polymerase with LRPPRC or SLIRP. The status of mt-mRNA poly A tail length has not yet been characterized in the tissues of LSFC subjects. Our group previously described the differences that exist amongst tissues of an LSFC subject and showed that the biochemical phenotypes of the disease are tissue-specific [71]. Thus, in the fourth chapter of this thesis, we use LSFC subject tissues to measure the poly A tail length of a subset of mt-mRNAs. We show that the percentage of poly-, oligo-, or non-adenylated mt-mRNAs varies amongst the human tissues. Furthermore, we demonstrate that the poly A tail length of three mitochondrial mRNAs (COX1, COX2, and ND3) is decreased in LSFC subject. Last, we show that all mt-mRNAs in liver are polyadenylated except ND6, and we characterize some features of these mRNAs at the 3′ end. In chapter 5, we demonstrate the interacting partners of LRPPRC variants

and describe the mechanism(s) underlying the pathogenesis of LSFC. The pull-down system or coimmunoprecipitation approach provides valuable information for investigating protein interactions, but it has two limitations. First of all, low abundance proteins may not be detected by this method. Second, the conditions that are used may not identify proteins that interact transiently or weakly. In order to overcome the limitations of the coimmunoprecipitation method, we took advantage of a recently developed technique called BioID [76]. BioID is designed to identify interacting proteins by biotinylating them with a promiscuous prokaryotic biotin ligase. The protein of interest is fused to this promiscuous biotin ligase (in frame with a downstream FLAG tag) and introduced to mammalian cells (Flp-In T-REx 293 cells with an inducible promoter). Transcription of the transgene is initiated with doxycycline (24 hours) and upon supplementation of the culture medium with biotin, the biotin ligase biotinylates proximal proteins, the interacting partners. Labeled proteins are captured on streptavidin beads and analyzed by mass spectrometry. This method identifies protein-protein interactions in a native environment *in vivo* independent of the strength of the interaction. The biotinylated proteins are purified using affinity columns and analyzed by mass spectrometry. The preys are scored based on the specificity of their interaction with the bait protein. The work in chapter 5 demonstrates that LRPPRC carrying the pathogenic amino acid substitutions have rapid turn-over. We show the defect cannot be corrected by expressing LRPPRC. We found CLPB interacting with LRPPRC variants and determined CLPB expression can stabilize Y172C LRPPRC. We propose that the steady-state levels of LRPPRC is tightly regulated at the post-transcriptional levels and that the mutated protein has short half-life.

Chapter 2 Materials and Methods

Animal care and generation of conditional Lrpprc knock-out mice

All experiments on mice were performed at Université de Montréal and approved by the animal care committee. Liver specific Lrpprc knock-out mice were generated as described by Cuillerier *et al* [97]. Briefly, the Lrpprc knock-out mice in C57BL/6N embryonic stem (ES) cells were produced by the KOMP repository (University of California, California). The mutated locus was transmitted through the germ line, and heterozygous Lrpprc +/lox-neo mice were produced. The neomycin resistance cassette was removed by crossing Lrpprc +/lox-neo with flp producing animal, resulted a mouse with loxP sites in intron 3 and 5. The homozygous Lrpprc loxP/loxP mice were produced after crossing Lrpprc +/loxP mice. Next, Lrpprc loxP/loxP mice were mated with mice produced Cre recombinase under the control of the albumin promoter in order to generate liver-specific Lrpprc knock-out animals. All knock-out animals were genotyped by isolated DNA from the tail based on the method published by Cuillerier *et al* [97]. For biochemical and molecular analyses, all mice (males and females) were euthanized by cervical dislocation at 5 or 10 weeks of age followed an overnight fast. After dissection, tissues were rapidly excised, and transferred to cold phosphate buffered saline (PBS, Bishop ALB001).

Mitochondrial isolation

The liver tissue was obtained from 5 and 10 weeks of age mice and was prepared in ice-cold 250 mM sucrose/ 10 mM Tris-HCl/1mM EDTA (PH=7.5). The tissue was minced by scissors; the pieces were transferred to a 15 ml glass tube and homogenized with 10 passes through a pre-chilled zero clearance homogenizer (Kimble/Kontes). The homogenized tissue extract was then centrifuged for 10 min at 600g, 4°C to obtain a post-nuclear supernatant. The supernatant was transferred in a clean tube and re-centrifuged at the same speed. Mitochondria were pelleted by centrifuging for 10 min at 10,000g, 4°C. After decanting the supernatant, the

mitochondrial pellet was washed once in the same buffer at the same speed. Protein concentration was measured by the Bradford method [98].

Electrophoresis and immunobloting

SDS–PAGE. Whole liver extracts or isolated mitochondria were extracted in 1.5% lauryl maltoside/ PBS, and 20 μg of protein per sample were loaded and run on either 10 or 12% polyacrylamide gels, then transferred to a nitrocellulose membrane and used for the detection of LRPPRC (1/1000; in house), SLIRP (1/50; in house), COX1 (1/2000; Abcam # ab14705), NDUFA9 (1/1000; Abcam # ab14713), SDHA (1/1000; Abcam # ab14715), ACTIN (1/1000; Genescript # A00702), PORIN (1/2000; Abcam # 14734). LRPPRC polyclonal antibodies were prepared by immunizing rabbits with peptides of 22 amino acids corresponding the sequence CEPPESFEFYAQQLRKLRENSS (antibody 295-313; Zymed laboratories, San Francisco, CA).

BN-PAGE. Blue-Native PAGE was used to separate samples on 6–15% polyacrylamide gradient gels. Mitoplasts were prepared from tissues by centrifugation of homogenized extracts and solubilized with 1% lauryl maltoside, and 10 μg of the solubilized proteins were used for electrophoresis [99]. Separated complexes were transferred to a nitrocellulose membrane using a semi-dry system (GE Healthcare Life Sciences), and immunoblot analysis was performed. Individual structural subunits of complexes I (NDUFA9; 1/1000; Abcam #ab14713), II (SDHA; 1/1000; Abcam #ab14715), III (CoreII; 1/100; in house), IV (COXI; 1/2000; Abcam #ab14705) and V (ATP5a; 1/5000; Abcam #ab14748) were detected by immunoblot analysis. For the two-dimensional analysis, strips of the first-dimension gel (BN-PAGE) were incubated for 45 min in 1% SDS and 1%-mercaptoethanol, and these strips were then run on a 10% tricine/SDS-PAGE to separate the proteins in the second dimension [100].

Sucrose density gradient

Mitochondria from wild- type and conditional LRPPRC knock-out mice (400 μg) were lysed in lysis buffer (260 mM sucrose, 100 mM KCl, 20 mM $MgCl_2$, 10 mM Tris-Cl [pH 7.4], 1% Triton X-100, 5 mM β-mercaptoethanol, protease inhibitor cocktail without EDTA [Roche]) on ice for 20 min. Lysates were cleared by centrifugation at 9,400 ×g for 45 min at 4°C and subsequently loaded on a 1 ml 10%-30% discontinuous sucrose gradient (10 mM Tris-Cl, 100 mM KCl, 20 mM $MgCl_2$) and centrifuged at 32,000 rpm for 130 min at 4°C in a Beckman SW60-Ti rotor (Beckman Coulter, Brea, CA, USA). After centrifugation, 14 fractions were collected from the top and used for immunoblotting.

Total RNA isolation from mouse tissue

Total RNA was isolated using Trizol reagent (Invitrogen). 100 mg of liver tissue in 1 ml of Trizol reagent was homogenized and incubated at room temperature for 5 min. 200 μl of chloroform was added to the previous mixture, shaken vigorously for 15 seconds and incubated at room temperature for 2-3 min. The sample was centrifuged 15 min at 12,000 g at 4°C. The aqueous phase, the colorless upper phase that corresponds to 60% of the volume of TRIzol, was transferred to a fresh tube. The RNA was precipitated by mixing the aqueous phase with 500 μl of isopropanol, incubated at room temperature for 10 min and centrifuged for 10 min at 12,000 g at 4°C. The RNA was visible as a pellet on the side of the tube. The RNA pellet was washed with 1 ml 75% ethanol and centrifuged at 7500g for 5 min at 4°C. Next, the RNA pellet was air dried and solubilized in RNase free water.

MPAT (mRNA poly A tail length) assay

This assay was based on the method described by Temperley *et al* [101]. A universal linker DNA oligonucleotide 5′-phospho-ATG TGA GAT CAT GCA CAG TCA TA-3′-NH2 was ligated to the 3′ termini of total RNA (2.5 μg) by T4 RNA ligase (New England Biolabs) at 37°C for 3h. The ligated RNA was subjected to phenol/chloroform extraction and ammonium acetate/ethanol precipitation. Briefly, 1 ml of acidic phenol/chloroform was mixed with 40 μl of chloroform/ isoamylalcohol. 200 μl of this mixture was added to the ligated RNA, vortexed for 1 min, and centrifuged for 2 min at room temperature at 12,000 g. The aqueous phase was transferred to a fresh tube containing 200 μl of chloroform/ isoamylalcohol, vortexed for 1 min, and centrifuged for 2 min at room temperature at 12,000 g. The aqueous phase was then mixed with 100 μl of 10M NH4acetate and 500 μl of 100% cold ethanol, vortexed and preserved at -80°C overnight. The sample was centrifuged for 10 min at 16,000 g at 4°C. After removing the supernatant, the pellet was washed with 70% cold ethanol and centrifuged for 10 min at 16,000 g at 4°C. The ligated RNA pellet was air dried, solubilized in RNase free water, and amplified using one-step RT-PCR kit (QIAGEN) with anti-linker primer. A first round of PCR (35 cycles) was applied using a gene-specific upper primer and the anti-linker primer, followed by a second round of 10-cycle PCR using a gene-specific lower primer and the anti-linker primer. Lastly, half of the reaction product was resolved by 10% polyacrylamide gel electrophoresis in TBE buffer, dyed with SYBR green (Invitrogen) and visualized by PhosphorImage, and the remaining half was cloned in TOPO TA cloning vector (Invitrogen) and a large number of clones were subjected to Sanger sequencing. The results were analyzed by Microsoft Excel. All Oligo-DNAs were listed in table 1.

Primers	Sequence
Anti-linker	5′ TAT GAC TGT GCA TGA TCT CAC AT 3′
Upper COX1	5′ TAC CAC GAC GCT ACT CAG AC 3′
Lower COX1	5′ TGC CCT CCA CCA TAT CAC AC 3′
COX2	5′ CTT TAT GCC CAT TGT CCT AG 3′
ND3	5′ CCA CTA CCA TGA GCA ATT C 3′

Table 2.1. Oligonucleotide sequences against mouse genes used in MPAT assay.

Histology

Haematoxylin/Eosin. For a general assessment of histopathology, livers were rapidly excised and fixed overnight in 10% formalin. Samples were embedded in paraffin and 5µm thick sections were stained with Haematoxylin and Eosin.

COX/SDH activity. Cytochrome c oxidase (COX) and succinate dehydrogenase (SDH) activity staining was adapted from [102]. Serial cryostat sections were cut 10µm thick, brought to room temperature and were left to air dry for 1 hour. The first section of each sample was incubated for COX activity staining (in mM: 3.75 DAB, 0.1 Cytochrome *c*, pinch of catalase in 0.1 NaPi buffer, pH 7,0) for 30 min at 37 °C. The second section was incubated for SDH activity staining (in mM: 130 Na- Succinate, 0.2 PMS, 0.1 Sodium Azide, 1.5 NBT in 0.1 NaPi buffer, pH 7,0) for 30 min at 37 °C. The third section was incubated for COX activity staining buffer first, washed with distilled water and incubated for SDH activity staining buffer to achieve double staining. Sections were washed with distilled water and mounted with glycerol gelatine. Slides were examined by light microscopy.

Transmission electron microscopy

Following anaesthesia (8% chloral hydrate; 600 mg/kg), mice were perfused with 10 ml PBS and 5 ml 2.5% glutaraldehyde via the vena cava. Livers were excised, sliced and fixed over night at 4 °C in 2.5% glutaraldehyde in phosphate buffer. After sample preparation, 90–100 nm thick sections were mounted onto a 200 mesh copper grid (Electron Microscopy Sciences) and imaged with a FEI Tecnai 12 120 kV transmission electron microscope equipped with an AMT XR80C 8 megapixel CCD camera as previously described [103].

Preparation of sub-mitochondrial particles

Sub-mitochondrial particles were prepared as in the previously published literature [104, 105, 106]. Frozen isolated liver mitochondria were thawed on ice and centrifuged for 10 min at 8000 g, 4 °C. The pellet was re-suspended in sonication buffer (in mM: 250 sucrose, 10 K-phosphate, 10 Tris-HCl, 2 EGTA, 2 $MgCl_2$; pH 7.4) and sonicated 5×15 s using a Branson sonicator at 50% amplitude. The suspension was centrifuged 10 min at 10 000Xg, 4 °C; the supernatant was transferred and centrifuged 60 min at 100 000Xg, 4 °C in a swinging-bucket rotor. The final pellet was re-suspended in a small volume (25 µl or less) of suspension buffer (in mM: 1 EDTA, 1 $MgCl_2$, 75 sodium phosphate; pH 7.4) and kept on ice until use.

Mitochondrial functions

Respirometry. Respiration was measured using Clark-type electrodes at 23 °C under continuous stirring based on previous protocols [107]. Mitochondria (0.3 mg prot/ml) were suspended in respiration buffer (in mM: 10 KCl, 5 K_2HPO_4, 10 MOPS, 9 Pi, 2,5 $MgCl_2$, 1mg/ml BSA; pH 7.4). Following baseline recording, respiration was measured following sequential additions: i) glutamate + malate (5:2.5 mM) for Complex-I (CI) or succinate (5 mM) for complex-II (CII), ii) ADP (1 mM), and iii) and carbonyl cyanide m-chlorophenylhydrazone (CCCP: 0.03 µM). To measure the oxidation of long-chain fatty acids, respiration was measured following supplementation with palmitoyl-carnitine (20 µM) in the presence of malate (2.5 mM) and ADP (1 mM). To measure the activity of complex-IV (CIV) under native conditions, maximal ADP stimulated respiration was measured in the presence of TMPD/ascorbate (5/0.3 mM), and titrated with increasing concentrations of potassium cyanide, which allowed to correct respiration values for the auto-oxidation of TMPD/ascorbate.

Ca_2-induced opening of the permeability transition pore (PTP). Mitochondria (0.5 mg prot./ml) were incubated in a sucrose buffer (in mM: 250 sucrose, 0.005 EGTA-Tris base, 10 Tris-MOPS; pH 7.55) containing succinate (5 mM), rotenone (1 μM) and Pi (10 mM). Changes in extra-mitochondrial calcium concentration were monitored fluorimetrically (Hitachi, F4500 spectrofluorometer) using Calcium-green 5N (1 μM, ex–em: 505–535 nm) as described previously [108]. Residual calcium concentration was adjusted to the same level at the beginning of every experiment by adding a small amount of EGTA. Calcium pulses (2.5 μmol/mg protein) were added at 2 min intervals until a Ca_2^+-induced Ca_2^+ release was observed. In some experiments, the following PTP inhibitors were added prior to Ca_2^+ pulses: Cyclosporin-A (1 μM), $MgCl_2$ + ADP + Oligomycin (1.2, 0.6, and 0.00127 mM respectively). In all experiments, Calcium Retention Capacity (CRC) was taken as the total amount of Ca_2^+ accumulated by mitochondria prior to the Ca_2^+ pulse triggering Ca_2^+ release.

Mitochondrial membrane potential. Mitochondria (0.25 mg prot./ml) were incubated at room temperature in a K-MES buffer (in mM: 110 K-MES, 35 KCl, 1 EGTA, 5 K_2HPO_4, 3 $MgCl_2$, 0.5 mg/ml BSA) supplemented with the potentiometric probe Rhodamine 123 (0.2 μM, ex-em: 503–525 nm) and either glutamate: malate (5: 2.5 mM) or succinate (5 mM). Membrane potential (ΔΨ) was calculated from changes in the concentration of extra-mitochondrial Rhodamine 123 as per [109] using the equation $\Delta\Psi=59 \times \log$ [Rhodamine]in/[Rhodamine]out. To calculate the intra-mitochondrial concentration of Rhodamine, the amount of Rhodamine taken-up by mitochondria was determined by measuring changes in fluorescence following addition of respiratory substrates. A matrix distribution volume of 1 μl/mg protein, and a non-specific binding of rhodamine to mitochondria of 30% was assumed in all groups [109].

Mitochondrial H_2O_2 release and membrane permeabilization. Mitochondria (0.2 mg prot./ml) were incubated at room temperature in a K-MES buffer (in mM: 110 K-MES, 35 KCl,

1 EGTA, 3 $MgCl_2$, 10 K_2HPO_4, 0.5 mg/ml BSA; pH 7,55) supplemented with the H_2O_2-sensitive probe Amplex red (1.5 μM; ex-em: 563–587nm) and horseradish peroxidase (1.2U/ml), as previously described [110]. Net mitochondrial H_2O_2 release was measured: i) under state 2 conditions in the presence of succinate (5 mM) alone or with glutamate-malate (5:2.5 mM) to elicit reverse electron flow, ii) under state 3 conditions following the addition of ADP (1 mM), and iii) under state 2 following inhibition of reverse electron flow with rotenone (1 μM). To assess mitochondrial H_2O_2 trapping, net H_2O_2 release was first measured under state 2 conditions and membranes were subsequently permeabilized by adding increasing pulses of digitonin (0.01% per pulse) at regular interval. An increase in H_2O_2 emission above basal levels was used as an indicator of H_2O_2 entrapment.

H_2O_2 Scavenging. H_2O_2 scavenging was measured fluorimetrically in a 96 well plate reader using a protocol modified from [110]. Briefly, mitochondrial aliquots (0.1 mg prot/ml) were distributed in 7 wells in K-MES buffer supplemented with glutamate (50 μM) and malate (20 μM). A pulse of 3 nmoles of H_2O_2 was added to the first well at t = 0 s, and to each subsequent well at 20 s intervals. At t = 100 s, 100 μl of K-MES buffer supplemented with 10 μM Amplex Red, and 0.5 U/ml horseradish peroxidase was added to all wells, and fluorescence corresponding to the amount of un-scavenged H_2O_2 remaining in each well was immediately measured in end-point measurement mode. In all experiments a control well containing no mitochondria was used as the baseline control.

Enzyme activities

Activities of CI (NADH-CoQ reductase), CII (succinate dehydrogenase), CIV (cytochrome *c* oxidase), CV (ATP synthase) and citrate synthase (CS) were measured spectrophotometrically in a plate reader using standard coupled enzyme assays adapted from

[107] and from [111] for CV. Activities were expressed in mU.min−1.mg mitochondrial prot−1. To facilitate comparisons, all enzyme activities were subsequently expressed as fold difference vs Lrpprc $^{+/+}$.

Mitochondrial membrane lipid composition using LC-MS analysis

Procedures for lipid extraction and analysis were adapted as previously described [112, 113]. Briefly, lipids were extracted from isolated mitochondria (200 µg protein), which had been spiked with six internal standards. Samples (equivalent to 2.6 µg of protein extract) were injected onto a 1290 Infinity HPLC coupled with a 6530 accurate mass QTOF (Agilent, Santa Clara, USA) via a dual electrospray ion source. Lipids were eluted on a Zorbax Eclipse plus C18, 2.1 × 100 mm, 1.8 µm (Agilent, Santa Clara, USA) kept at 40°C with a gradient of 83 min and were analysed in both negative and positive scan mode. Each feature or entity characterized by a specific mass and retention time, were identified using Mass Hunter B.07.00 software (Agilent, Santa Clara, USA). A frequency filter of 100% was applied and signal intensities were normalized using Quantile algorithm with Mass Profiler Pro. software (MPP, Agilent, Santa Clara, USA). MS entities that discriminated the two conditions based on a false discovery rate of 5% and a fold change >2, were subjected to tandem mass spectrometry for lipid identification. Note that for cholesterol, identification was also confirmed by LC-MS analysis of the corresponding standard.

Statistical analyses

Unless indicated, data in chapter 3 are presented as mean ± SEM. Unpaired student's t-test or a one-way analysis of variance (ANOVA) followed by Bonferroni multiple comparison post hoc analysis was used to determine significant difference between two or among multiple

groups, respectively. Statistically significant differences were considered for $P < 0.05$. All analyses were performed on Prism 6.0 for Mac OS-X. For lipidomics analysis, data were analyzed with Mass Profiler Professional (MPP) using unpaired student's t-test followed by Benjamini Hochberg correction and statistical significance was set at a false discovery rate of 5%; data are depicted as a volcano plot.

Subject

The human tissues used in this thesis were taken from an LSFC subject homozygous for a common C1119T transition (p. A354V) in LRPPRC with typical clinical features of the LSFC disease as described by Morin *et al*, 1993 [53].

Total RNA isolation and MPAT assay (human tissues)

Total RNA was isolated using Trizol reagent (Invitrogen). Approximately100 mg of human tissue (liver, heart, skeletal muscles) was homogenized in 1 ml of Trizol reagent and incubated at room temperature for 5 min. Then, 200 µl of chloroform was added and the mixture, was shaken vigorously for 15 seconds and incubated at room temperature for 2-3 min. The sample was centrifuged 15 min at 12,000 g at 4°C. The aqueous phase, the colorless upper phase that corresponds to 60% of the volume of TRIzol, was transferred to a fresh tube. The RNA was precipitated by mixing the aqueous phase with 500 µl of isopropanol, incubated at room temperature for 10 min, and centrifuged for 10 min at 12,000 g at 4°C. The RNA pellet, which was visible on the side of the tube, was washed with 1 ml 75% ethanol and centrifuged at 7500g for 5 min at 4°C. Next, the RNA pellet was air dried and solubilized in RNase free water. The mRNA poly A tail length (MPAT) assay was performed as described previously, and the following primers were used for specific amplification of human mitochondrial mRNAs. The

PCR product was cloned into TOPO TA vector, and approximately 12 clones were sequenced (tables 3.2-3.4).

primers	Sequence
Anti-linker	5′ TAT GAC TGT GCA TGA TCT CAC AT 3′
Upper COX1	5′ AGA ACC CTC CAT AAA CCT GGA 3′
Lower COX1	5′ CAC ATT CGA AGA ACC CGT AT 3′
COX2	5′ ACG ACC GGG GGT ATA CTA CG 3′
COX3	5′ AAC ATC ACT TTG GCT TCG 3′
ND1	5′ GAA TTC GAA CAG CAT ACC 3′
ND2	5′ ACC TCA ATC ACA CTA CTC 3′
ND3	5′ AAT TGC CCT CCT TTT ACC C 3′
ND4	5′ CTC CCT CTA CAT ATT TAC CAC 3′
ND5	5′ CAT CAT ACT CTT TCA CCC AC 3′
ND6	5′ AGT TGG AAT AGG TTG TTA GC 3′
CYTB	5′ ATC ATT GGA CAA GTA GCA TC 3′
ATP6	5′ CCC TCT ACA CTT ATC ATC TTC 3′

Table 2.2. The sequence of oligonucleotides against human mitochondrial genes used in MPAT assay.

Plasmids

CLPB/pDONR221 was obtained from DNASU (central repository for plasmid clones and collections, The Biodesign Institute, Arizona State University, 1001 S. McAllister Ave, Tempe, AZ 85287-6401) and a BirA-FLAG construct was generated via Gateway cloning into pcDNA5-pDEST-BirA-FLAG-C-ter. The wt LRPPRC/pDONR223 was obtained from Addgene (23521) and point mutations (A354V and Y172C) were introduced into the LRPPRC sequence by

polymerase chain reaction–directed mutagenesis (Agilent Technologies, 200522), and constructs (wt LRPPRC-BirA-FLAG, A354V LRPPRC-BirA-FLAG, and Y172C LRPPRC-BirA-FLAG) were generated via Gateway cloning into pcDNA5-pDEST-BirA-FLAG-C-ter. Constructs wt LRPPRC, A354V LRPPRC and Y172C LRPPRC were generated via Gateway cloning into pBabe and PLXSH retroviral vectors. All constructs were validated by Sanger sequencing.

Cell lines

Immortalized subject Fibroblasts (subjects 1, 2, and 3) and age matched controls (controls 1 and 2), Flp-In T-REx 293, and 143B cell lines were grown in high-glucose Dulbecco's modified Eagle's medium (DMEM) supplemented with 10% fetal bovine serum, at 37°C in an atmosphere of 5% CO_2.

BioID

Human cell lines (Flp-In T-REx 293) were seeded at 250,000 cells per well in a 6 wells plate in 2 ml high glucose Dulbecco's modified Eagle's medium (DMEM) (Wisent) supplemented with 10% fetal bovine serum (Wisent), 10% penicillin/streptomycin (100 U/ml, Thermo Fisher) at 37°C in an atmosphere of 5% CO_2. The following day, cells were transfected in the presence of 200 ng of wt-LRPPRC-BirA-FLAG, A354V LRPPRC-BirA-FLAG, and Y172C LRPPRC-BirA-FLAG, 2 µg of pOG44 in 250 µl of 1× Opti-MEM (Invitrogen) mixed with 5 µl of Lipofectamine 2000 reagent in 250 µl of 1× Opti-MEM. The Opti-MEM/Lipofectamine solution was added to the Opti MEM/plasmid solution and incubated 20 min before addition to the cells (in medium without antibiotics). The medium was changed 4 h after transfection. The next day, transfected cells were passaged into 10 cm^2 plates, and the following day selection was started by the addition of hygromycin (Calbiochem) at a final

concentration of 200 μg/ml. The selection media was changed every 2–3 days until clear visible colonies were present. Up to six colonies per construct were picked and expanded, and the localization and the expression level of the construct were assessed by immunofluorescence using anti-FLAG (Sigma, F1804). The selected clones were scaled up to six 15 cm^2 plates for treatment and harvesting. Cells were grown to 70% confluency before induction of protein expression using 1 μg/ml tetracycline (Sigma), and media supplementation with 50 μM biotin for protein labeling. Cells were harvested 24 h later as follows: the media was decanted, cells were washed twice with 5 ml of PBS per 15 cm^2 plate and then harvested by scraping in 5 ml of PBS. Cells from three 15 cm^2 plates were pelleted at 800 rpm for 3 min, PBS was aspirated and pellets transferred to a −80°C freezer. Purification of biotinylated proteins followed by their identification by mass spectrometry was performed as described by Couzens *et al* [114].

Electrophoresis and immunoblotting

Mitoplasts prepared from fibroblasts or Flp-In T-REx 293 cells by treatment with 0.8 mg digitonin/mg protein were run in the first dimension on non-denaturing, blue-native gels (BN-PAGE) as detailed elsewhere [99]. The native complexes were visualized with the following antibodies against the following subunits in all native gels: complex I, ND1 (a gift from Anne Lombes, Paris); complex II, SDHA (Abcam ab14715); complex III, core1 (Abcam ab110252); complex IV, COX IV (Abcam ab110261) and complex V, ATP alpha (Abcam ab14748). For the two-dimensional analysis, strips of the first-dimension gel were incubated for 45 min in 1% SDS and 1% β-mercaptoethanol, and then 10% polyacrylamide SDS-PAGE was used to separate the proteins in the second dimension.

Denaturing SDS-PAGE was used for the electrophoretic separation of whole-cell extracts, isolated mitochondria from cell lines, or fractions from alkaline carbonate extraction. Whole cells or isolated mitochondria were extracted on ice with 1.5% dodecyl maltoside/phosphate buffered saline (PBS) and mixed with sample buffer without prior centrifugation. Twenty micrograms of protein were then electrophoresed, transferred to a nitrocellulose membrane and analyzed by immunoblotting with the following antibodies: FLAG (Sigma F1804), LRPPRC (in house), SLIRP (Abcam ab51523), SDHA (abcam ab14715), Actin (genescript A00702).

Antibodies

The following antibodies were used in this study: anti-FLAG (Sigma F1804), anti-LRPPRC (in house), anti-SLIRP (Abcam ab51523), anti-SDHA (Abcam ab14715), anti-PORIN (Abcam ab14734), anti-NDUFA9 (Abcam ab14713), anti-COX IV (Abcam ab110261), anti-ATP5A1 (Abcam ab14748), anti-UQCRC2 (Abcam ab14745), anti- COX1 (Abcam ab14705), anti-ACTIN (GeneScript A00702), anti-BIOTIN (Abcam Ab53494), anti-CLPB (Sigma HPA039006), anti-TOMM20 (Santa cruz, Sc-11415), anti-AFG3L2 (in house), anti-PNPT1 (Proteintech 14487-1-AP), anti-CLPP (Proteintech 15698), CLPX (Abcam ab122644), anti-OPA1 (in house), anti-YME1L (Proteintech 11510), anti-HTRA2 (Proteintech 15775-1-AP), anti-IMMT (Abnova, H00010989-M01), anti-HSP75 (Abcam ab126946), anti-HSP10 (Santa cruz Sc-376313), anti-PORIN (Calbiochem 529534), anti-LONP1 (Proteintech 15440).

Pulse labeling of mitochondrial translation products

In vitro labeling of mitochondrial translation products was performed as previously described by Leary *et al*, 2009 [115]. Briefly, cells were pulse-labeled for 60 min at 37°C in methionine/cysteine-free DMEM containing 200 μCi/ml of a [35S] methionine/cysteine mix (Perkin Elmer) and 100 μg/ml of either emetine or anisomycin to inhibit cytosolic translation. To assess the mitochondrial translation rate, the cells were chased for 10 min (PULSE). To assess the stability of the newly synthesized peptides the cells were chased for 17 hours (CHASE) in regular DMEM, or for 8, 16 and 32 hours in a time course experiment. For chase studies, cells were incubated for 23 hours in 40 μg /ml chloramphenicol to inhibit mitochondrial translation prior to labeling. Total cellular protein (50 μg) harvested from cells after chasing was resuspended in loading buffer with a pH of 6.7 containing 93 mM Tris-HCl, 7.5% glycerol, 1% SDS, 0.25 mg bromophenol blue/ml and 3% mercaptoethanol, sonicated for 3–8 seconds, loaded

and run on 15-20% polyacrylamide gradient gels. The labeled mitochondrial translation products were detected through direct autoradiography.

Estimating protein half-life

Inducible Flp-In T-REx 293 cells expressing wt LRPPRC-BirA-FLAG, A354V LRPPRC-BirA-FLAG, and Y172C LRPPRC-BirA-FLAG were used. The expression of the protein was induced by the addition of tetracycline, and it was stopped after 24 hours. The cells were washed three times and were collected at 0, 6, 12, 24, 36, 48 hours after removing tetracycline from the media. The steady-state level of FLAG was measured and normalized to the levels of actin. The experiment was repeated four times and paired student's t-test or a two-way analysis of variance was used to determine significant difference between two groups. Statistically significant differences were considered for $P < 0.05$.

Immunofluorescence experiments

Glass coverslips were treated with poly-D-lysine hydrobromide (Sigma P6407-5NG) for 20 min at room temperature. 293 cells were plated on treated coverslips, induced by tetracycline for 24 hours, and fixed for 20 min with 4% Formaldehyde (Sigma, F8775) in PBS at 37°C. Cells were permeabilized for 15 min with a solution of Triton 0.05% (Bishop, TRX506) in PBS and blocked for nonspecific sites for 30 min in PBS-BSA 5%. Coverslips were then incubated for 1 h with the primary antibody in blocking solution and 30 min with appropriate anti-species secondary antibodies coupled with Alexa fluorochromes (Invitrogen) in blocking solution. DAPI (1:2000) was added for nuclear staining. Coverslips were mounted in Dako Fluorescence mounting medium. Cells were imaged with an Olympus IX83 microscope connected to a

Yokogawa CSU-X confocal scanning unit. Images were analyzed using ImageJ software Fiji [116].

siRNA transfection

Stealth RNA interference duplex constructs (Invitrogen) was used for transient knock-down of CLPB, AFG3L2, OMA1, and HTRA2 in fibroblasts. Stealth siRNA duplexes were transiently transfected into cells using Lipofectamine RNAiMAX (Invitrogen), according to the manufacturer's specifications. Briefly, lipofectamine and RNA duplexes (48 nM) were diluted in Opti-MEM ® Reduced Serum Medium. BLOCK-iT™ Alexa Fluor ® Red Fluorescent Oligo was used to assess the transfection efficiency (transfection performed in parallel with the other stealth constructs) and as a mock oligo transfection control (All reagents from Invitrogen). Transfection was repeated on day 3, and cells were retreated with 48 nM Stealth RNA interference duplex constructs, Lipofectamine RNAiMAX, and Opti-MEM media.

For transient knock-down of CLPB, CLPP, AFG3L2, YME1L, LONP1, and OMA1 in Flp-In T-REx 293 cells, stealth siRNA duplexes (Invitrogen) were transiently transfected into cells using Lipofectamine RNAiMAX and Opti-MEM media. The media was changed to regular DMEM the following day. The expression of the FLAG tagged protein was induced by tetracycline on day 3. On day 4, the cells were chased by changing media to regular DMEM. Half of the cells were harvested for immunoblot analysis and labeled as time 0. The remaining cells were pelleted 24 hours later and marked as time 24h.

Stealth RNA interference	constructs
CLPB	CCCGCUCCAUCAAACAUGAGGUAGA
CLPP	GCCUUGUUAUCGCACAGCUCCUCUU
CLPX	AAUAUCUUCGCCUACAUAUCCAGCC
SPG7	CCUCAAGGUUGAAGCAGAAGAAUAA
AFG3L2	GGUAUUGGAGAAACCUUACAGUGA
YME1L	UUCGAUGGCAGAUUGGGUUUCUGGA
OMA1	CAGCAGUCCCUAGUCUGUCAGUAUU
LONP1	GGACGUCCUGGAAGAGACCAAUAUU
HTRA2	GGGAGGUGAUUGGAGUGAACACCAU

Table 2.3. List of siRNAs and the constructs used in 293 cell lines.

Alkaline carbonate extraction

Freshly prepared mitochondria from 293 cells (from two 15 cm^2 plates per sample) were pelleted at 15,000 g for 10 min at 4°C. 100 μg of isolated mitochondria were resuspended to a final concentration of 1 mg/ml in 100 mM sodium carbonate (Na_2CO_3) pH 12 plus protease inhibitor, and incubated on ice for 30 min. Half of the volume (50 μl) was reserved as "input" sample. The remaining (50 μl) was centrifuged at maximum speed in a benchtop ultracentrifuge for 1h at 4ºC. The supernatant was stored as "sup" sample, and the pellet was gently rinsed twice with ice cold ddH_2O. The "pellet" was dissolved in a volume of SDS-PAGE loading buffer equal to that of the input and sup fractions (50 μl). The samples were loaded on SDS-PAGE gel to visualize appropriate proteins.

Treatment of 293 cell lines with molecular chaperons

293 cell lines (wt- and Y172C-LRPPRC-BirA-FLAG) were thawed one week in advance. On the day one, the following chaperons were added to the media (DMEM): 10 mM 4-phenylbutyrate (PBA), 1 M trimethylamine n-oxide (TMAO), 7.5% Glycerol, and 5% dimethyl sulfoxide (DMSO). The following day, cells were treated with tetracycline, fresh PBA and TMAO. At this stage, the cells treated with glycerol and DMSO died. On the third day, cells were harvested and lysed with 1.5% DDM and the lysate were subjected to 8% SDS-PAGE gel and immunoblotted with nitrocellulose membranes.

Chapter 3 characterization of liver-specific *Lrpprc* knock-out mice

3.1. Missense mutation in LRPPRC (p. A354V) in mouse leads to lethality early in the development

As described by our group [71], biochemical phenotypes of the LSFC disease in tissues isolated from one patient are heterogeneous. To investigate the reason, we studied a knock-in mouse carrying A354V Lrpprc mutation. In contrast to human cases, homozygous embryos died at embryonic days 8 and 10 (Figure 3.7). Out of 70 genotyped mice 5% were homozygous for knock-in allele, 65% were heterozygous, and 28% were homozygous for wild-type allele. Ruzzenente *et al* also showed that LRPPRC is essential for embryonic development in mice [75]. Knowing that liver is severely affected in LSFC [54, 56], we studied conditional knock-out mice in which LRPPRC was specifically depleted in the liver.

3.2. Loss of LRPPRC in liver results in delayed growth, and pronounced liver histopathological abnormalities

The liver-specific homozygous knock-out mice were viable, had a normal appearance and locomotor activity under normal cage bound conditions, but had reduced body weight at 5 weeks old compared to littermate controls (Figure 3.8 A). Livers of knock-out mice displayed several macroscopic abnormalities. Liver mass was 25% greater than in control animals (Figure 3.8 B), liver lobes displayed scattered pale coalescing areas, characteristic of multifocal hepatic necrosis, and the gall bladder was severely swollen. Microscopically, the geometry of liver lobules was disrupted and numerous blood vessels were dilated (Figure 3.8 C). Consistent with a C-IV deficiency, a severe reduction of COX staining was present in liver sections from knock-out mice. Furthermore, the normal peri-portal zonation of nuclear encoded CII (e.g. SDH) activity was lost in favour of a more homogeneous distribution across liver lobules (Figure 3.8 D). Of note, immunoblot analysis indicated the presence of residual amounts of LRPPRC (Figure 3.1 A-

E), which could be because of liver regeneration as previously observed in liver-specific COX10 knock-out mice [117].

3.3. Loss of LRPPRC in mouse liver resembles the biochemical phenotypes observed in LSFC disease

SDS-PAGE analysis of mitochondrial pellets isolated from liver tissue of wild- type and Lrpprc knock-out mouse demonstrates a decrease in the steady-state levels of LRPPRC, SLIRP, and COX1 (a mitochondrial subunit of cyochrome *c* oxidase) (Figure 3.1 A-E). We next sought to investigate the level of OXPHOS complexes by BN-PAGE assay, and we mainly observed severe deficiency of complex IV accompanied by disassembly of complex V, a phenotype that is not observed in LSFC patients. This could be explained by the presence of residual protein in patient and almost complete absence of LRPPRC in the liver of conditional knock-out mice.

Analysis of OXPHOS assembly in 10-week-old mice suggests up-regulation of other OXPHOS complexes in addition to a severe COX defect and disassembled complex V (Figure 3.2 A-B). The presence of up-regulated OXPHOS complexes in Lrpprc knock-out livers could be due to compensatory mechanisms in response to lack of fully assembled complex IV and that could contribute to decrease the deleterious phenotype.

According to previously published by Sasarman *et al*, the LRPPRC/SLIRP complex is undetectable in human heart [71]. In order to further analyze the formation of this complex in mouse tissues, we isolated mitochondria from heart, liver, and skeletal muscle, in addition to liver isolated from Lrpprc$^{-/-}$ sample. Next, we tested this by BN-PAGE assay followed by second dimension gel (Figure 3.3 A-B). To our surprise, we found that LRPPRC/SLIRP complex is detectable in the heart and liver, and it migrates differently as compared with skeletal muscle. Altogether, these data suggest that LRPPRC/SLIRP form a complex in all three described

tissues; however, it seems likely that the complex is post-translationally modified in the heart and liver in comparison to skeletal muscle.

3.4. The steady-state levels of a subset of mitochondrial mRNAs are decreased in conditional LRPPRC knock-out mice

Several studies suggest that LRPPRC interacts with mitochondrial mRNAs [69,74, 75]. Thus, loss of LRPPRC in liver-specific Lrpprc knock-out mice should impact the steady-state levels of mitochondrial mRNAs. To investigate this, we isolated total RNA from liver of conditional LRPPRC knock-out mice and measured the steady-state levels of all mitochondrial mRNAs by qRT-PCR. The results clearly show a decrease in the levels of all mitochondrial COX subunits (COX1, COX2, and COX3), cytb, ND1, ND4/4L, and ATP6. The levels of other mitochondrial mRNAs seem to be normal, but the levels of the two mitochondrial rRNAs were increased (Figure 3.4).

Next, we asked whether the steady-state level of mitochondrial ribosomal subunits is correspondingly altered. To test this, we analyzed ribosome assembly on sucrose density gradients and observed enhanced level of mitochondrial ribosomal small and large subunits in conditional LRPPRC knock-out mice (Figure 3.5). This observation was also confirmed by SDS-PAGE. A good correlation was obtained between qRT-PCR data and the results of the sucrose density gradient: both indicated the presence of compensatory translation machinery including large and small ribosomal proteins and RNAs in mitochondria isolated from conditional LRPPRC knock-out mice.

3.5. LRPPRC is essential for polyadenylation of some mitochondrial mRNAs

LRPPRC deficiency has an impact on the steady-state levels of most mtDNA-encoded transcripts in mice, particularly COX1-3 and ATP6, while rRNA levels were slightly increased. We therefore asked whether changes in the levels of mitochondrial mRNAs correlate with the length of ploy A tail in conditional LRPPRC knock-out mice. Thus, we analyzed the poly A tail length of selected mitochondrial mRNAs, including COX1, COX2, and ND3 mRNAs using MPAT assay. Interestingly, a high proportion (70-91%) of transcripts for COX1, COX2, and ND3 were oligo adenylated with less than 10 As or lacked stop codons and had short and variable chain lengths. However, there was no relationship between the severity of mRNA downregulation and the poly A tail length based on ND3 (Figure 3.6).

Altogether, we showed that some mitochondrial mRNAs harbor posttranscriptional modifications in mouse and that the poly A tail length of a subset of mitochondrial mRNAs is decreased in conditional Lrpprc knock-out mice. Further investigation is required to characterize the factors that are involved in this process.

3.6. The length of COX1 mRNA 3′ end varies in mouse heart

Ruzzenente *et al* [75] showed that COX1 mRNA in mouse heart is polyadenylated with 55 As, but oligoadenylated with less than 10 As in the heart-specific Lrpprc knock-out mice. To validate our MPAT assay with the results obtained by [75], we isolated total RNA from the heart of a wild-type mouse and measured the poly A tail length of the COX1 mRNA. Interestingly, we noticed variable length of poly A (8-66 A′s) and 3′UTR (14-71 nucleotides) for this mRNA.

3.7. Loss of hepatic LRPPRC induces a multi-faceted bioenergetic phenotype

We investigated whether mitochondria from *Lrpprc*$^{-/-}$ mice displayed abnormalities at the level of the phosphorylation machinery, particularly the ATP synthase (CV). As shown in Figure 3.9 A, CV activity was similar in the two experimental groups. However, an important loss of sensitivity to inhibition by oligomycin was noted in *Lrpprc*$^{-/-}$ samples, suggesting a CV defect. BN-PAGE analysis in DDM-solubilized mitochondrial extracts indicated a reduction in the amount of assembled CV monomers in knock-out mouse (Figure 3.9 B). Moreover, lower molecular weight ATPα immuno-reactive bands were visible, suggesting an accumulation of sub-assembled CV (Figure 3.9 B). CN-PAGE and in-gel activity measurements were also performed in digitonin-solubilized mitochondria to resolve CV dimers (Figure 3.9 C). These experiments confirmed the assembly defect, and further indicated an important reduction in the amount of assembled CV dimers in *Lrpprc*$^{-/-}$ mice.

Respirometry studies were performed to examine the bioenergetic consequences of these OXPHOS defects. While subtle differences in baseline state 2 respiration were apparent, the most striking abnormality was a 40–60% reduction of maximal ADP-stimulated respiration in the presence of CI or CII substrates (Figure 3.10 A). This reduction was attributable to the ATP synthase defect, rather than to loss of CIV activity, since mitochondria from control and Lrpprc$^{-/-}$ mice had similar maximal respiration rates following uncoupling with CCCP (Figure 3.10 A). Since the activity of CIV measured in solubilized extracts was reduced by 80% in Lrpprc$^{-/-}$ mitochondria (Figure 3.9 A), the surprizing capacity of residual CIV to support normal rates of respiration was investigated by monitoring CIV activity in its native membrane environment using TMPD/Ascorbate as a respiratory substrate (Figure 3.10 B). Under those conditions, CIV activity of Lprrpc$^{-/-}$ mitochondria was only 30% lower than in controls ($P = 0.07$), indicating that the detergent extraction step used for the spectrophotometric assessment of CIV activity

amplifies the defect in Lrpprc$^{-/-}$ mitochondria. Interestingly, CIV was significantly more sensitive to cyanide (Figure 3.10 C) in Lrpprc$^{-/-}$ mitochondria compared to controls, indicating a greater vulnerability to inhibition.

Mitochondria from Lrpprc$^{-/-}$ mice also showed a 50% reduction in ADP-stimulated respiration in the presence of palmitoyl-CoA (Figure 3.10 A). Because the respiration rates observed with palmitoyl-CoA, are less than half those achieved with CII substrates, this result suggests that in addition to causing OXPHOS defects, Lrpprc deficiency has a direct impact on mitochondrial fatty acid oxidation capacity.

3.8. The ATP synthase assembly defect associated with LRPPRC deficiency alters the mitochondrial permeability transition pore

Recent studies suggest that ATP synthase dimers may constitute the structural core of the PTP [124, 125]. In the presence of increased Ca^{2+} concentrations and Pi, which are key triggers of pore opening, Ca^{2+} is suggested to displace Mg^{2+} from catalytic sites on the F1 sector. Under this condition, CV would adopt a conformation that induces pore formation at the interface between the two CV monomers. In this model, the OSCP subunit, located on the lateral stalk of CV is suggested to act as a negative modulator of PTP opening, presumably by limiting access of the Ca^{2+} binding sites on the F1 ATPase [124, 125]. Importantly, this negative modulation is suggested to be relieved when Cyclophilin-D (CypD), a key pore-sensitizing protein present in the mitochondrial matrix, is recruited to OSCP [124, 125].

Given the CV assembly defect observed in knock-out mice, Ca^{2+} retention capacity (CRC) experiments were performed in the presence of Pi to determine whether pore regulation was altered. As shown in Figure 3.11 A and D, CRC was nearly two-fold greater in mitochondria from knock-out mice, indicating a striking resistance to PTP opening. CRC was also performed in the presence of Mg^{2+}, ADP, and oligomycin, to delineate the nature of this resistance. Under this condition, CRC was increased by 2.3–2.5 fold in both experimental groups, indicating normal sensitivity in *Lrpprc*$^{-/-}$ mitochondria to ligands of the catalytic F1 sector, and the OSCP subunit (Figure 3.11 C and D). Furthermore, OSCP levels in the whole mitochondrial lysate and extracts used for CN-PAGE were similar between the two experimental groups (Figure 3.11 F). CRC experiments were also performed in the presence of Cyclosporin-A (CsA), which delays PTP opening by preventing recruitment of CypD to OSCP [124, 125]. As expected, CsA increased resistance to Ca^{2+}-induced PTP opening by more than 2.5 folds in control mice. In contrast, mitochondria from *Lrpprc*$^{-/-}$ mice were largely insensitive to CsA (Figure 3.11 B and D). Lack of sensitivity to CsA is normally observed in cells that express low levels of CypD [106, 107], and in tissues from CypD-KO mice [108]. However, this was not the case in *Lrpprc*$^{-/-}$ mice since total mitochondrial CypD content was two folds higher than in controls (Figure 3.11 E). Together, these data indicate that in *Lrpprc*$^{-/-}$ mitochondria the CV assembly defect leads to intrinsic resistance to pore opening, through a loss of regulation by CypD.

3.9. Hepatic LRPPRC deficiency induces pronounced changes in mitochondrial H_2O_2 dynamics

An important factor believed to underlie cellular dysfunction in genetic mitochondrial diseases is enhanced production of mitochondrial ROS, which can disrupt normal ROS-dependent cellular signal transduction, and trigger oxidative damage to cellular components [109, 110]. To address whether LRPPRC deficiency had an impact on mitochondrial ROS dynamics, net mitochondrial H_2O_2 release was measured in respiring mitochondria. Strikingly, mitochondria from *Lrpprc*$^{-/-}$ mice released tenfold less H_2O_2 compared to controls in conditions where superoxide production is promoted through reverse electron flow (*i.e.* during state 2 respiration with succinate ± glutamate/malate) (Figure 3.12 A). To investigate factors underlying this striking difference, mitochondrial membrane potential, which is an important determinant of superoxide production, was measured. As shown in Figure 3.12 B, membrane potential was reduced by 2–3 mV in *Lrpprc*−/−, which can account for no more than ∼7% of the difference in H_2O_2 release observed vs wild type [111, 112].

To determine whether enhanced ROS scavenging was responsible for the dramatic reduction of mitochondrial H_2O_2 release in *Lrpprc*$^{-/-}$ mice, the capacity to scavenge a pulse of exogenous H_2O_2 was also measured directly in respiring mitochondria. This scavenging rate represents the sum of the rate of all mitochondrial H_2O_2 consuming systems. Surprisingly, mitochondria from *Lrpprc*$^{-/-}$ mice were completely unable to scavenge exogenous H_2O_2 (Figure 3.12 C). The level of key antioxidant enzymes was therefore measured. The expression of SOD2 was similar in the two groups, while the levels of catalase were modestly reduced, suggesting no major collapse of the antioxidant machinery (Figure 3.12 D). This observation was overall compatible with the results of the H_2O_2 release experiment, since a collapse of antioxidant systems would have caused an increase in H_2O_2 release, not a drastic reduction as observed.

Together, the lack of endogenous H_2O_2 emission and exogenous H_2O_2 scavenging pointed to a major barrier hindering H_2O_2 diffusion in and out of mitochondria in *Lrpprc* deficient mice.

To address this possibility, respiring mitochondria were titrated with increasing concentration of digitonin (0.01 to 0.03%) to achieve progressive membrane permeabilization. As shown in Figure 3.12 E, addition of digitonin to *Lrpprc*$^{-/-}$ mitochondria progressively raised the amount of H_2O_2 released in the media to the level observed in non-permeabilized mitochondria from control mice, suggesting trapping of H_2O_2 in mitochondria from *Lrpprc*$^{-/-}$ mice. To test this hypothesis, H_2O_2 production was measured in inside-out sub-mitochondrial particles, where respiratory chain complexes generate H_2O_2 directly in the incubation medium, bypassing the normal diffusion step across the lipid bilayer. In this condition, H_2O_2 release was actually higher in *Lrpprc*$^{-/-}$ compared to control (Figure 3.12 F), confirming that LRPPRC deficiency induced a strong reduction of mitochondrial permeability to H_2O_2.

To investigate the underlying mechanism, the expression of aquaporin-8 channels, which are known to facilitate the diffusional transport of H_2O_2 across the inner mitochondrial membrane [113, 118] was measured. AQP-8 content was 35% higher in *Lrpprc*−/− mice, indicating that changes in AQP8 expression were not responsible for the altered H_2O_2 diffusion (Figure 3.12 G). Non-targeted lipidomic analysis was also performed to examine potential changes in the membrane lipid composition. In *Lrpprc*$^{-/-}$ mitochondria, 65 features reached the established significance threshold (FC > 2 and FDR < 5%, corresponding to a p value of 0.01) (Figure 3.13 A). From these features, thirty-three distinct lipids were identified in *Lrpprc*$^{-/-}$ mitochondria of which 14 were upregulated and 18 downregulated. Interestingly, increased lipids were essentially glycerophospholipids mostly represented by phosphatidylcholines (PC) and few phosphatidylethanolamine (PE), while decreased lipid species were more diversified. The latter included in particular 7 triglycerides, 2 diglycerides, 6 sphingomyelins, as well as cholesterol and

cholesterol sulfate (Figure 3.13 B). Together, these results indicated that loss of LRPPRC triggers broad changes in the lipid composition of mitochondrial membranes, which likely underlie the impairment of H_2O_2 diffusion in and out of mitochondria.

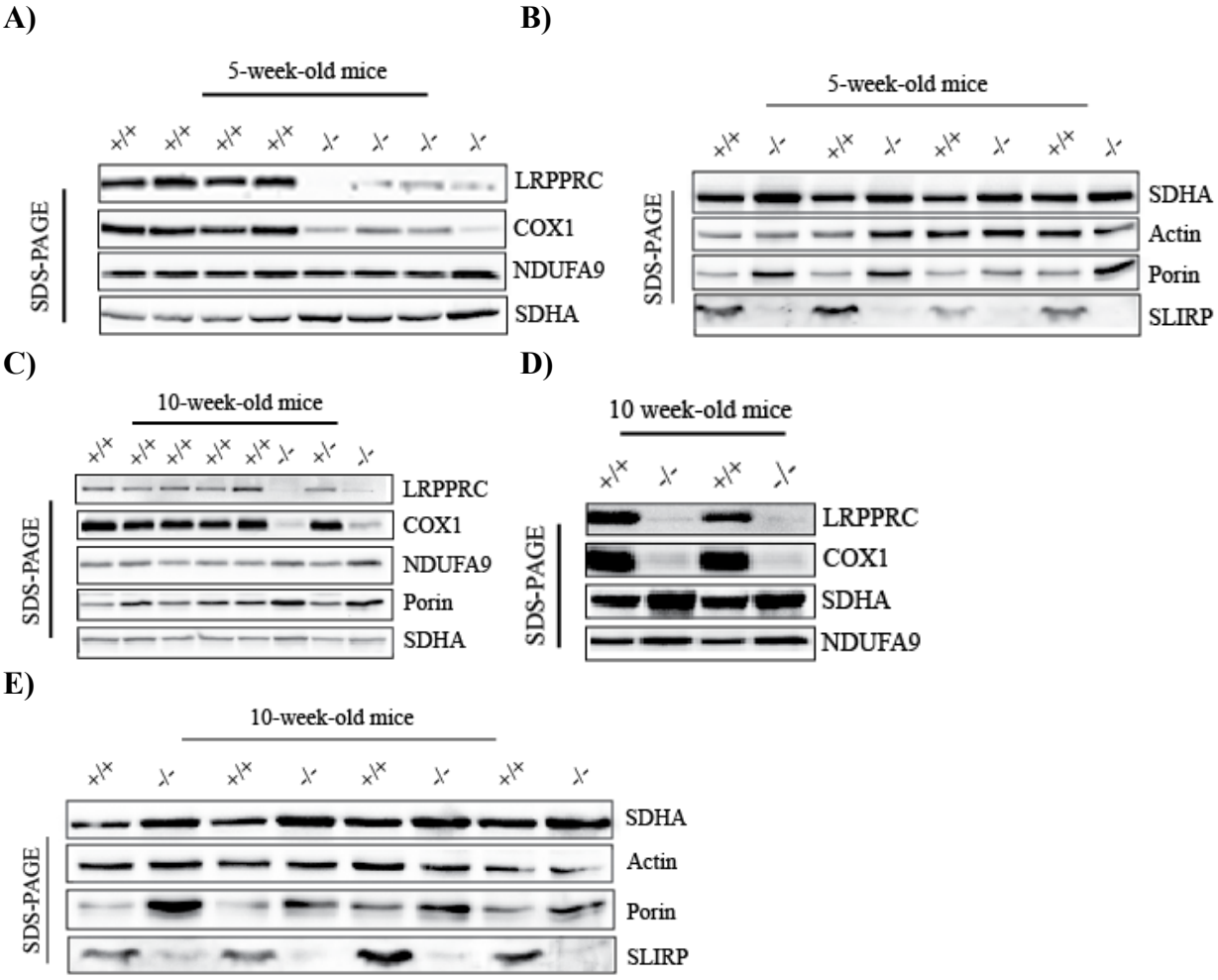
A)
5-week-old mice
+/+ +/+ +/+ +/+ -/- -/- -/- -/-
SDS-PAGE
LRPPRC
COX1
NDUFA9
SDHA
B)
5-week-old mice
+/+ -/- +/+ -/- +/+ -/- +/+ -/-
SDS-PAGE
SDHA
Actin
Porin
SLIRP
C)
10-week-old mice
+/+ +/+ +/+ +/+ +/+ -/- -/- -/-
SDS-PAGE
LRPPRC
COX1
NDUFA9
Porin
SDHA
D)
10 week-old mice
+/+ -/- +/+ -/-
SDS-PAGE
LRPPRC
COX1
SDHA
NDUFA9
E)
10-week-old mice
+/+ -/- +/+ -/- +/+ -/- +/+ -/-
SDS-PAGE
SDHA
Actin
Porin
SLIRP

Figure 3.1. **Decreased levels of LRPPRC, COX1, and SLIRP in liver-specific LRPPRC knock-out mice.** Mitochondria was isolated from the liver tissue of wild-type (+/+) and liver specific LRPPRC knock-out mice (-/-) at 5 and 10 weeks of age and was run in 10% polyacrylamide gel (Panels A, B, C, D, and E). The blots were incubated with the antibodies against the proteins indicated at the right side of the picture. The 70-KDa subunit of complex II, Porin and Actin were used as a loading control.

A)

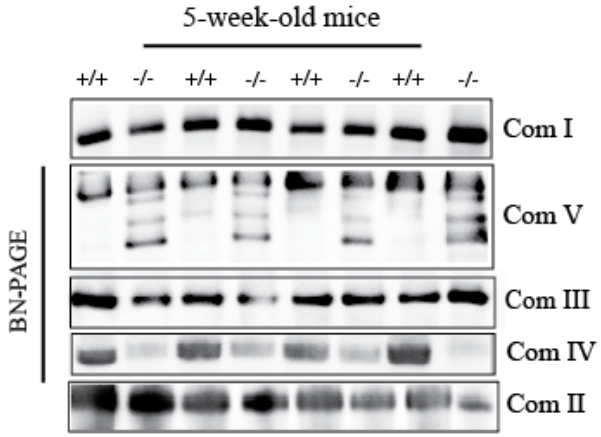
5-week-old mice
+/+ -/- +/+ -/- +/+ -/- +/+ -/-
Com I
Com V
Com III
Com IV
Com II
BN-PAGE

B)

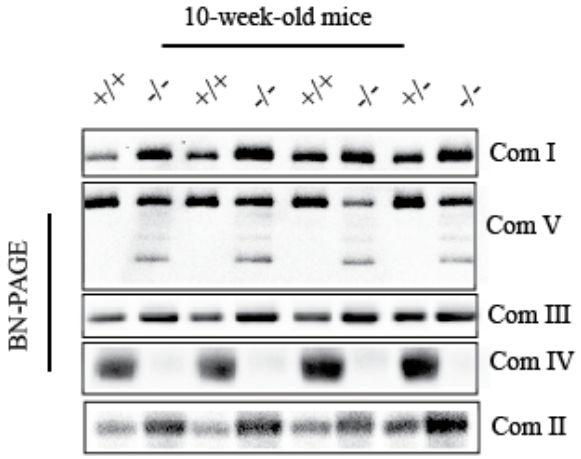
10-week-old mice
Com I
Com V
Com III
Com IV
Com II
BN-PAGE

Figure 3.2. **OXPHOS deficiency in liver-specific LRPPRC knock-out mice resembles to that of LSFC patient.** BN-PAGE analysis of the assembled OXPHOS complexes in liver mitochondria was performed using wild-type (+/+) and LRPPRC knock-out (-/-) mice at 5 and 10 weeks of age (panel A and B). Each of the five OXPHOS complexes (Com I-V) was visualized with a subunit specific antibody.

A)

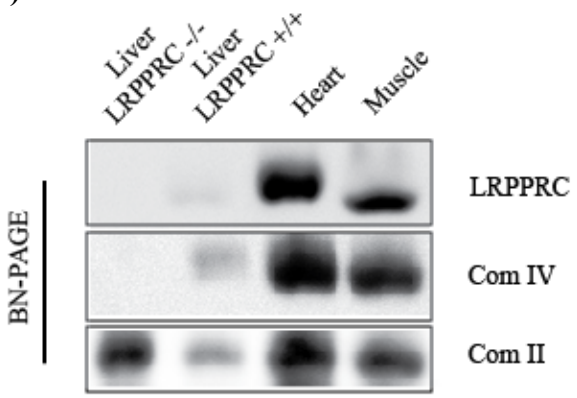
Liver LRPPRC -/-
Liver LRPPRC +/+
Heart
Muscle
BN-PAGE
LRPPRC
Com IV
Com II

B)

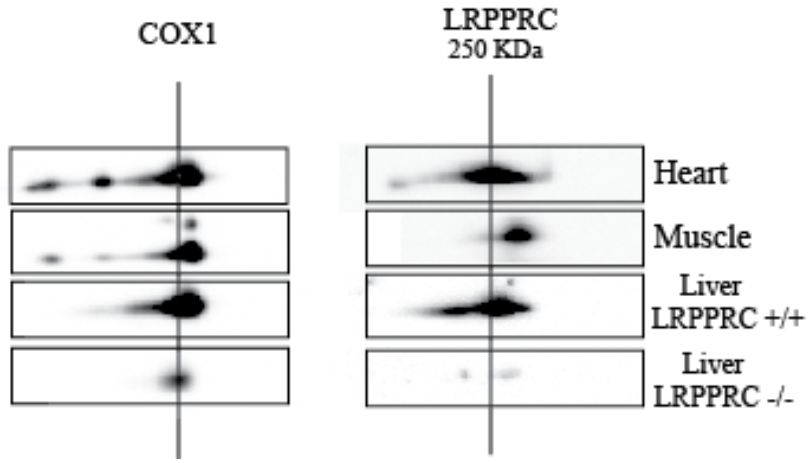
COX1
LRPPRC
250 KDa
Heart
Muscle
Liver LRPPRC +/+
Liver LRPPRC -/-

Figure 3.3. LRPPRC complex migrates differently in mouse tissues. Panel A shows First dimension BN-PAGE analysis of the LRPPRC–SLIRP complex with antibodies against LRPPRC, complexes II and IV (COX), in skeletal muscle, heart, and liver isolated from control (+/+) and liver specific LRPPRC knock-out (-/-) mice. Panel B shows Extracts from control tissues and cells were run in the first dimension on a non-denaturing, blue native gel (BN-PAGE), after which individual lanes were cut out and run on the second dimension on a denaturing gel (SDS-PAGE). Antibodies were then used to detect LRPPRC and SLIRP, as indicated.

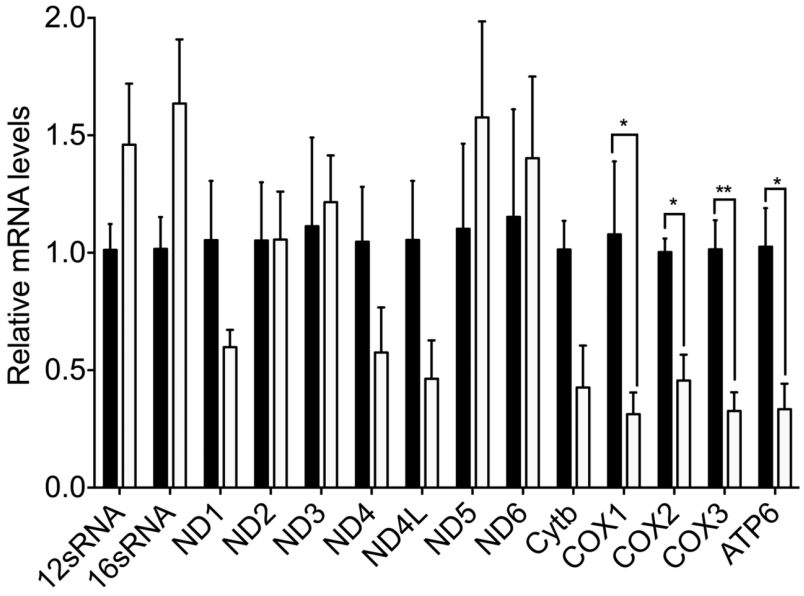
Relative mRNA levels
2.0
1.5
1.0
0.5
0.0
*
*
**
*
12sRNA
16sRNA
ND1
ND2
ND3
ND4
ND4L
ND5
ND6
Cytb
COX1
COX2
COX3
ATP6

Figure 3.4. LRPPRC deficiency decreases the steady-state levels of a subset of mitochondrial mRNAs. Expression of mitochondrial ribosomal subunits, and of selected mitochondrial and nuclear encoded transcripts in wild-type (+/+) and knock-out (-/-) mice. Data were obtained at 10 weeks of age ($n = 3–5$). The Y and X axes show relative mRNA levels and the name of mt RNAs, respectively. Black and white bars represent wild-type and knock-out mouse, respectively.

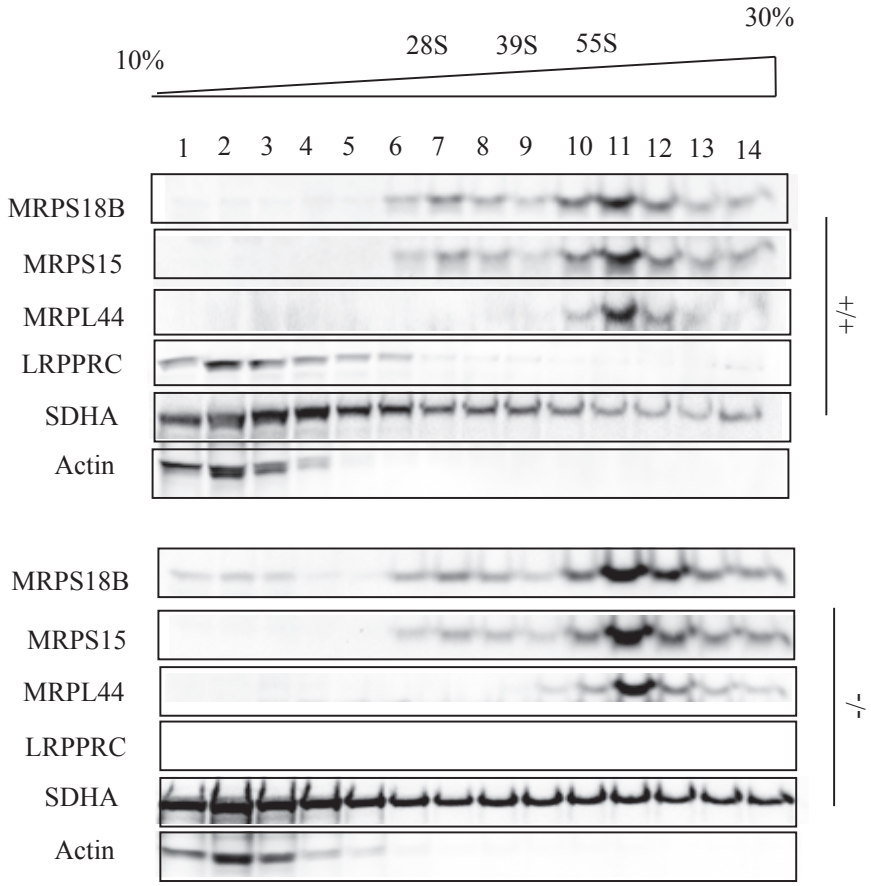
10%
30%
28S
39S
55S
1 2 3 4 5 6 7 8 9 10 11 12 13 14
MRPS18B
MRPS15
MRPL44
LRPPRC
SDHA
Actin
+/+
MRPS18B
MRPS15
MRPL44
LRPPRC
SDHA
Actin
-/-

Figure 3.5. Analysis of ribosome assembly in LRPPRC knock-out liver. Cleared mitochondrial lysates from wild-type (+/+) in top panel and liver specific LRPPRC knock-out (-/-) mice in bottom panel were loaded on a discontinuous sucrose gradient (10-30%) and centrifuged, after which fractions were collected for immunoblot analysis with antibodies against subunits of the large (MRPL44) and small (MRPS15 and 18B) mitochondrial ribosomal subunits. The approximate migration of the small (28S) and of the large (39S) mitochondrial ribosomal subunits and the monosome (55S) are indicated for reference.

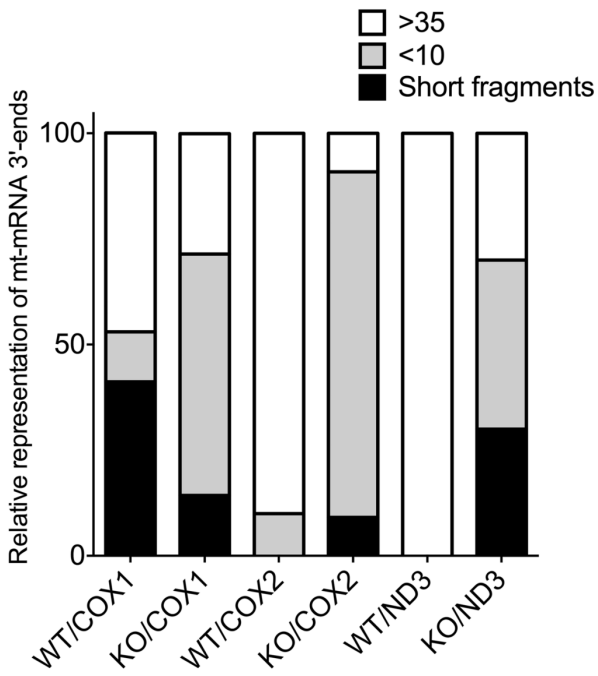
>35
<10
Short fragments
Relative representation of mt-mRNA 3'-ends
100
50
0
WT/COX1
KO/COX1
WT/COX2
KO/COX2
WT/ND3
KO/ND3

Figure 3.6. The length of a subset of mt-mRNA poly A tail is decreased in liver-specific Lrpprc knock-out mice. The Y and X-axes show the relative representation of mt-mRNAs 3′ ends and COX1, COX2, and ND3 mRNAs, respectively. White bars, grey bars, black bars indicate poly, oligo, and nonadenylated mRNAs, respectively. The data were obtained at 10 weeks of age with 3 experimental replicates per group using pooled RNA from 3 WT (wild-type) and 3 KO (knock-out) mice.

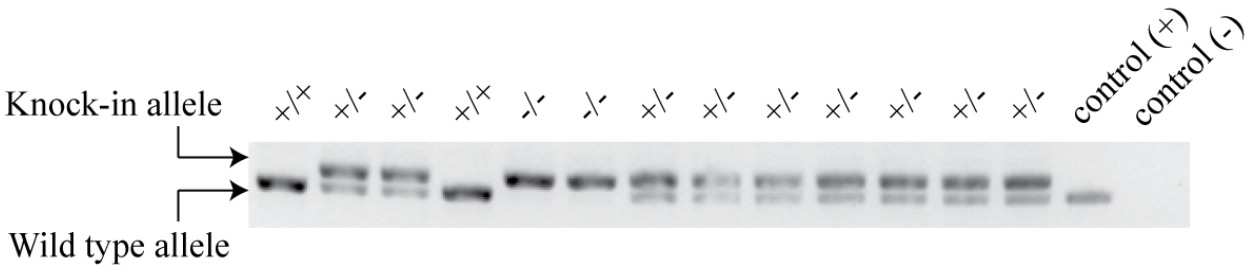
Knock-in allele
Wild type allele
+/+
+/-
+/-
+/+
-/-
-/-
+/-
+/-
+/-
+/-
+/-
+/-
+/-
control (+)
control (-)

Figure 3.7. LRPPRC mutation (p. A354V) leads to lethality in embryonic mouse. The DNA of 70 samples (including embryos, babies, and adult mice) was isolated, and 13 samples from developed embryos were run on 1% agarose gel as shown. The arrowheads show wild-type and knock in allele. +/+, +/-, and -/- indicate wild-type, heterozygous, and homozygous mice, respectively. The two embryos carrying a homozygous knock-in allele were removed from the womb at 9 and 10 days of development.

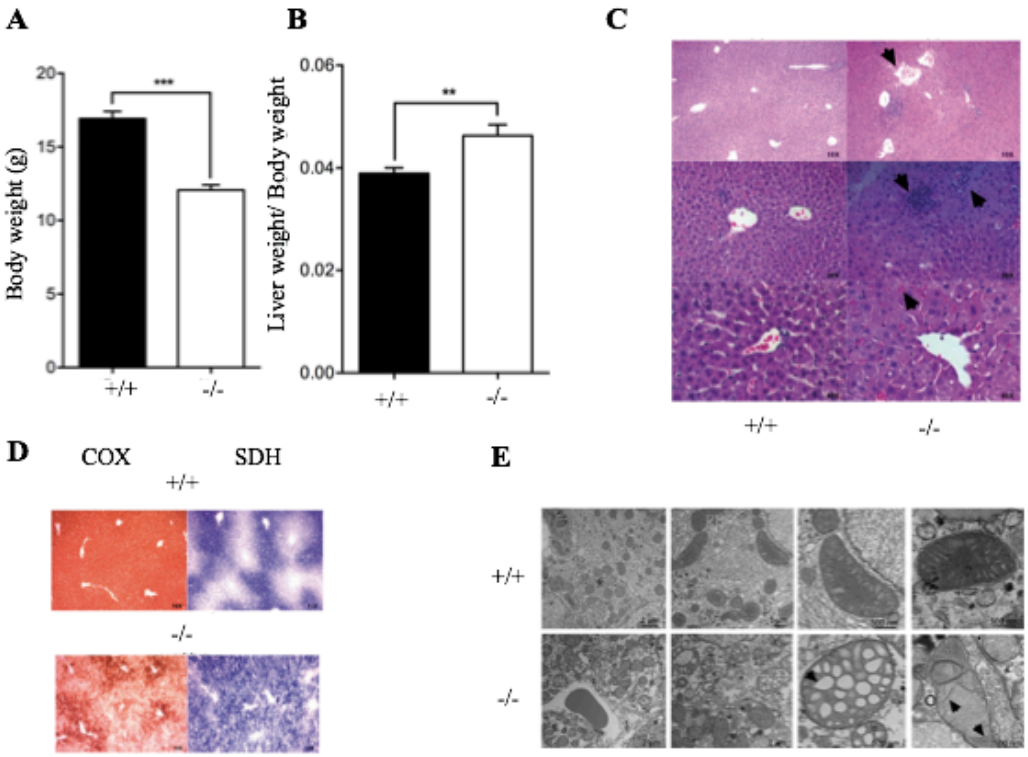
A
B
C
Body weight (g)
20
15
10
5
0
***
+/+
-/-
Liver weight/ Body weight
0.06
0.04
0.02
0.00
**
+/+
-/-
+/+
-/-
D
COX
SDH
+/+
-/-
E
+/+
-/-

Figure 3.8. General phenotype and liver histology in normal and liver-specific LRPPRC deficient mice. Panels A and B show mean body weight (n = 30), and ratio of liver to body weight (n = 16–17) in +/+ and −/− mice. Panel C shows representative images of H&E staining. Loss of lobular structure and dilated vessels (top), focal necrosis and infiltration of inflammatory cells (middle), and cholestasis (bottom) are visible in the −/− samples (arrows). Panel D shows representative images of serial liver sections stained for COX (brown staining) and SDH (blue staining) activity. Panel E shows transmission electron micrographs from both mouse strains. Arrows point to large vacuolar structures and stacked cristae, which were commonly observed in −/− mitochondria. Difference between +/+ and −/− was assessed with a Student t-test: **P < 0.01; ***P < 0.001.

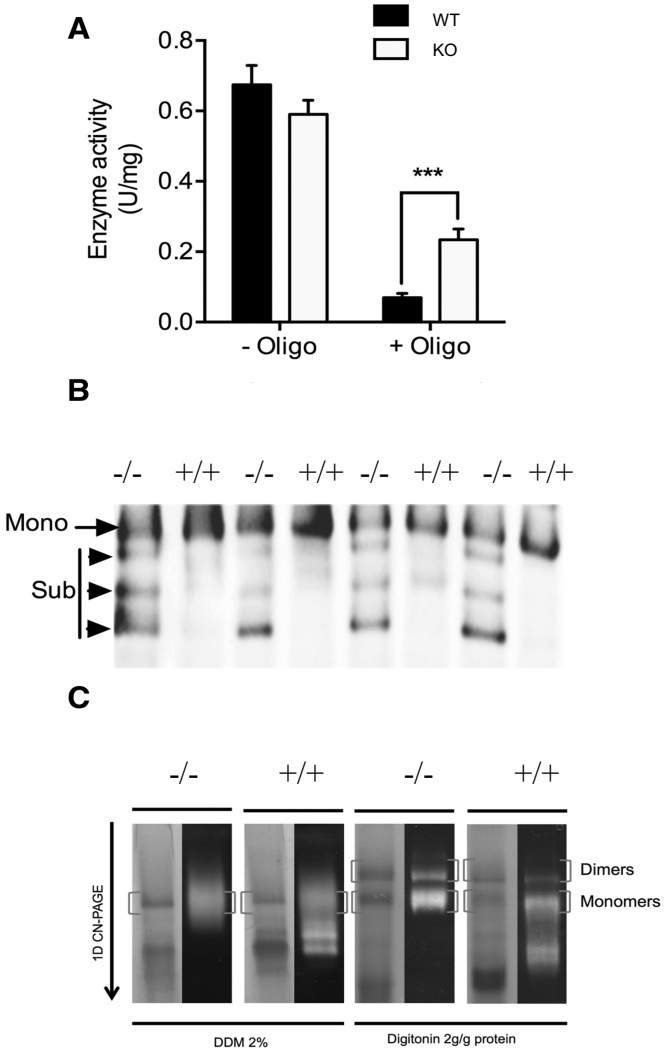
A
WT
KO
Enzyme activity (U/mg)
0.8
0.6
0.4
0.2
0.0
***
- Oligo
+ Oligo
B
-/- +/+ -/- +/+ -/- +/+ -/- +/+
Mono
Sub
C
-/- +/+ -/- +/+
1D CN-PAGE
Dimers
Monomers
DDM 2%
Digitonin 2g/g protein

Figure 3.9. Impact of LRPPRC deficiency on ATP synthase (CV) activity and assembly. Panel A: Enzyme activity measured spectrophotometrically in mitochondrial extracts in the absence and presence of the CV inhibitor Oligomycin (1.2 μM). Data are expressed as fold changes vs wild type values (n = 6–8). Panel B: BN-PAGE blot of DDM-solubilized mitochondria from wild-type and knock-out mice. Membranes were probed with anti-ATPα Mono: CV monomers, Sub: Sub-assembled CV complexes. Panel C: Supramolecular assembly of CV revealed by in gel activity measurement. CN-PAGE was performed in duplicates for each sample. The first gel was used for in gel activity measurements (right lanes for each sample), while the other gel was stained with coomassie blue. Experiments were performed following extraction with DDM, which fully dissociates CV into monomers or with digitonin to preserve dimeric, and oligomeric CV complexes. Blots are representative of at least 3 independent experiments. Significantly different from the knock-out group: $^{**}P < 0.01$.

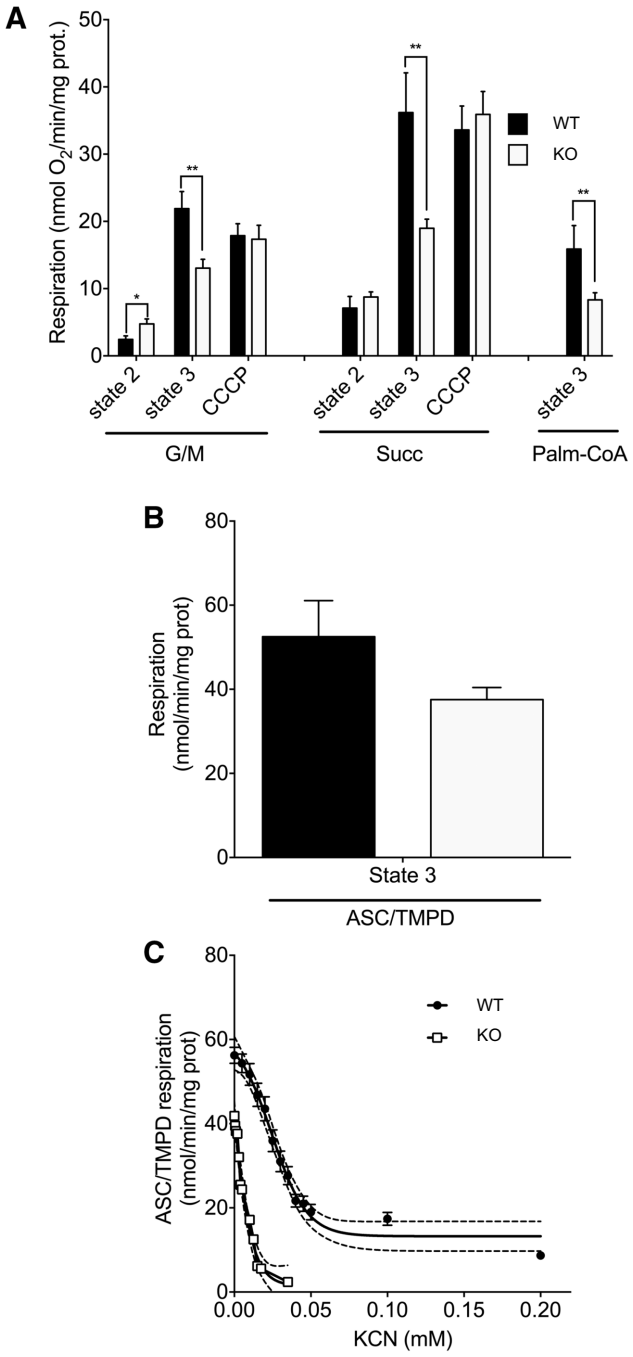
A
Respiration (nmol O2/min/mg prot.)
50
40
30
20
10
0
WT
KO
*
**
**
**
state 2
state 3
CCCP
state 2
state 3
CCCP
state 3
G/M
Succ
Palm-CoA
B
Respiration (nmol/min/mg prot)
80
60
40
20
0
State 3
ASC/TMPD
C
ASC/TMPD respiration (nmol/min/mg prot)
80
60
40
20
0
WT
KO
0.00
0.05
0.10
0.15
0.20
KCN (mM)

Figure 3.10. Impact of LRPPRC deficiency on the mitochondrial bioenergetics phenotype. Panel A: Baseline state 2, state 3 (1 mM ADP), and CCCP (0.03 μM)-uncoupled respiration in liver mitochondria energized with CI (glutamate/malate [GM: 5/2.5 mM]), CII (Succinate 5 mM) substrates, or following stimulation of long-chain fatty acid oxidation (palmitoyl-CoA [20 μM]) (n = 5–9). Panel B: Maximal state 3 respiration in isolated liver mitochondria energized with CIV substrates (ascorbate/TMPD: 9mM/0.9mM) (n = 5). Panel C: Titration of CIV-driven (Ascorbate/TMPD 9/0.9 mM) state 3 respiration with potassium cyanide (KCN) in wild-type (WT) and knock-out (KO) mitochondria. Best fit and 95% confidence intervals are shown for each dataset (n = 5).

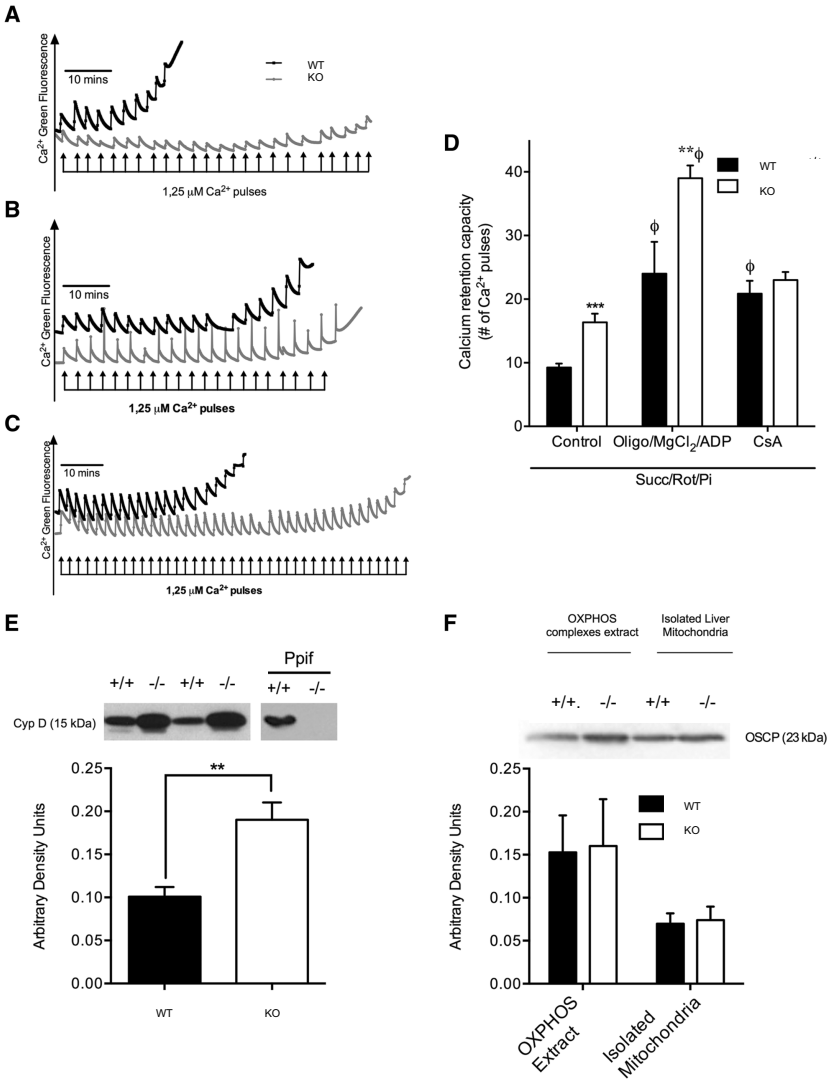
A
10 mins
WT
KO
Ca2+ Green Fluorescence
1,25 μM Ca2+ pulses
B
10 mins
Ca2+ Green Fluorescence
1,25 μM Ca2+ pulses
C
10 mins
Ca2+ Green Fluorescence
1,25 μM Ca2+ pulses
D
Calcium retention capacity
(# of Ca2+ pulses)
WT
KO
Control
Oligo/MgCl2/ADP
CsA
Succ/Rot/Pi
E
Ppif
+/+ -/- +/+ -/-
+/+ -/-
Cyp D (15 kDa)
Arbitrary Density Units
WT
KO
F
OXPHOS complexes extract
Isolated Liver Mitochondria
+/+ -/- +/+ -/-
OSCP (23 kDa)
Arbitrary Density Units
WT
KO
OXPHOS Extract
Isolated Mitochondria

Figure 3.11. Impact of LRPPRC deficiency on the permeability transition pore

Panel A-C: Representative tracings of mitochondrial calcium retention capacity (CRC) in isolated liver mitochondria exposed to consecutive pulses of calcium (2.5 μmole/mg protein per pulse). All experiments were performed in the presence of Succinate (5 mM), Rotenone (1 μM) and Pi (10 mM). In panel B and C, the incubation buffer was respectively supplemented with Cyclosporin-A (1μM), or a combination of ADP (12 μM), $MgCl_2$ (0.6 mM) and Oligomycin (27 μM). Panel D: Average Calcium Retention Capacity observed in the three experimental conditions described in A-C (n = 8–11). Panel E: Immunoblot and densitometric analysis of Cyclophilin-D (CypD) content in isolated liver mitochondria from wild-type (+/+) and knock-out (-/-) mitochondria. Mitochondrial lysates from wild-type (+/+) and CypD deficient Ppif (-/-) mice were run as controls (n = 6). Panel F: Immunoblot and densitometric analysis of OSCP content in whole mitochondrial lysates and OXPHOS extracts obtained following digitonin treatment. Significantly different from wild type mice: **$P < 0.01$, ***$P < 0.001$; Significantly different from control condition: Φ: $P < 0.001$.

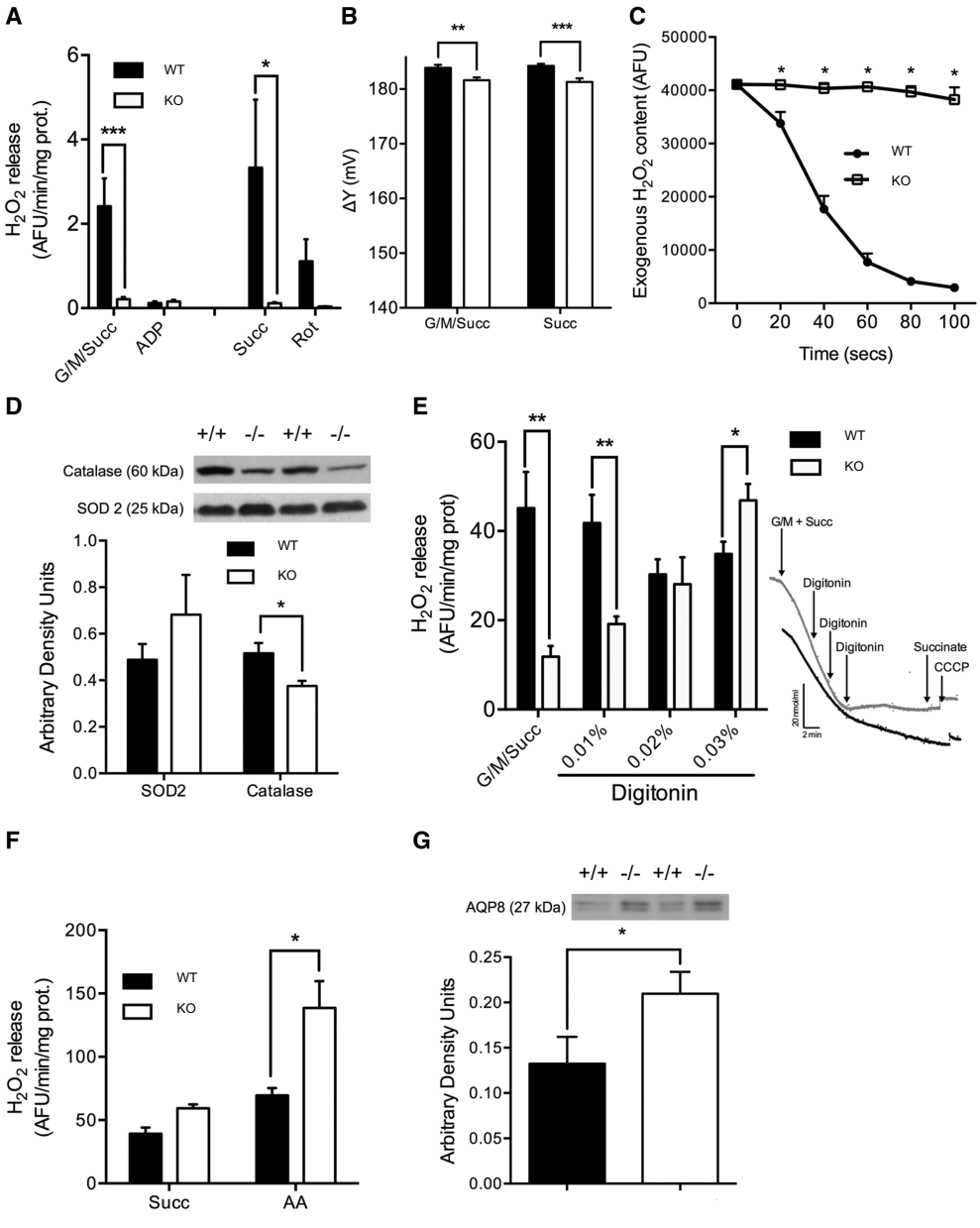
A
B
C
D
E
F
G
WT
KO
H_2O_2 release (AFU/min/mg prot.)
G/M/Succ
ADP
Succ
Rot
ΔY (mV)
Exogenous H_2O_2 content (AFU)
Time (secs)
+/+ -/- +/+ -/-
Catalase (60 kDa)
SOD 2 (25 kDa)
Arbitrary Density Units
SOD2
Catalase
H_2O_2 release (AFU/min/mg prot)
0.01%
0.02%
0.03%
Digitonin
G/M + Succ
Succinate
CCCP
20 nmol/ml
2 min
AA
AQP8 (27 kDa)

Figure 3.12. Impact of LRPPRC deficiency on mitochondrial dynamics: Panel A: Net H_2O_2 release from mitochondria under state 2 and state 3 (1 mM ADP) conditions in the presence of substrates for CI + CII (G/M/Succ: 5/2.5/5 mM) (n = 8–16). In some experiments (n = 3), net H_2O_2 release was measured in the presence of succinate alone (Succ: 5 mM) and rotenone (1 μM) was added to confirm that H_2O_2 release occurred mainly through reverse electron back flow to CI. Panel B: Mitochondrial membrane potential measured on respiring isolated liver mitochondria energized with complex I + II (G/M/Succ: 5/2.5/5 mM) or complex II (succinate 5mM) substrates. (n = 6). Panel C: Immunoblot and densitometric analysis of SOD2 and catalase content in mitochondria from wild type and knock-out mice (n = 6). Panel D: Kinetics of scavenging of an exogenous H_2O_2 load (3 nmoles) by mitochondria energized with CI substrates (Gutamate/Malate: 50/20 μM) (n = 6). Panel E: Net H_2O_2 release from mitochondria under state 2 conditions in the presence of substrates for CI + CII (G/M/Succ: 5/2.5/5 mM). Following baseline measurements, digitonin was progressively added and changes in H_2O_2 release were monitored (n = 6). Insets in panel E shows progressive inhibition of respiration in +/+ (black tracing), −/− (grey tracing) in response to progressive permeabilization with digitonin. Panel F: H_2O_2 production measured in sub-mitochondrial particles (SMP) in the presence of succinate (5 mM) alone, or with Antimycin-A (AA: 2 μM) (n = 4). Panel G: Immunoblot and densitometric analysis of AQP8 content in mitochondria from wild type and knock-out mitochondria (n = 6). Significantly different from wild type mice: *P < 0.05, **P < 0.01, ***P < 0.001.

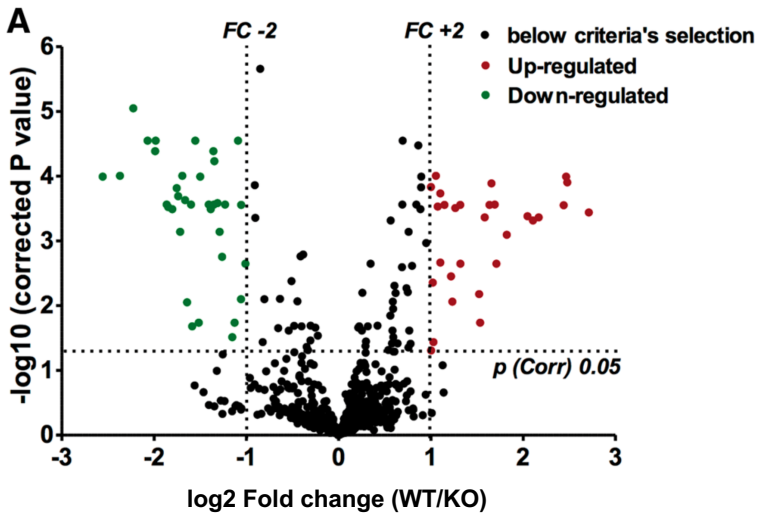
A
FC -2
FC +2
below criteria's selection
Up-regulated
Down-regulated
-log10 (corrected P value)
p (Corr) 0.05
log2 Fold change (WT/KO)

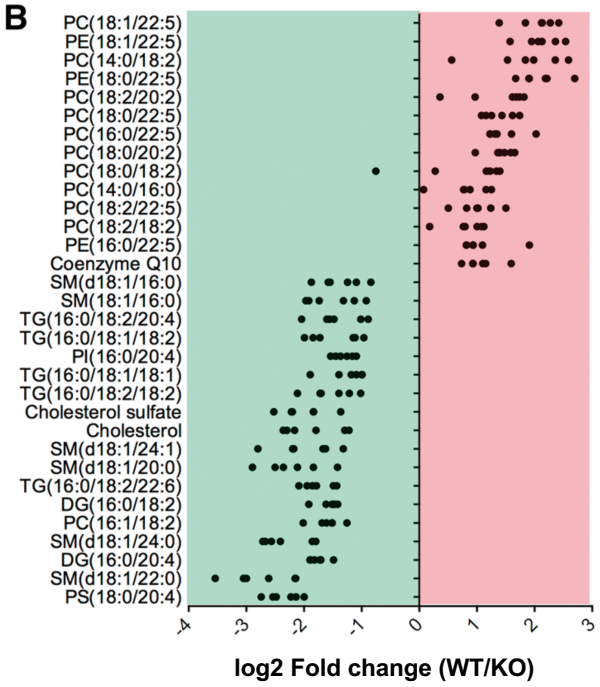
B
PC(18:1/22:5)
PE(18:1/22:5)
PC(14:0/18:2)
PE(18:0/22:5)
PC(18:2/20:2)
PC(18:0/22:5)
PC(16:0/22:5)
PC(18:0/20:2)
PC(18:0/18:2)
PC(14:0/16:0)
PC(18:2/22:5)
PC(18:2/18:2)
PE(16:0/22:5)
Coenzyme Q10
SM(d18:1/16:0)
SM(18:1/16:0)
TG(16:0/18:2/20:4)
TG(16:0/18:1/18:2)
PI(16:0/20:4)
TG(16:0/18:1/18:1)
TG(16:0/18:2/18:2)
Cholesterol sulfate
Cholesterol
SM(d18:1/24:1)
SM(d18:1/20:0)
TG(16:0/18:2/22:6)
DG(16:0/18:2)
PC(16:1/18:2)
SM(d18:1/24:0)
DG(16:0/20:4)
SM(d18:1/22:0)
PS(18:0/20:4)
log2 Fold change (WT/KO)

Figure 3.13. Impact of LRPPRC deficiency on mitochondrial membrane lipid composition. Panel A: Volcano plot showing entities that were identified as differentially expressed, either up or downregulated, in knock-out mitochondria according to the following selection criteria: fold change > 2 and corrected p value < 0.05. Panel B: Individual lipid species found to be significantly up or down-regulated on knock-out mitochondria. Each dot represents a Log2-transformed ratio of an individual knock-out mitochondria relative to the mean value obtained in the wild-type group (n = 6 per group).

Chapter 4 characterization of LSFC tissues using the MPAT assay

4.1. Enrichment of oligo- and non-adenylated mt-mRNAs in LSFC tissues

Polyadenylation of newly synthesized transcripts in different organelles and organisms has been studied [119]. In eukaryotic cytosol, polyadenylation stabilizes mRNA transcripts, but in bacteria, archea, chloroplasts and plant mitochondria this phenomenon is a signal for mRNA degradation [119, 120, 121]. In mammalian mitochondria, the exact role of polyadenylation is still unclear, but it has been shown that LRPPRC is involved in polyadenylation of most mt-mRNAs [75]. In this chapter, I investigated the polyadenylation profile of three mt-mRNAs for COX1, COX2, and ND3 in tissues from an LSFC subject carrying a missense mutation in LRPPRC (A354V LRPPRC). Analysis of liver tissue of conditional LRPPRC knock-out mice suggest that the steady-state levels of some mt-mRNAs including COX1 and COX2 are reduced while the levels of other mt-mRNAs such as ND3 remain unchanged. COX1, COX2, and ND3 mRNAs are therefore selected for further investigations at the post transcriptional levels.

For all three mRNAs, a non-homogeneous PCR pattern was observed after performing MPAT assay in different human tissues (Figure 4.1 A, 4.2 A, and 4.3 A). For example, all COX1 and COX2 transcripts were found to be poly adenylated (>40 As) in skeletal muscles, while in heart and liver the tail length of poly A varied from 0 to >40 As (Figure 4.1 and 4.2 B). The results were slightly different for ND3, for example, about 75% of the transcripts were polyadenylated (>40 As) in skeletal muscle, 80% were oligo-adenylated (10-40 As) in liver, and <50% were non- or polyadenylated in heart (Figure 4.3 B). In our experiments, we also found a remarkable percentage of transcripts lacking a stop codon with short and variable chain length (short fragments) that did not seem to correlate with the loss of LRPPRC in LSFC subject tissues.

Interestingly, analysis of the COX1 and COX2 3′ends in the tissues (skeletal muscle, heart, and liver) of the LSFC subject suggests a shift from poly adenylated transcripts towards oligo or non-adenylated ones, yet a small percentage (<40 %) remained polyadenylated (Figure 4.1 and 4.2 C). For ND3 mRNA, the majority of the transcripts were found oligo-adenylated in these tissues (Figure 4.3 C).

4.2. Lack of homogeneity in mitochondrial mRNAs features

Investigation of human mt-mRNAs in Hep G2 cells [120] showed that some features of mitochondrial mRNAs such as tail length of poly A, presence of 3′ or 5′ untranslated regions, and the number of A′s required to add the stop codon differ from one mRNA to another. Similarly, in our experiments where we investigated the 3′-ends of mt-mRNAs isolated from liver, we observed a lack of homogeneity in their features. For example, except for ND6, all mitochondrial mRNAs contained a poly A tail of 27 to 68 A′s. In addition, most mt-mRNAs are not flanked by 3′ untranslated regions except COX1, COX2, ND5, and ND6 where the 3′ UTR corresponds to tRNAser, a 25 nucleotide non-coding sequence, and ND5/ND6 sequences, respectively (table 4.4).

A)

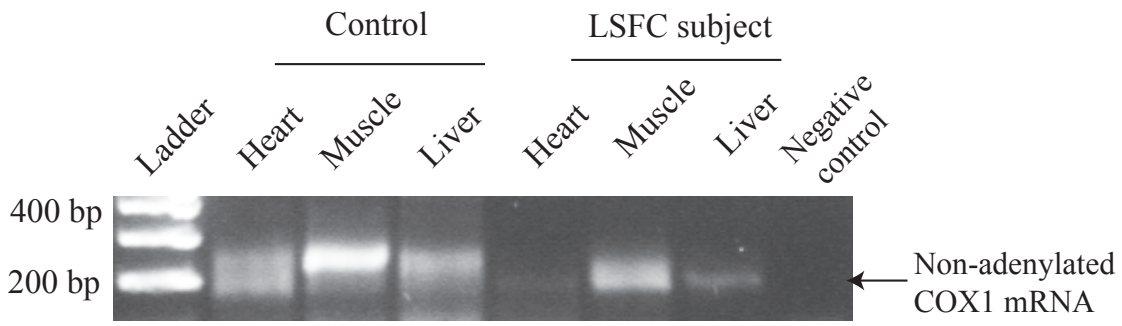
Control
LSFC subject
Ladder
Heart
Muscle
Liver
Heart
Muscle
Liver
Negative control
400 bp
200 bp
Non-adenylated COX1 mRNA

B)

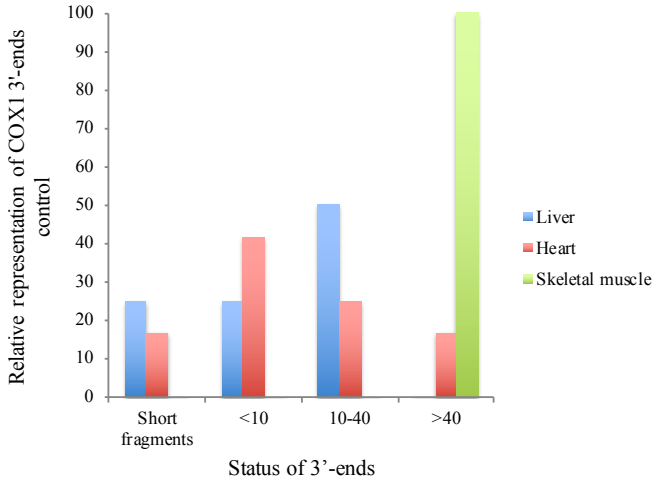
Relative representation of COX1 3'-ends control
100
90
80
70
60
50
40
30
20
10
0
Short fragments
<10
10-40
>40
Status of 3'-ends
Liver
Heart
Skeletal muscle

C)

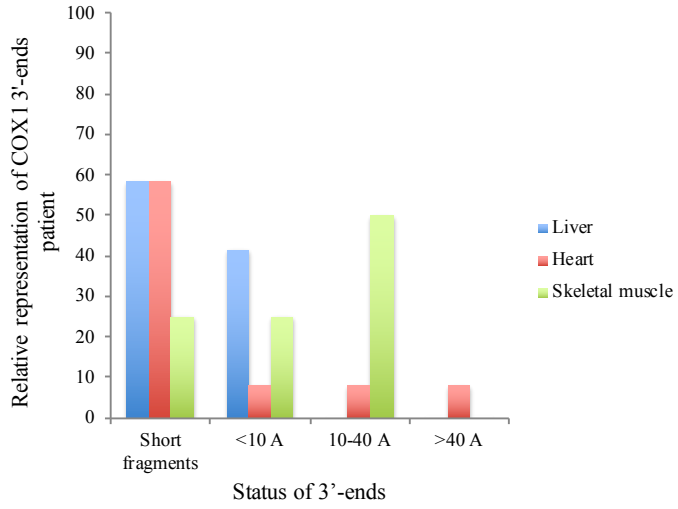
Relative representation of COX1 3'-ends patient
100
90
80
70
60
50
40
30
20
10
0
Short fragments
<10 A
10-40 A
>40 A
Status of 3'-ends
Liver
Heart
Skeletal muscle

Figure 4.1. The tail length of poly A for COX1 mRNA varies in tissues and is reduced in LSFC subject. Panel A shows MPAT assay for COX1 transcripts in several human tissues including liver, heart, and skeletal muscles of a control and of an LSFC subject, the arrowhead shows nonadenylated COX1 mRNAs. Panel B and C show the relative representation of poly (>40), olig (10-40), and nonadenylated (<10) COX1 mRNAs in tissues of a healthy individual and of an LSFC subject, respectively. Short fragments refer to COX1 transcripts terminated before the stop codon.

	Control			**LSFC subject**		
Tissues / **3′end**	Liver	Heart	Skeletal muscles	Liver	Heart	Skeletal muscles
Short fragments	3/12	2/12	0/12	7/12	7/10	3/12
<10	3/12	5/12	0/12	5/12	1/10	3/12
10-40	6/12	3/12	0/12	0/12	1/10	6/12
>40	0/12	2/12	12/12	0/12	1/10	0/12
3′UTR (71 nt)	7/12	8/12	12/12	4/12	2/10	5/12
3′UTR (63-71)	2/12	2/12	0/12	1/12	1/10	4/12

Table 4.1. Sequencing data representing the 3′end of COX1 mRNA. Table depicting the 3′UTR and the number of poly (>40), oligo (10-40), or nonadenylated (<10) COX1 mRNAs in control and LSFC subject tissues. Numbers are presented over the total number of sequenced clones.

A)

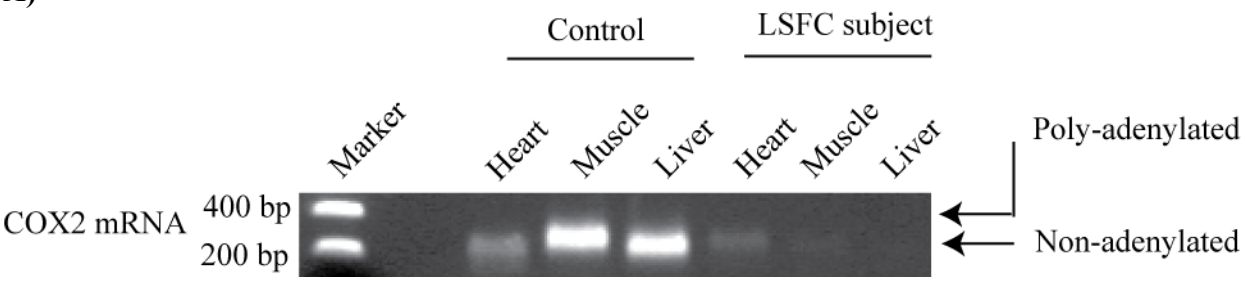
Control
LSFC subject
Marker
Heart
Muscle
Liver
Heart
Muscle
Liver
Poly-adenylated
COX2 mRNA
400 bp
200 bp
Non-adenylated

B)

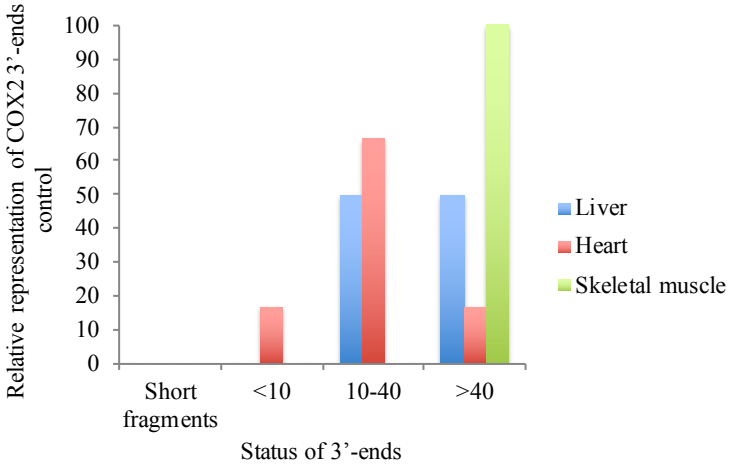
Relative representation of COX2 3'-ends control
100
90
80
70
60
50
40
30
20
10
0
Short fragments
<10
10-40
>40
Status of 3'-ends
Liver
Heart
Skeletal muscle

C)

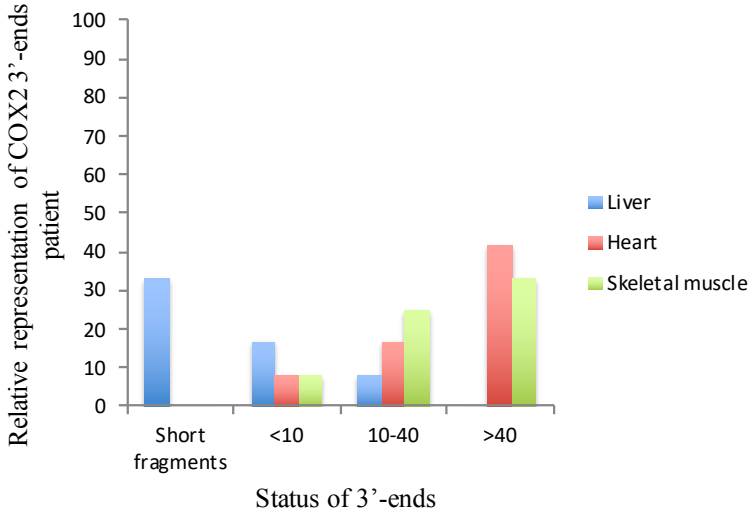
Relative representation of COX2 3'-ends patient
100
90
80
70
60
50
40
30
20
10
0
Short fragments
<10
10-40
>40
Status of 3'-ends
Liver
Heart
Skeletal muscle

Figure 4.2. The variability of the poly A tail length of COX2 mRNA in control tissues and enrichment of nonadenylated COX2 in LSFC subject. Panel A shows MPAT assay for COX2 transcripts in tissues including liver, heart, and skeletal muscles of a control and of an LSFC subject, the arrowhead indicates nonadenylated COX2 mRNAs. Panel B and C show the relative representation of poly (>40), oligo (10-40), and nonadenylated (<10) COX2 mRNAs in tissues of a control and of an LSFC subject, respectively. Short fragments refer to COX2 transcripts terminated before the stop codon.

	Control			**LSFC subject**		
Tissues / **3′end**	Liver	Heart	Skeletal muscles	Liver	Heart	Skeletal muscles
Short fragments	0/12	0/12	0/12	4/11	0/8	0/8
A(s) <10	0/12	2/12	0/12	6/11	1/8	1//8
A(s) 10-40	6/12	8/12	0/12	1/11	2/8	3/8
A(s) >40	6/12	2/12	12/12	0/11	5/8	4/8
3′UTR (25 nt)	12/12	12/12	12/12	2/11	7/8	7/8
3′UTR (0-25)	0/12	0/12	0/12	5/11	1/8	0/8

Table 4.2. Sequencing data representing the 3′end of COX2 mRNA. Table depicting the 3′UTR and the number of poly (>40), oligo (10-40), or nonadenylated (<10) COX2 mRNAs in control and LSFC subject tissues. Numbers are presented over the total number of sequenced clones.

A)

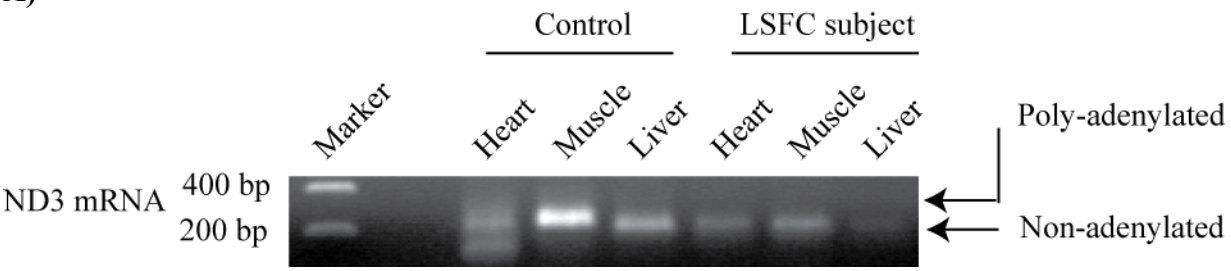
Control
LSFC subject
Marker
Heart
Muscle
Liver
Heart
Muscle
Liver
ND3 mRNA
400 bp
200 bp
Poly-adenylated
Non-adenylated

B)

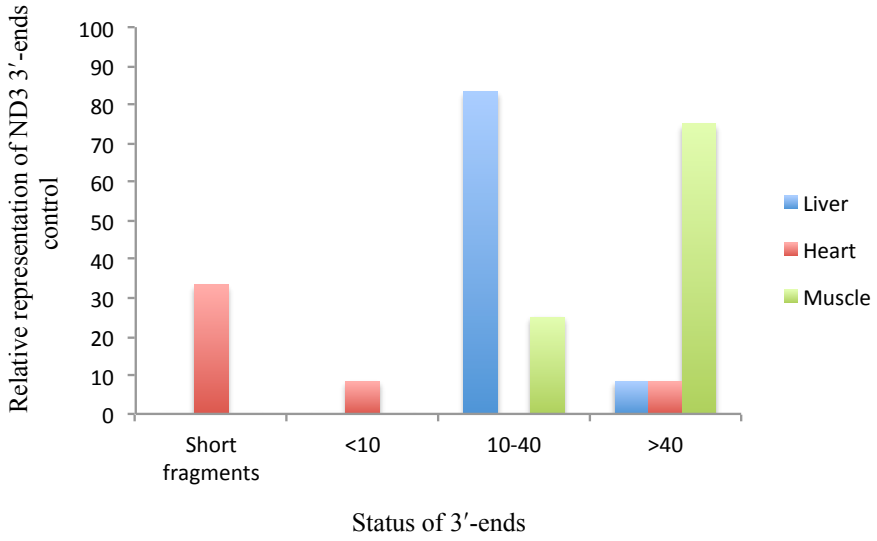
Relative representation of ND3 3′-ends control
100
90
80
70
60
50
40
30
20
10
0
Short fragments
<10
10-40
>40
Liver
Heart
Muscle
Status of 3′-ends

C)

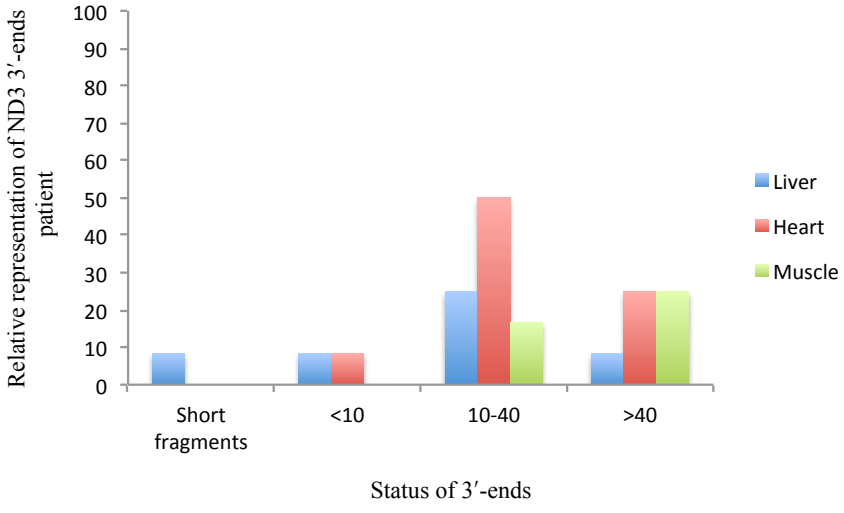
Relative representation of ND3 3′-ends patient
100
90
80
70
60
50
40
30
20
10
0
Short fragments
<10
10-40
>40
Liver
Heart
Muscle
Status of 3′-ends

Figure 4.3. ND3 mRNA polyadenylation profile in control and LSFC tissues differs from COX1 and COX2. Panel A shows MPAT assay for ND3 transcripts in a variety of tissues including liver, heart, and skeletal muscles of a control and of an LSFC subject, the arrowhead shows nonadenylated ND3 mRNAs. Panel B and C show the relative representation of poly (>40), oligo (10-40), and nonadenylated (<10) ND3 mRNAs in tissues of a healthy individual and of an LSFC subject, respectively. Short fragments refer to ND3 transcripts terminated before the stop codon

	Control			**LSFC subject**		
Tissues / **3′end**	Liver	Heart	Skeletal muscles	Liver	Heart	Skeletal muscles
Short fragments	0	4/6	0/12	1/6	0/10	0/5
A(s) <10	0	1/6	0/12	1/6	1/10	0/5
A(s) 10-40	10/11	0/6	3/12	3/6	6/10	2/5
A(s) >40	1/11	1/6	9/12	1/6	3/10	3/5
3′UTR	N/A	N/A	N/A	N/A	N/A	N/A

Table 4.3. Sequencing data representing the 3′end of ND3 mRNA. Table depicting the 3′UTR and the number of poly (>40), oligo (10-40), or nonadenylated (<10) ND3 mRNAs in control and LSFC subject tissues. Numbers are presented over the total number of sequenced clones.

mRNA	3' Trailer	Poly A tail length
COX1	63-71	35-62
COX2	25	30-68
COX3	0	33-45
ATP8/ATP6	0	39-53
CYTB	0	34-43
ND1	0	36
ND2	0	33
ND3	0	27-66
ND4L/ND4	0	37-49
ND5	300-362	40
ND6	630	0

Table 4. 4. Features of human mitochondrial mRNAs in liver. Generally, mitochondrial mRNAs isolated from human liver are polyadenylated (except ND6) and do not contain 3′ UTR except COX1, COX2, ND5, and ND6.

Chapter 5 Investigation of the pathogenesis of LRPPRC mutations using human cell lines

5.1. p. Y172C variant in LRPPRC results in combined deficiency of complexes IV and I in fibroblasts

Mutations in LRPPRC leads to complex IV defect in fibroblasts [69]. Here, we investigated fibroblasts from a male Finnish subject harbouring a missense mutation in LRPPRC that transforms amino acid tyrosine to cysteine at position 172. BN-PAGE analysis of isolated OXPHOS complexes revealed assembly defects of complex IV and to a milder extent complex I. All other OXPHOS complexes appeared to be normally assembled (Figure 5.1 B). Using denaturing SDS-PAGE, the steady-state levels of complex IV and I subunits were measured and a pronounced defect in COX1 and NDUFA9 levels was observed (Figure 5.1 A). To determine whether the rates of synthesis of the individual mtDNA-encoded COX and complex I subunits were altered, we pulse-labeled the mitochondrial translation products in subject fibroblasts. Remarkably, we found defects in the rate of synthesis of all the COX and ND subunits (Figure 5.1 C). The rates of synthesis of cytb, ATP6 and ATP8 were similar to control.

5.2. Expressing LRPPRC from retroviral vector fails to increase the expression of LRPPRC

Immunoblot analysis of mitochondrial extracts using polyclonal antibodies directed against LRPPRC showed that the steady-state levels of LRPPRC was low (about 20 %) in LSFC subjects compared to control (Figure 5.2 A). To investigate whether the lack of LRPPRC protein was responsible for the COX defect, wild-type, A354V, and Y172C LRPPRC was expressed in subject fibroblasts using a retroviral expression vector. In all cases, the steady-state levels of LRPPRC, SLIRP, and COX1 proteins were slightly increased or stayed unchanged (Figure 5.2 A-C). Moreover, using a different expression vector PLXSH (Figure 5.2 C) or different cell lines 143B and HEK293 cells (Figure 5.3 D), we failed to increase the expression levels of LRPPRC

in control and LSFC subject fibroblasts. As LRPPRC forms a stable complex with SLIRP, we asked as to whether we could increase the levels of LRPPRC or SLIRP proteins by co-expressing both in control and LSFC subject fibroblasts (Figure 5.3 A-C). To our surprise, the level of LRPPRC was increased 1.4 folds in control fibroblasts, but this level was not altered in an LSFC subject. The steady-state level of SLIRP protein was not increased in either control or subject (Figure 5.3 C). This led us to measure the levels of LRPPRC and SLIRP transcripts in co-expressing cell lines (control and LSFC subject). In fact, the RNA levels for both LRPPRC and SLIRP was increased about 3-fold in control, and only for SLIRP, the transcript level was increase about 4-fold in LSFC subject fibroblasts (Figure 5.3 B).

5.3. Comparing the interacting partners of wt- to A354V- and Y172C- LRPPRC in 293 cell lines

One of the preliminary experiments in BioID was to assure that the FLAG tagged protein was expressed. Therefore, two clones of 293 cells that were homogenously expressing wt, A354V, or Y172C LRPPRC-BirA-FLAG were harvested, and after extracting proteins, the steady-state levels of FLAG tagged proteins were monitored by anti-FLAG (Figure 5.4 A-B). Interestingly, the mutant proteins were expressed at low levels compared to wild-type LRPPRC. The same decrease was previously demonstrated in fibroblasts or tissues of LSFC subjects. Probing the membrane with a biotin antibody, also showed that the proximal proteins are biotinylated (Figure 5.4 B). Next, the same samples were loaded in an 8% SDS-PAGE gel and probed with LRPPRC antibody (Figure 5.5 A) to compare the expression level of FLAG tagged LRPPRC to the endogenous protein. Interestingly, the steady-state level of wt LRPPRC-BirA-FLAG was about 50% that of the endogenous protein. Thus, we decided to induce 239 cells with tetracycline more than 24 hours to increase the expression of FLAG tagged protein. However,

the protein was not expressed more than 50% of the endogenous even after 72 hours of tetracycline induction (Figure 5.5 B). It is important before carrying out the actual BioID experiment to confirm that the tagged protein is actually targeted to the correct cellular compartment, and this was verified by immunofluorescence using anti-FLAG. FLAG tagged LRPPRC, either wild-type or mutant, localized to mitochondria (Figure 5.4 C). There was a near perfect co-localization of wild-type FLAG tagged LRPPRC with endogenous protein, whereas the pathogenic LRPPRC (A354V or Y172C LRPPRC-BirA-FLAG) variants were mostly present in small foci.

5.4. BirA-FLAG LRPPRC (wt and mutant) is associated with the membrane

Sasarman *et al* [71], showed that about 50% of LRPPRC and SLIRP proteins are present in an insoluble fraction upon alkaline carbonate extraction of isolated mitochondria from HEK293 cells. This result prompted us to compare the solubility of wild-type to A354V and Y172C LRPPRC in 293 cells, and accordingly, we found the membrane association of both wild-type and mutant LRPPRC in 293 cells (Figure 5.6 A).

5.5. Y172C and A354V LRPPRC variants destabilize the protein

Our preliminary results (Figure 5.4 A) made us to further scrutinize the causality of the decrease in the steady-state levels of A354V and Y172C-LRPPRC-BirA-FLAG in 293 cells. We postulated that this reduction could be due to impaired protein synthesis or increased protein turnover because of the instability of the mutant protein. To address this, we measured the protein half-life using inducible 293 cells expressing wild-type, A354V, Y172C LRPPRC-BirA-FLAG. Figure 5.8 shows that the protein level of A354V and Y172C LRPPRC variant declined rapidly in contrast to the wild-type protein. The half-life for wt-LRPPRC is about 26.3 hours,

whereas this was reduced for A354V and Y172C LRPPRC to 18.2 and 11.4 hours, respectively.

5.6. CLPB interacts with A354V or Y172C LRPPRC-BirA-FLAG

As described previously, the A354V and Y172C LRPPRC variants are unstable and have a short half-life; however, it is unclear what protein interacts with these variants. we addressed this question using BioID and as the results are illustrated in Figure 5.9, where we used bait to bait comparison meaning the preys interacting with A354V or Y172C LRPPRC were compared to the preys interacting with wt LRPPRC. Caseinolytic peptidase B homolog (CLPB) specifically interacted with A354V and Y172C LRPPRC variants, several proteins of the mitochondrial ribosome, other mitochondrial enzymes, as well as some heat-shock proteins DNAJA3, and HSPE1. We performed BioID of CLPB, and there was no interaction with LRPPRC suggesting the specificity of the CLPB interaction with A354V and Y172C LRPPRC variants.

Many proteins including some RNA binding proteins, mitochondrial ribosomal subunits, mitochondrial enzymes, and SLIRP were found to interact with both wt and A354V or Y172C LRPPRC variants. Using BN-PAGE and second-dimension, we also showed that wt and Y172C LRPPRC-BirA-FLAG is present in a complex with SLIRP and with the endogenous LRPPRC (Figure 5.7).

Next, we measured the impact of CLPB deficiency on the stability of Y172C LRPPRC variant by transiently knocking-down CLPB in 293 cells expressing wt and Y172C LRPPRC-BirA-FLAG. Interestingly, the steady-state levels of Y172C LRPPRC-BirA-FLAG was decreased, but no change was observed on the levels of wt LRPPRC-BirA-FLAG (Figure 5.10), further suggesting the specificity of the CLPB interaction with LRPPRC variants. Therefore, we asked whether we could rescue the reduction in the levels of Y172C LRPPRC by expressing CLPB. In fact, as indicated in figure 5.10, the steady-state levels of Y172C LRPPRC variant is

increased by expressing CLPB in 293 cell lines.

5.7. Y172C LRPPRC variant is degraded faster in the absence of OMA1 and AFG3L2

Knowing that LRPPRC variants are less stable in comparison to wt LRPPRC-BirA-FLAG, we decided to perform an experiment to identify the mitochondrial protease(s) by which Y172C or A354V LRPPRC-BirA-FLAG are degraded. Thus, we knocked down some major components of mitochondrial quality control machinery along with CLPB in 293 cells expressing wt and Y172C-LRPPRC-BirA-FLAG (Figure 5.11 A-D and Figure 5.12). Surprisingly, the steady-state levels of Y172C LRPPRC were further reduced in the absence of AFG3L2 and OMA1. Next, we aimed to investigate the impact of CLPB, AFG3L2, and OMA1 knock down on LRPPRC levels in control and LSFC subject fibroblasts (Figure 5.13 A and 5.14 A).

To our surprise, the steady-state levels of LRPPRC and SLIRP remained unchanged in the absence of CLPB, AFG3L2, and OMA1. In addition, expressing CLPB failed to increase the steady-state levels of LRPPRC and SLIRP and the levels of Complex IV in LSFC subject fibroblasts (Figure 5.13 B-C and 5.14 A).

A)

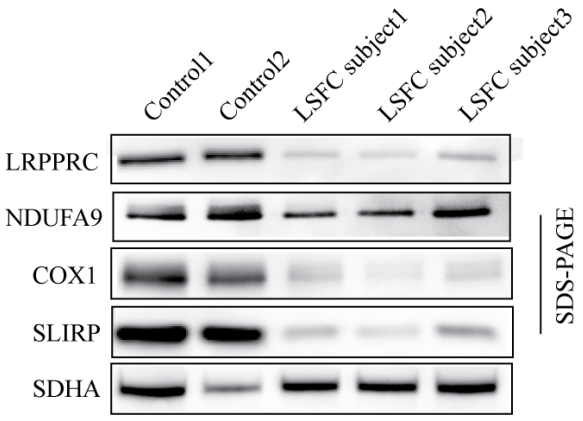
Control1
Control2
LSFC subject1
LSFC subject2
LSFC subject3
LRPPRC
NDUFA9
COX1
SLIRP
SDHA
SDS-PAGE

B)

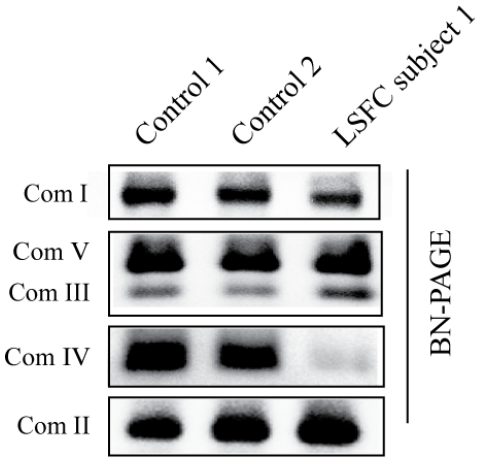
Control 1
Control 2
LSFC subject 1
Com I
Com V
Com III
Com IV
Com II
BN-PAGE

C)

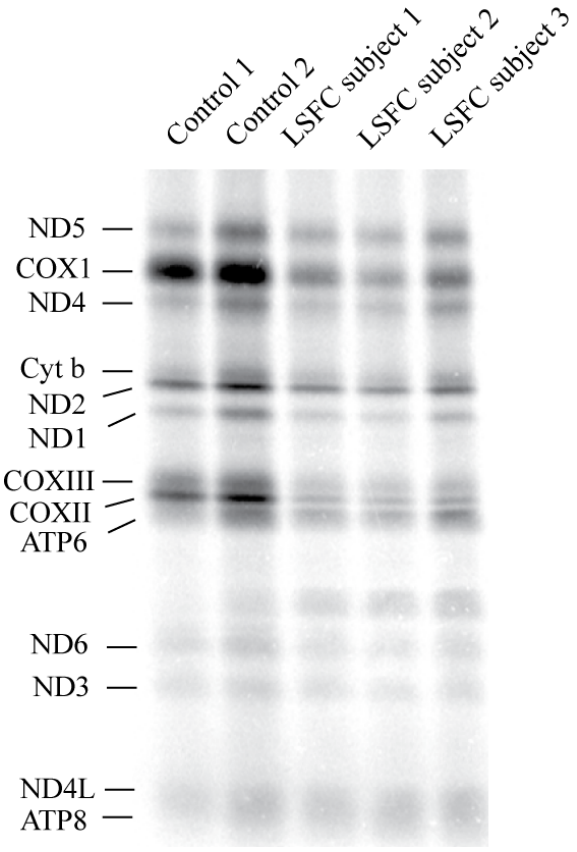
Control 1
Control 2
LSFC subject 1
LSFC subject 2
LSFC subject 3
ND5
COX1
ND4
Cyt b
ND2
ND1
COXIII
COXII
ATP6
ND6
ND3
ND4L
ATP8

Figure 5.1. Impact of LRPPRC deficiency on mitochondrial OXPHOS assembly in a Finnish LSFC subject. Panel A shows immunoblot analysis of whole cell extracts from subject1 fibroblasts (Finnish LSFC subject carrying homozygous mutation at c. 515A>G (p. Y172C)), subject 2 and 3 fibroblasts (Quebec LSFC subjects carrying homozygous mutation at c.515A>G (p. Y172C)). The blot was probed with LRPPRC, SLIRP, NDUFA9, COX1, and SDHA as a loading control. Panel B shows Blue-native PAGE analysis of the five OXPHOS complexes in two controls and Finnish LSFC subject (Subject 1) revealed by subunit-specific antibodies against OXPHOS complexes. Panel C shows Pulse-chase labeling of newly synthesized mitochondrial polypeptides (indicated on the left; ND, subunits of complex I; COX, subunits of complex IV; cyt b, subunit of complex III; ATP, subunits of complex V) in subject and control fibroblasts.

A)

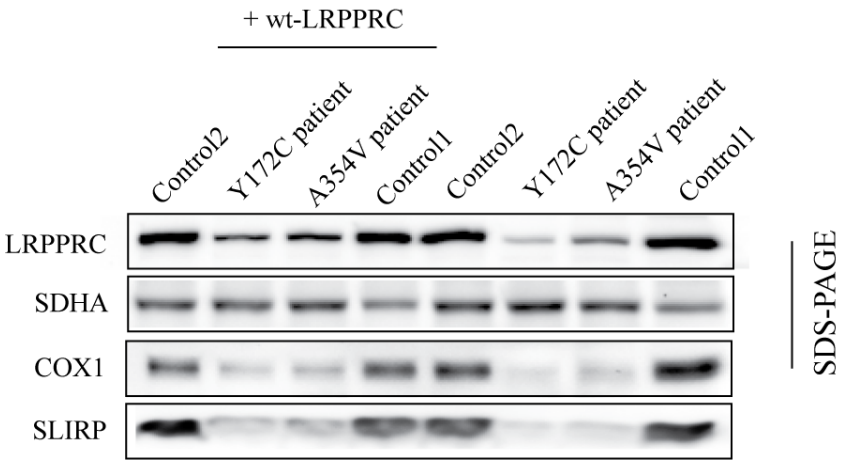
+ wt-LRPPRC
Control2
Y172C patient
A354V patient
Control1
Control2
Y172C patient
A354V patient
Control1
LRPPRC
SDHA
COX1
SLIRP
SDS-PAGE

B)

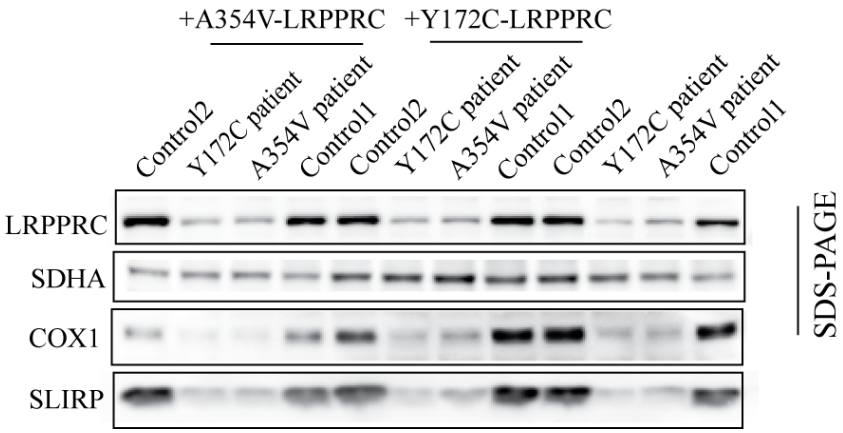
+A354V-LRPPRC
+Y172C-LRPPRC
Control2
Y172C patient
A354V patient
Control1
Control2
Y172C patient
A354V patient
Control1
Control2
Y172C patient
A354V patient
Control1
LRPPRC
SDHA
COX1
SLIRP
SDS-PAGE

C)

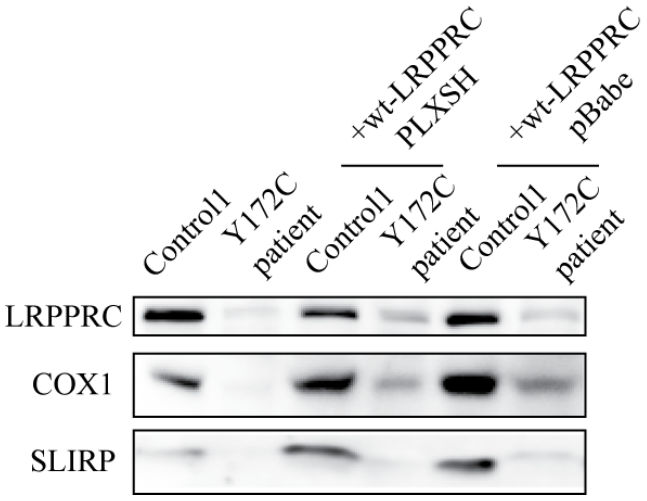
+wt-LRPPRC PLXSH
+wt-LRPPRC pBabe
Control1
Y172C patient
Control1
Y172C patient
Control1
Y172C patient
LRPPRC
COX1
SLIRP

Figure 5.2. Failure to rescue the biochemical defects of LRPPRC deficiency in LSFC subject fibroblasts. Immunoblot analysis of control and LSFC subject fibroblasts, Finnish subject with p. Y172C and Saguenay subject with p. A354V mutation in LRPPRC, expressing (A) wt-LRPPRC from a pBabe retroviral expression vector, (B) A354V- and Y172C-LRPPRC in pBabe retroviral expression vector (C) wt-LRPPRC in PLXSH retroviral expression vector. The blots were probed with LRPPRC, SLIRP, COX1 antibodies and SDHA antibody was used as a loading control.

A)

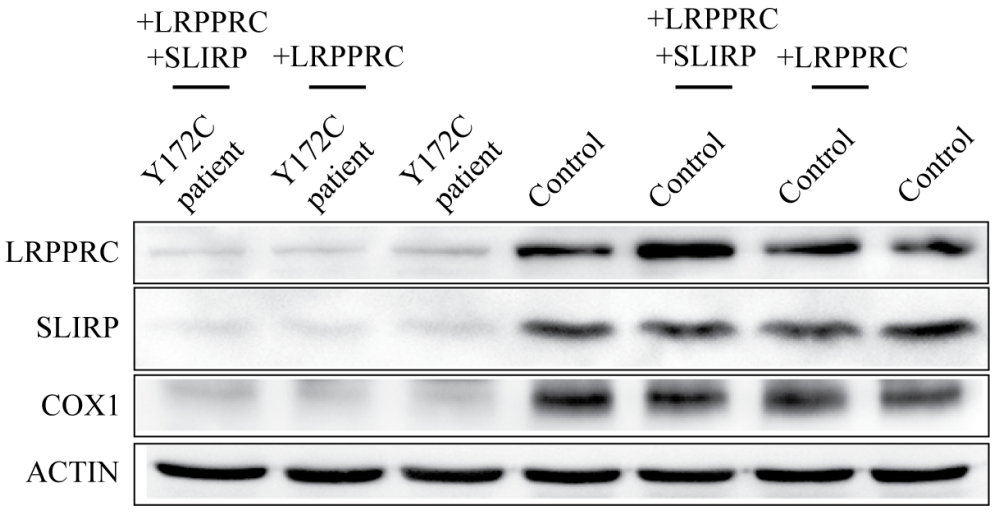
+LRPPRC
+SLIRP
+LRPPRC
+LRPPRC
+SLIRP
+LRPPRC
Y172C patient
Y172C patient
Y172C patient
Control
Control
Control
Control
LRPPRC
SLIRP
COX1
ACTIN

B)

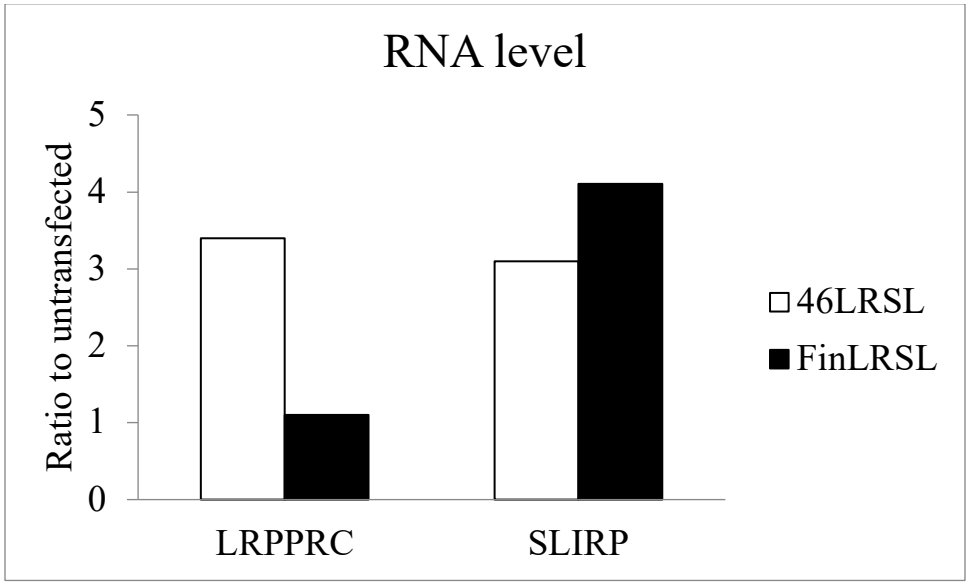
RNA level
Ratio to untransfected
5
4
3
2
1
0
LRPPRC
SLIRP
46LRSL
FinLRSL

C)

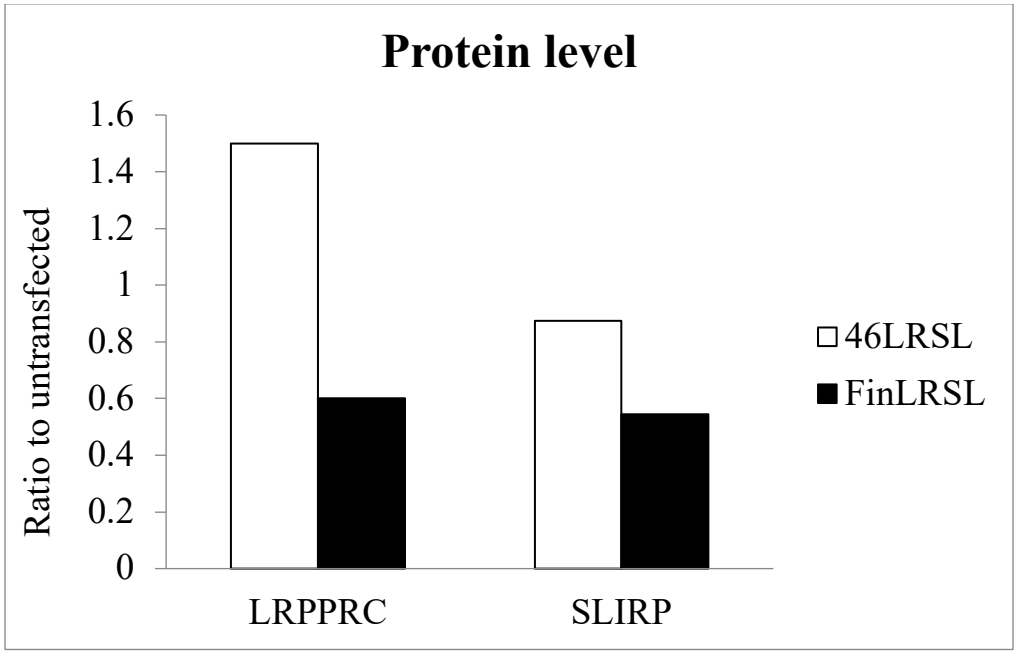
Protein level
Ratio to untransfected
1.6
1.4
1.2
1
0.8
0.6
0.4
0.2
0
LRPPRC
SLIRP
46LRSL
FinLRSL

D)

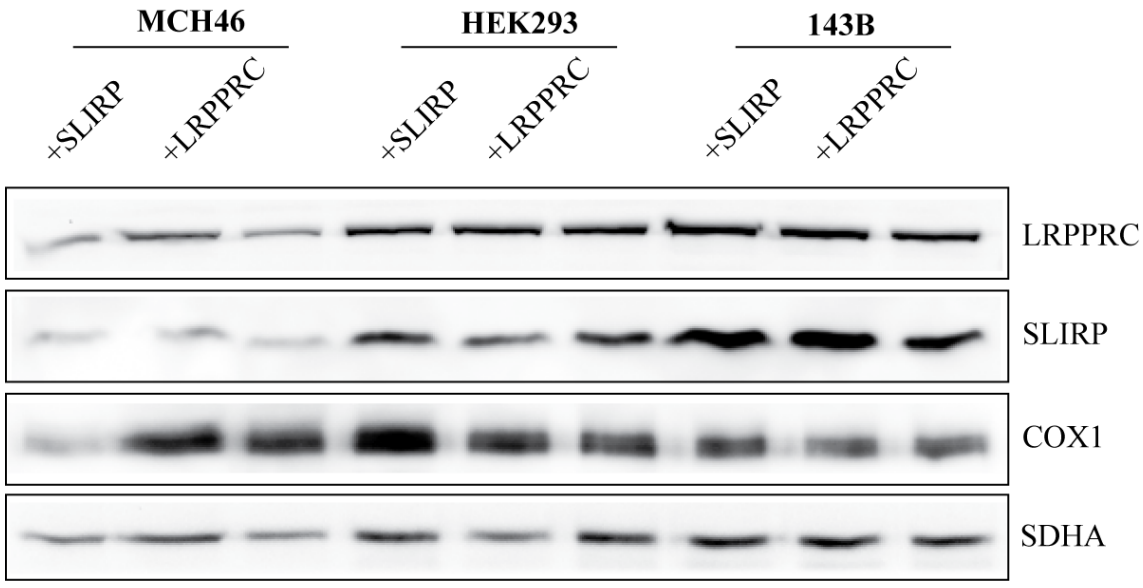
MCH46
HEK293
143B
+SLIRP
+LRPPRC
+SLIRP
+LRPPRC
+SLIRP
+LRPPRC
LRPPRC
SLIRP
COX1
SDHA

Figure 5.3. Expression of LRPPRC or co-expression of LRPPRC/SLIRP fails to rescue the biochemical defects in LSFC subject fibroblasts. Panel A shows SDS-PAGE analysis of expressing (+LRPPRC) and co-expressing (+LRPPRC/+SLIRP) cell lines (control and LSFC subject fibroblasts) blotted with LRPPRC, SLIRP, and COX1 antibodies. Actin is a loading control. Quantification of LRPPRC and SLIRP panel B transcripts panel C proteins in control (46) and LSFC subject (Fin) fibroblasts. The Y axis represents the ratio of the transcripts to un-transfected cell lines, and the X axis shows LRPPRC and SLIRP transcripts. 46LRSL stands for Control fibroblasts co-expressing LRPPRC and SLIRP, and FinLRSL refers to LSFC subject fibroblasts co-expressing LRPPRC and SLIRP. Panel D shows the expression of LRPPRC (+LRPPRC) and SLIRP (+SLIRP) in different human cell lines (143B osteosarcoma, HEK293 embryonic kidney cells, and MCH46 fibroblasts). The blot is probed with LRPPRC, SLIRP, and COX1 antibodies. SDHA was used a loading control.

A)

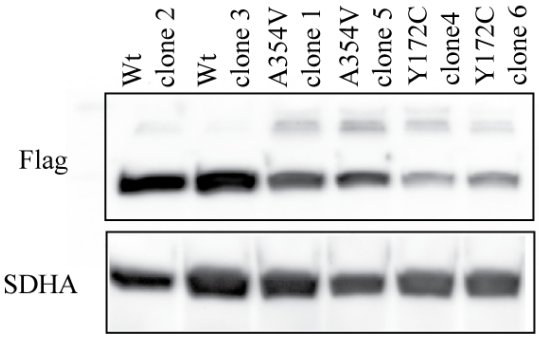
Wt clone 2
Wt clone 3
A354V clone 1
A354V clone 5
Y172C clone4
Y172C clone 6
Flag
SDHA

B)

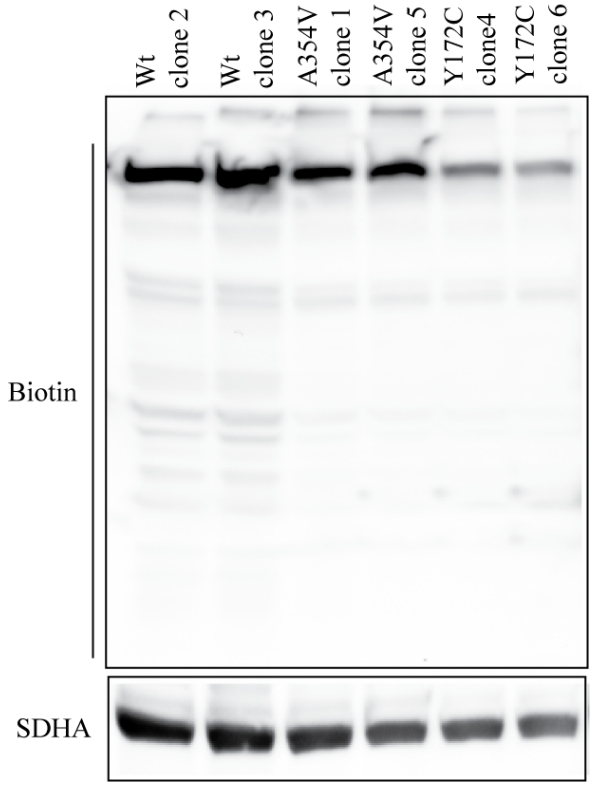
Wt clone 2
Wt clone 3
A354V clone 1
A354V clone 5
Y172C clone4
Y172C clone 6
Biotin
SDHA

C)

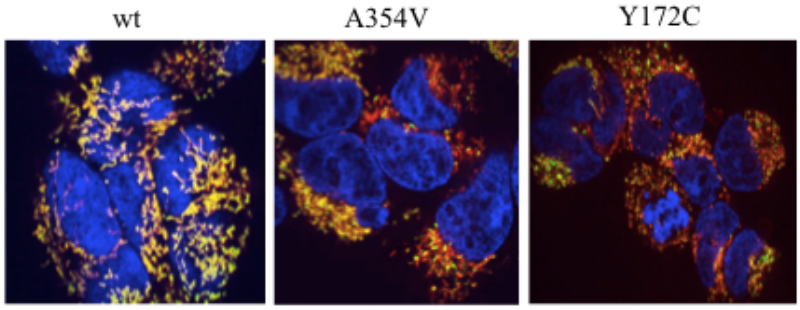
wt
A354V
Y172C

Figure 5.4. The steady-state levels of tagged mutant LRPPRC is lower than the wild type in 293 cell lines. Validation of BioID fusion proteins. Flp-In T-REx 293 cells stably expressing wt LRPPRC-BirA-FLAG, A354V LRPPRC-BirA-FLAG, and Y172C LRPPRC-BirA-FLAG were analyzed using WB and IF. (A) Following SDS-PAGE, tagged proteins were probed with FLAG antibody (B) the same blot was probed with anti-biotin antibody (C) Following IF, wt-LRPPRC-BirA-FLAG, A354V LRPPRC-BirA-FLAG, and Y172C LRPPRC-BirA-FLAG were probed by anti-FLAG and the endogenous LRPPRC was probed by anti-LRPPRC. Tagged LRPPRC staining is shown in green and the endogenous LRPPRC staining is shown in red. The images were obtained using confocal microscopy and processed by ImageJ.

A)

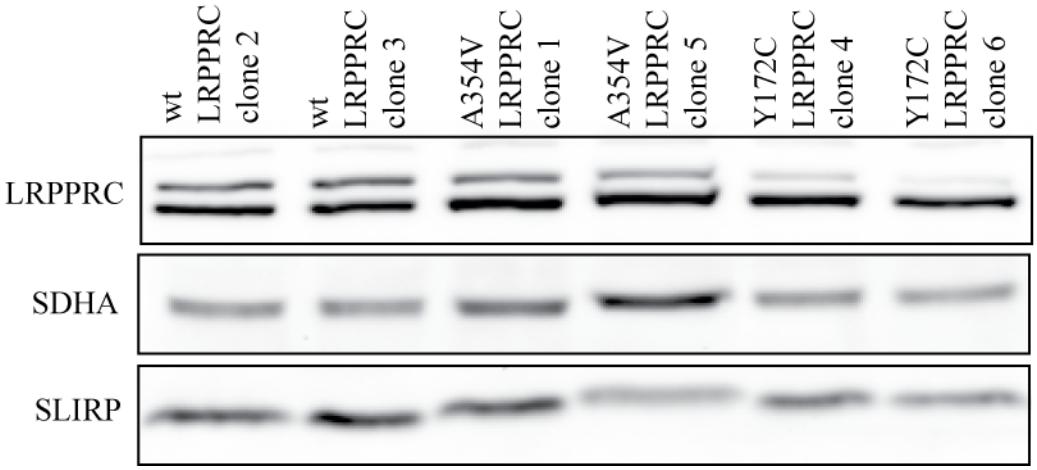
wt LRPPRC clone 2
wt LRPPRC clone 3
A354V LRPPRC clone 1
A354V LRPPRC clone 5
Y172C LRPPRC clone 4
Y172C LRPPRC clone 6
LRPPRC
SDHA
SLIRP

B)

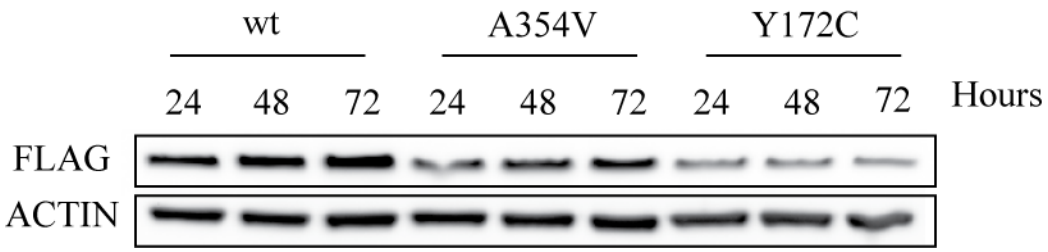
wt
A354V
Y172C
24 48 72 24 48 72 24 48 72 Hours
FLAG
ACTIN

Figure 5.5. Comparison of the expression levels of wt LRPPRC-BirA-FLAG to the endogenous protein in 293 cells. Panel A shows SDS-PAGE analysis of 293 cell lines expressing wt, A354V and Y172C LRPPRC-BirA-FLAG. The blot was probed with antibodies against LRPPRC and SLIRP. Panel B shows the expression levels of tagged LRPPRC after inducing 293 cell lines with tetracycline for the period of 24, 48, and 72 hours. The blot was probed with FLAG antibody.

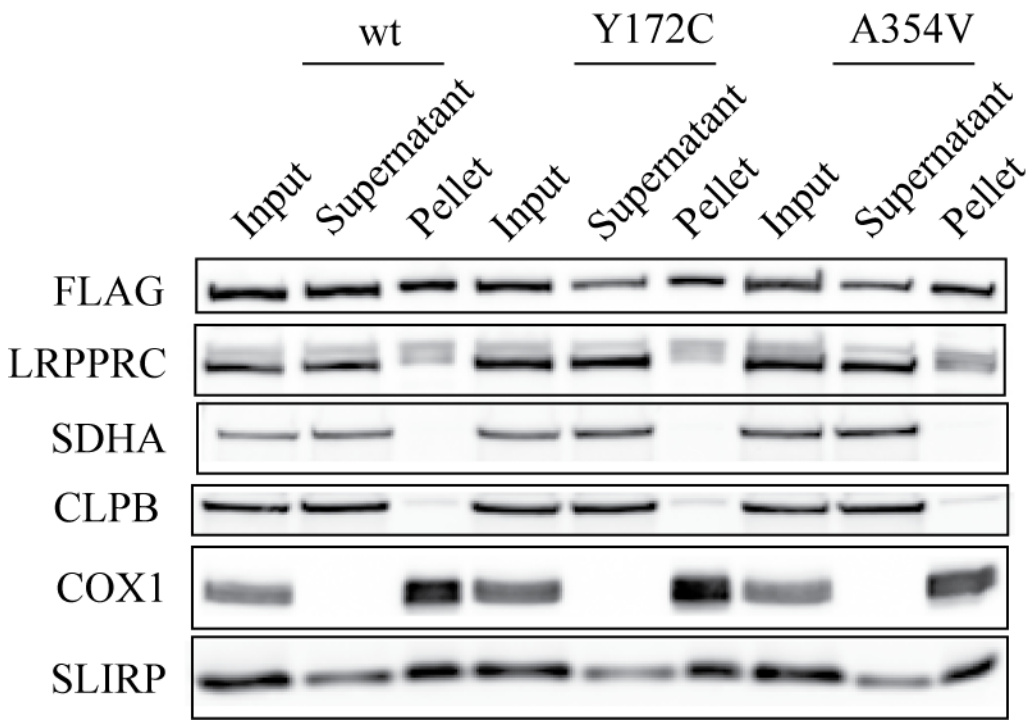
wt
Y172C
A354V
Input
Supernatant
Pellet
Input
Supernatant
Pellet
Input
Supernatant
Pellet
FLAG
LRPPRC
SDHA
CLPB
COX1
SLIRP

Figure 5.6. LRPPRC BirA-FLAG is associated with the insoluble fraction. The panel shows Alkaline carbonate extracts of mitochondria from 293 cells that were analyzed by immunoblotting with antibodies against FLAG, LRPPRC, SLIRP and the following protein controls: COX I (multiple pass, integral inner membrane), SDHA (soluble, inner membrane-associated), CLPB (soluble, inter membrane space).

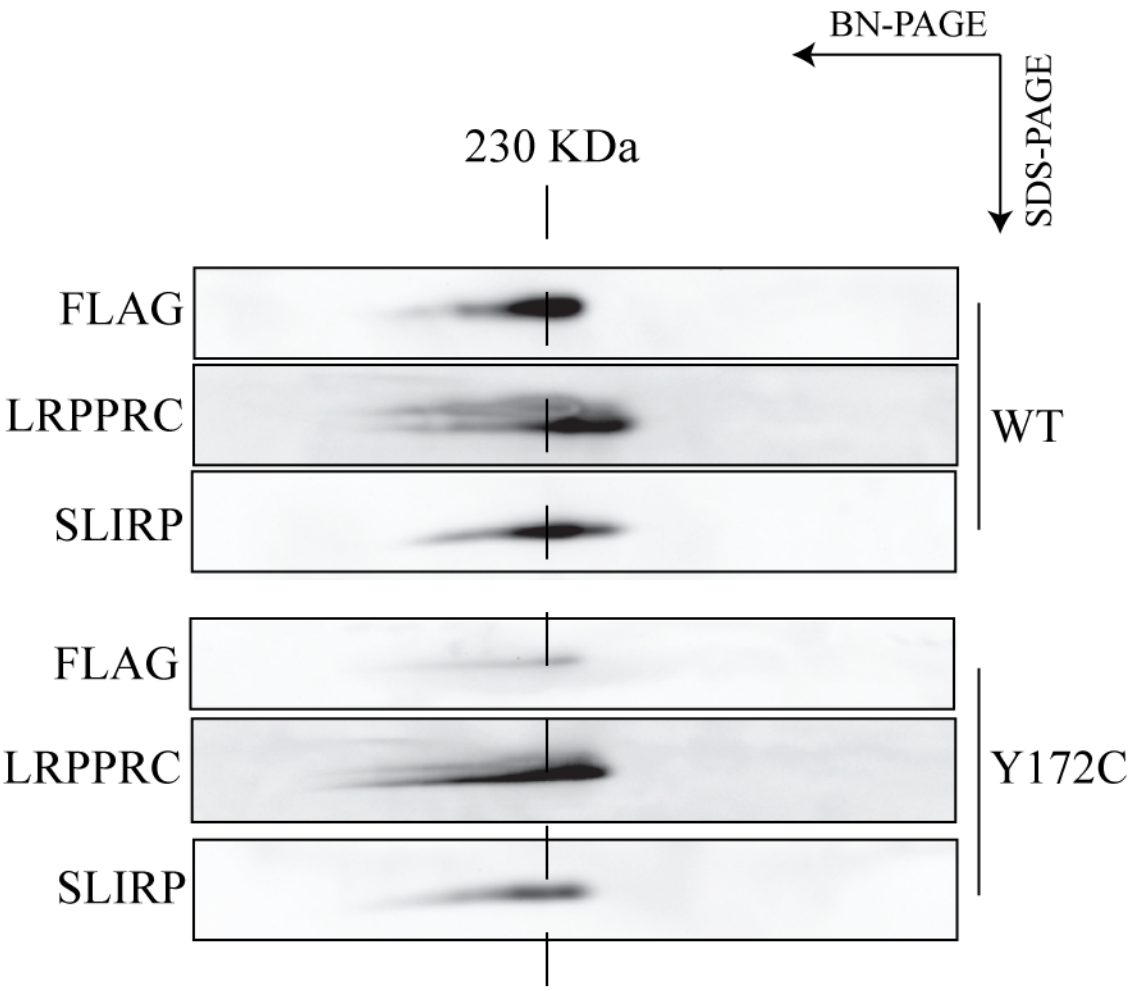
BN-PAGE
SDS-PAGE
230 KDa
FLAG
LRPPRC
SLIRP
WT
FLAG
LRPPRC
SLIRP
Y172C

Figure 5.7. Characterization of LRPPRC/SLIRP complex by 2D gel electrophoresis.

293 cell lines (wt- and Y172C-LRPPRC-BirA-FLAG) were subjected to second dimension (2D) denaturing experiment. A cocktail of antibodies directed against the indicated proteins was used to probe the immunoblots panel A wt-LRPPRC-BirA-FLAG and panel B Y172C-LRPPRC-BirA-FLAG.

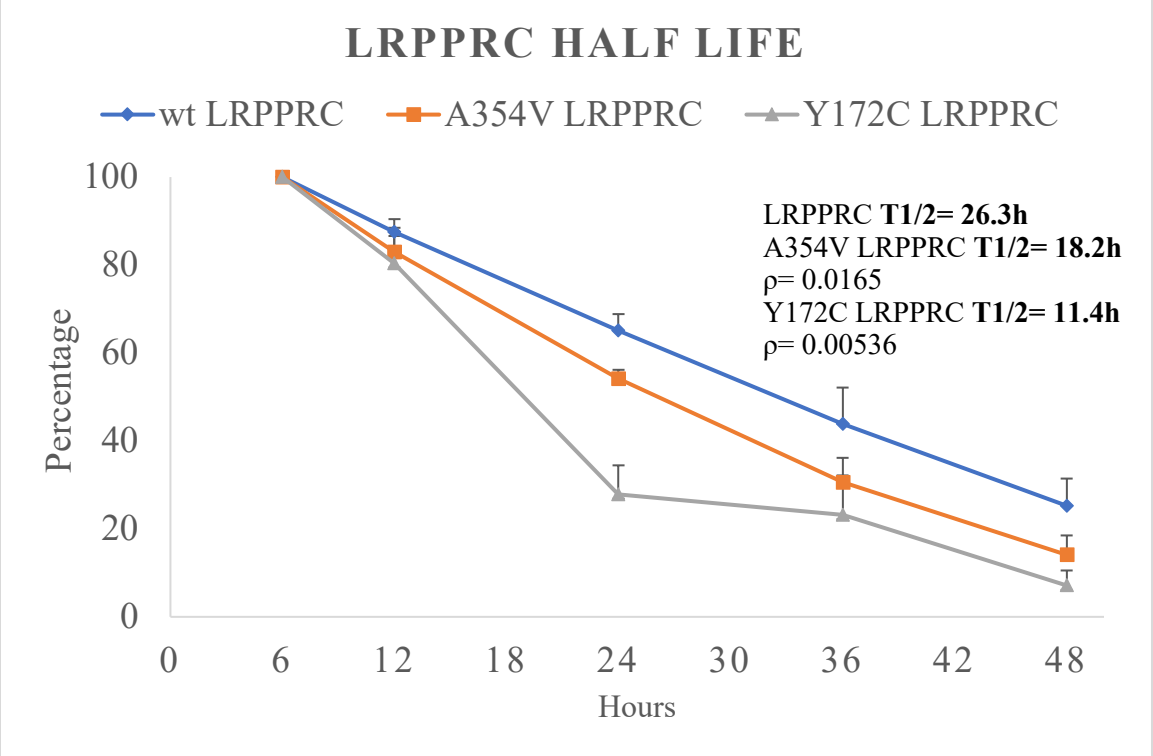
LRPPRC HALF LIFE
wt LRPPRC
A354V LRPPRC
Y172C LRPPRC
Percentage
100
80
60
40
20
0
0
6
12
18
24
30
36
42
48
Hours
LRPPRC T1/2= 26.3h
A354V LRPPRC T1/2= 18.2h
ρ= 0.0165
Y172C LRPPRC T1/2= 11.4h
ρ= 0.00536

Figure 5.8. Half-lives of wild-type and LRPPRC pathogenic variants. 293 cells stably expressing wt, A354V, Y172C LRPPRC-BirA-FLAG under an inducible promoter were harvested at different time points after removing the protein expression inducing factor (tetracycline) from the media. Protein levels were determined from the cell lysates using Image J and normalized with the control. Statistical analysis was assessed by the Student t-test from 4 experimental replicates, and the P value is as indicated. The Y-axis represents the percentage of quantified proteins over the control, and X-axis indicates the time points.

Bait	Prey gene	Prey protein	Avg Spectra	AvgSAINT	Fold Change
A354V	AARS2	NP_065796.1	10	0.98	13.85
WT	AASS	NP_005754.2	6.33	1	63.33
WT	ABCB7	NP_001258625.1	8.83	1	88.33
A354V	ABCB7	NP_001258625.1	5.67	1	56.67
Y172C	ABCB7	NP_001258625.1	3	0.99	30
WT	ABHD10	NP_060864.1	2	0.98	20
WT	ACAD9	NP_054768.2	18.83	1	188.33
A354V	ACAD9	NP_054768.2	18	1	180
Y172C	ACAD9	NP_054768.2	20	1	200
WT	ACADM	NP_001120800.1	6	1	60
A354V	ACADM	NP_001120800.1	5.83	1	58.33
Y172C	ACADM	NP_001120800.1	6.2	0.99	62
A354V	ACADVL	NP_001257376.1	5.5	1	55
Y172C	ACADVL	NP_001257376.1	7.2	1	72
WT	ACAT1	NP_000010.1	9.67	1	96.67
A354V	ACAT1	NP_000010.1	5.83	1	58.33
Y172C	ACAT1	NP_000010.1	6.2	1	62
WT	ACOT1	NP_001032238.1	156	1	48.41
A354V	ACOT1	NP_001032238.1	104.33	1	32.38
Y172C	ACOT1	NP_001032238.1	93	1	28.86
WT	ACOT2	NP_006812.3	25.5	1	51
A354V	ACOT2	NP_006812.3	15.67	1	31.33
Y172C	ACOT2	NP_006812.3	30.2	1	60.4
WT	ACOT9	NP_001028755.2	5.67	0.98	17
A354V	ACOT9	NP_001028755.2	8.83	0.99	26.5
Y172C	ACOT9	NP_001028755.2	7	0.99	21
WT	AFG3L2	NP_006787.2	49.17	1	491.67
A354V	AFG3L2	NP_006787.2	37.33	1	373.33
Y172C	AFG3L2	NP_006787.2	50.8	1	508
WT	ALAS1	NP_954635.1	15.67	1	156.67

A354V	ALAS1	NP_954635.1	9.5	1	95
Y172C	ALAS1	NP_954635.1	8	1	80
WT	ALDH2	NP_000681.2	2.83	0.96	17
A354V	ALDH2	NP_000681.2	3.67	0.98	22
WT	ALDH4A1	NP_003739.2	4.33	1	43.33
Y172C	ANGEL2	NP_653168.2	1.8	0.96	18
WT	ATAD3A	NP_060658.3	23	0.97	4.81
A354V	ATAD3A	NP_060658.3	40.5	1	8.48
WT	ATP5B	NP_001677.2	162.5	1	15.64
A354V	ATP5B	NP_001677.2	140	1	13.48
Y172C	ATP5B	NP_001677.2	137.4	1	13.23
A354V	ATP5C1	NP_005165.1	26.5	1	3.64
Y172C	ATP5C1	NP_005165.1	36.6	1	5.03
A354V	ATP5D	NP_001678.1	2.17	0.99	21.67
WT	ATP5F1	NP_001679.2	13.67	1	41
A354V	ATP5F1	NP_001679.2	28.83	1	86.5
Y172C	ATP5F1	NP_001679.2	33	1	99
WT	ATP5J	NP_001676.2	4.17	1	41.67
WT	ATP5J2-PTCD1	NP_001185808.1	43	1	55.29
A354V	ATP5J2-PTCD1	NP_001185808.1	41.17	1	52.93
Y172C	ATP5J2-PTCD1	NP_001185808.1	36.8	1	47.31
Y172C	ATP5L	NP_006467.4	1.8	0.96	18
A354V	ATP5O	NP_001688.1	13.17	0.97	10.77
Y172C	ATP5O	NP_001688.1	14.4	0.97	11.78
WT	ATPAF1	NP_073582.3	15.67	1	156.67
A354V	ATPAF1	NP_073582.3	5.67	1	56.67
Y172C	ATPAF1	NP_073582.3	6	1	60
WT	ATPIF1	NP_057395.1	3	1	30
Y172C	BCKDK	NP_005872.2	5.6	0.98	20.16
WT	BCS1L	NP_001073335.1	16.33	1	163.33
A354V	BCS1L	NP_001073335.1	7.5	1	75
Y172C	BCS1L	NP_001073335.1	11.4	1	114
WT	C10orf2	NP_001157284.1	10.5	1	105
WT	C17orf80	NP_001094091.	19	1	190
Y172C	C17orf80	NP_001094091.1	11	1	110

WT	C6orf203	NP_001135940.1	2	0.98	20
WT	C8orf82	NP_001001795.1	1.67	0.97	16.67
WT	CARS2	NP_078813.1	16.5	1	165
A354V	CARS2	NP_078813.1	9.33	1	93.33
Y172C	CARS2	NP_078813.1	7.6	1	76
A354V	CBR4	NP_116172.2	4.67	1	46.67
Y172C	CBR4	NP_116172.2	2.6	0.98	26
WT	CDK5RAP1	NP_057492.2	3.33	1	33.33
A354V	CDK5RAP1	NP_057492.2	8.33	1	83.33
Y172C	CDK5RAP1	NP_057492.2	8	1	80
A354V	CLPB	NP_110440.1	24.67	1	63.43
Y172C	CLPB	NP_110440.1	21.2	1	54.51
WT	CLPP	NP_006003.1	7.5	1	22.5
A354V	CLPP	NP_006003.1	4.83	0.96	14.5
Y172C	CLPP	NP_006003.1	7	0.95	21
WT	CLPX	NP_006651.2	45.67	1	21.08
A354V	CLPX	NP_006651.2	66.5	1	30.69
Y172C	CLPX	NP_006651.2	73	1	33.69
WT	CLUH	NP_056044.3	3.67	1	36.67
A354V	CLUH	NP_056044.3	46.17	1	461.67
Y172C	CLUH	NP_056044.3	6	1	60
WT	COQ5	NP_115690.3	15.33	1	153.33
A354V	COQ8A	NP_064632.2	6.17	1	61.67
WT	COX4I1	NP_001852.1	5	0.99	18
A354V	COX4I1	NP_001852.1	4.33	1	15.6
WT	COX5A	NP_004246.2	7.83	1	78.33
A354V	COX5A	NP_004246.2	6	1	60
Y172C	COX5A	NP_004246.2	3.2	1	32
A354V	COX7A2	NP_001856.2	3	1	30
Y172C	COX7A2	NP_001856.2	2.4	0.98	24
WT	DAP3	NP_387506.1	167.83	1	1678.33
A354V	DAP3	NP_387506.1	108.5	1	1085
Y172C	DAP3	NP_387506.1	117.4	1	1174
WT	DARS2	NP_060592.2	11.33	0.97	11.33
A354V	DARS2	NP_060592.2	16.17	0.99	16.17
Y172C	DARS2	NP_060592.2	12.4	0.98	12.4
WT	DBT	NP_001909.3	128.83	1	6.37
A354V	DBT	NP_001909.3	114.83	1	5.68
Y172C	DBT	NP_001909.3	130.6	1	6.46
A354V	DDX28	NP_060850.2	5.5	1	55

WT	DHX30	NP_055781.2	83.83	1	23.22
A354V	DHX30	NP_055781.2	92.67	1	25.66
Y172C	DHX30	NP_055781.2	89.2	1	24.7
WT	DLST	NP_001924.2	55	1	141.43
A354V	DLST	NP_001924.2	43.83	1	112.71
Y172C	DLST	NP_001924.2	36.6	1	94.11
A354V	DNAJA3	NP_005138.3	28.33	1	4.77
WT	EARS2	NP_001077083.1	11.17	1	67
A354V	EARS2	NP_001077083.1	8.5	1	51
Y172C	EARS2	NP_001077083.1	8.2	0.99	49.2
WT	ECHS1	NP_004083.3	22.5	1	225
A354V	ECHS1	NP_004083.3	14.33	1	143.33
Y172C	ECHS1	NP_004083.3	11.4	1	114
Y172C	ECI1	NP_001171500.1	2.2	0.98	22
WT	ECSIT	NP_057665.2	11.67	1	116.67
A354V	ECSIT	NP_057665.2	3.67	1	36.67
Y172C	ECSIT	NP_057665.2	3.8	1	38
WT	ELAC2	NP_060597.4	21	1	54
A354V	ELAC2	NP_060597.4	20.67	1	53.14
Y172C	ELAC2	NP_060597.4	15.2	1	39.09
WT	ERAL1	NP_005693.1	21.5	1	77.4
A354V	ERAL1	NP_005693.1	17.83	1	64.2
Y172C	ERAL1	NP_005693.1	19.8	1	71.28
WT	ETFA	NP_001121188.1	25.33	1	19.83
A354V	ETFA	NP_001121188.1	22.33	1	17.48
Y172C	ETFA	NP_001121188.1	21.4	1	16.75
WT	ETFB	NP_001976.1	17.33	1	173.33
A354V	ETFB	NP_001976.1	17.5	1	175
Y172C	ETFB	NP_001976.1	14	1	140
WT	FASTKD1	NP_078898.3	2.5	0.99	25
A354V	FASTKD1	NP_078898.3	3.17	1	31.67
WT	FASTKD2	NP_001129665.1	26.17	1	261.67
A354V	FASTKD2	NP_001129665.	23.33	1	233.33
Y172C	FASTKD2	NP_001129665.1	26.2	1	262
A354V	FASTKD3	NP_076996.2	3.17	1	31.67

WT	FASTKD5	NP_068598.1	24.33	1	243.33
A354V	FASTKD5	NP_068598.1	41.17	1	411.67
Y172C	FASTKD5	NP_068598.1	33.2	1	332
WT	FDX1	NP_004100.1	3.5	1	35
Y172C	FDX1	NP_004100.1	2.2	0.98	22
WT	FLAD1	NP_001171820.1	4.17	1	37.5
WT	GADD45GIP1	NP_443082.2	9.5	1	95
A354V	GADD45GIP1	NP_443082.2	4.17	1	41.67
A354V	GARS	NP_002038.2	5.67	0.97	25.5
WT	GATB	NP_004555.1	10.17	1	101.67
A354V	GATB	NP_004555.1	4.67	1	46.67
Y172C	GATB	NP_004555.1	4.8	1	48
WT	GATC	NP_789788.1	4.17	1	41.67
A354V	GATC	NP_789788.1	2.5	0.99	25
WT	GCDH	NP_000150.1	2.67	1	26.67
WT	GFM1	NP_079272.4	9.67	1	96.67
A354V	GFM1	NP_079272.4	14	1	140
Y172C	GFM1	NP_079272.4	17	1	170
WT	GLS	NP_001243239.1	52.33	1	523.33
A354V	GLS	NP_001243239.1	24.33	1	243.33
Y172C	GLS	NP_001243239.1	23.8	1	238
WT	GLUD1	NP_005262.1	49.5	1	10.48
A354V	GLUD1	NP_005262.1	43.67	0.99	9.25
Y172C	GLUD1	NP_005262.1	67.6	1	14.32
WT	GRSF1	NP_001091947.1	40	1	400
A354V	GRSF1	NP_001091947.1	21	1	210
Y172C	GRSF1	NP_001091947.1	21.6	1	216
WT	GSTK1	NP_001137151.1	2.5	0.98	22.5
WT	GTPBP10	NP_149098.2	22.67	1	226.67
A354V	GTPBP10	NP_149098.2	9.67	1	96.67
Y172C	GTPBP10	NP_149098.2	8.4	1	84
Y172C	GTPBP3	NP_598399.2	4.8	0.96	21.6
A354V	GTPBP8	NP_054889.2	2.17	0.98	21.67
Y172C	GTPBP8	NP_054889.2	3.8	1	38
WT	GUF1	NP_068746.2	13.17	1	131.67

A354V	GUF1	NP_068746.2	13.83	1	138.33
Y172C	GUF1	NP_068746.2	9.8	1	98
WT	HADH	NP_001171634.2	5.67	1	56.67
A354V	HADH	NP_001171634.2	4.17	1	41.67
Y172C	HADH	NP_001171634.2	5	1	50
WT	HADHA	NP_000173.2	10	0.99	13.85
A354V	HADHA	NP_000173.2	29.17	1	40.38
Y172C	HADHA	NP_000173.2	44.8	1	62.03
A354V	HADHB	NP_000174.1	3.5	0.97	21
WT	HARS2	NP_036340.1	6.33	1	63.33
A354V	HARS2	NP_036340.1	14.5	1	145
Y172C	HARS2	NP_036340.1	9.6	1	96
A354V	HAX1	NP_006109.2	5.83	0.99	10.5
WT	HINT2	NP_115982.1	9.33	1	93.33
A354V	HINT2	NP_115982.1	4.67	1	46.67
Y172C	HINT2	NP_115982.1	6.8	1	68
WT	HNRNPAB	NP_112556.2	26.67	1	6
A354V	HNRNPAB	NP_112556.2	16	0.99	3.6
WT	HNRNPDL	NP_112740.1	13.67	1	12.3
A354V	HNRNPDL	NP_112740.1	8.33	0.99	7.5
Y172C	HNRNPDL	NP_112740.1	8.8	0.99	7.92
WT	HNRNPK	NP_112552.1	105.83	1	4.12
WT	HNRNPL	NP_001524.2	131.5	1	7.64
A354V	HNRNPL	NP_001524.2	87.5	1	5.08
Y172C	HNRNPL	NP_001524.2	119	1	6.91
WT	HNRNPR	NP_001095868.1	44.17	1	7.04
A354V	HNRNPR	NP_001095868.1	35.33	1	5.63
Y172C	HNRNPR	NP_001095868.1	40.8	1	6.5
WT	HNRNPUL1	NP_653333.1	13.33	1	14.12
A354V	HNRNPUL1	NP_653333.1	8.83	1	9.35
WT	HSD17B10	NP_004484.1	92.17	1	9.7
A354V	HSD17B10	NP_004484.1	51.5	1	5.42
Y172C	HSD17B10	NP_004484.1	49.2	1	5.18
WT	HSDL2	NP_115679.2	28.17	1	36.21
A354V	HSDL2	NP_115679.2	11.17	1	14.36
Y172C	HSDL2	NP_115679.2	12.4	1	15.94
A354V	HSPE1	NP_002148.1	5	1	50

Y172C	HSPE1	NP_002148.1	3	0.99	30
WT	IARS2	NP_060530.3	85.33	1	17.86
A354V	IARS2	NP_060530.3	66.83	0.99	13.99
Y172C	IARS2	NP_060530.3	64.2	0.99	13.44
WT	IBA57	NP_001010867.1	18.67	1	18.67
A354V	IBA57	NP_001010867.1	14.33	1	14.33
Y172C	IBA57	NP_001010867.1	15.4	1	15.4
WT	IDH3A	NP_005521.1	2.5	0.99	25
WT	IDH3B	NP_008830.2	5.67	0.95	6.8
A354V	IDH3B	NP_008830.2	8.83	1	10.6
WT	IGF2BP1	NP_006537.3	29.17	1	3.32
A354V	IMMT	NP_001093639.1	7.67	0.95	6.9
Y172C	IMMT	NP_001093639.1	11.2	0.98	10.08
WT	ISCA1	NP_112202.2	3.17	0.99	31.67
A354V	IVD	NP_002216.2	2.5	1	25
WT	KIAA0391	NP_055487.2	9.5	1	95
A354V	KIAA0391	NP_055487.2	21.83	1	218.33
Y172C	KIAA0391	NP_055487.2	24.6	1	246
WT	LARS2	NP_056155.1	13.67	1	61.5
A354V	LARS2	NP_056155.1	15.67	1	70.5
Y172C	LARS2	NP_056155.1	14	1	63
WT	LETM1	NP_036450.1	52	1	187.2
A354V	LETM1	NP_036450.1	36	1	129.6
Y172C	LETM1	NP_036450.1	31.6	1	113.76
WT	LOC100507855	XP_003119578.1	13.5	1	135
A354V	LOC100507855	XP_003119578.1	5.33	1	53.33
WT	LONP1	NP_004784.2	3.67	0.96	7.33
A354V	LONP1	NP_004784.2	4.33	0.98	8.67
WT	LYPLAL1	NP_620149.1	4.17	1	41.67
WT	LYRM4	NP_065141.3	3.17	1	31.67
A354V	LYRM4	NP_065141.3	3.17	1	31.67
Y172C	LYRM4	NP_065141.3	2.6	0.98	26
WT	MDH2	NP_005909.2	9	1	90
A354V	MDH2	NP_005909.2	7.83	1	78.33
Y172C	MDH2	NP_005909.2	6.8	1	68
WT	ME2	NP_002387.1	3.33	1	33.33

A354V	ME2	NP_002387.1	3.67	1	36.67
Y172C	ME2	NP_002387.1	4.6	1	46
WT	METTL15	NP_001107000.1	9.5	1	95
A354V	METTL15	NP_001107000.1	3.5	0.99	35
Y172C	METTL15	NP_001107000.1	3.2	0.99	32
WT	METTL17	NP_073571.1	2.33	0.98	23.33
Y172C	METTL17	NP_073571.1	2	0.97	20
WT	MGME1	NP_443097.1	4.33	1	43.33
WT	MMAB	NP_443077.1	31	1	310
A354V	MMAB	NP_443077.1	6.5	1	65
Y172C	MMAB	NP_443077.1	9	1	90
WT	MRM3	NP_060616.1	13.33	1	133.33
A354V	MRM3	NP_060616.1	9	1	90
Y172C	MRM3	NP_060616.1	10.4	1	104
WT	MRPL1	NP_064621.3	11.83	1	118.33
A354V	MRPL1	NP_064621.3	6.5	1	65
Y172C	MRPL1	NP_064621.3	6	1	60
WT	MRPL10	NP_660298.2	8.5	1	85
WT	MRPL12	NP_002940.2	19.5	1	58.5
A354V	MRPL12	NP_002940.2	11.5	1	34.5
Y172C	MRPL12	NP_002940.2	13.6	1	40.8
WT	MRPL13	NP_054797.2	12.33	1	123.33
A354V	MRPL13	NP_054797.2	16.17	1	161.67
Y172C	MRPL13	NP_054797.2	16	1	160
WT	MRPL14	NP_115487.2	5.5	1	55
WT	MRPL15	NP_054894.1	22.33	1	223.33
A354V	MRPL15	NP_054894.1	16.67	1	166.67
Y172C	MRPL15	NP_054894.1	13.6	1	136
WT	MRPL16	NP_060310.1	4.67	1	42
A354V	MRPL16	NP_060310.1	2.67	0.98	24
WT	MRPL17	NP_071344.1	8	1	80
A354V	MRPL17	NP_071344.1	7.67	1	76.67
Y172C	MRPL17	NP_071344.1	6.6	1	66
WT	MRPL18	NP_054880.2	5	1	50
A354V	MRPL18	NP_054880.2	3.67	1	36.67
Y172C	MRPL18	NP_054880.2	4	0.99	40
WT	MRPL19	NP_055578.2	15.5	1	155
A354V	MRPL19	NP_055578.2	6.67	1	66.67
Y172C	MRPL19	NP_055578.2	6.4	1	64

WT	MRPL2	NP_057034.2	4.5	1	45
A354V	MRPL2	NP_057034.2	4.67	1	46.67
WT	MRPL20	NP_060441.2	17.67	1	176.67
A354V	MRPL20	NP_060441.2	13.17	1	131.67
Y172C	MRPL20	NP_060441.2	9.8	1	98
WT	MRPL21	NP_852615.1	17	1	170
A354V	MRPL21	NP_852615.1	13.83	1	138.33
Y172C	MRPL21	NP_852615.1	9.8	1	98
WT	MRPL22	NP_054899.2	9.5	1	95
A354V	MRPL22	NP_054899.2	14	1	140
Y172C	MRPL22	NP_054899.2	15.2	1	152
WT	MRPL23	NP_066957.3	8.67	1	86.67
A354V	MRPL23	NP_066957.3	5.17	1	51.67
Y172C	MRPL23	NP_066957.3	7.2	1	72
WT	MRPL24	NP_078816.2	13.83	1	138.33
A354V	MRPL24	NP_078816.2	4.5	1	45
Y172C	MRPL24	NP_078816.2	8	1	80
WT	MRPL27	NP_057588.1	8.5	1	85
A354V	MRPL27	NP_057588.1	7.33	1	73.33
Y172C	MRPL27	NP_057588.1	6	1	60
WT	MRPL28	NP_006419.2	12.5	1	125
A354V	MRPL28	NP_006419.2	12.67	1	126.67
Y172C	MRPL28	NP_006419.2	18.6	1	186
WT	MRPL3	NP_009139.1	18	1	180
A354V	MRPL3	NP_009139.1	13.33	1	133.33
Y172C	MRPL3	NP_009139.1	14	1	140
WT	MRPL30	NP_660213.1	5.5	1	55
A354V	MRPL30	NP_660213.1	7	1	70
Y172C	MRPL30	NP_660213.1	11.4	1	114
WT	MRPL37	NP_057575.2	16.17	1	58.2
A354V	MRPL37	NP_057575.2	11.17	0.99	40.2
Y172C	MRPL37	NP_057575.2	9.6	0.99	34.56
WT	MRPL38	NP_115867.2	12.17	1	121.67
A354V	MRPL38	NP_115867.2	6.67	1	66.67
Y172C	MRPL38	NP_115867.2	9.2	1	92
WT	MRPL39	NP_542984.2	13.33	1	133.33
A354V	MRPL39	NP_542984.2	13.67	1	136.67
Y172C	MRPL39	NP_542984.2	9.6	1	96
WT	MRPL4	NP_057040.2	34	1	340
A354V	MRPL4	NP_057040.2	20.17	1	201.67
Y172C	MRPL4	NP_057040.2	16.4	1	164

WT	MRPL40	NP_003767.2	9	1	90
WT	MRPL41	NP_115866.1	14.5	1	145
A354V	MRPL41	NP_115866.1	9.17	1	91.67
Y172C	MRPL41	NP_115866.1	9.2	1	92
WT	MRPL42	NP_751917.1	19	1	190
A354V	MRPL42	NP_751917.1	7.67	1	76.67
Y172C	MRPL42	NP_751917.1	5	0.99	50
WT	MRPL43	NP_789762.1	24.67	1	246.67
A354V	MRPL43	NP_789762.1	19.5	1	195
Y172C	MRPL43	NP_789762.1	11.6	1	116
WT	MRPL44	NP_075066.1	38.67	1	348
A354V	MRPL44	NP_075066.1	28	1	252
Y172C	MRPL44	NP_075066.1	23	1	207
WT	MRPL45	NP_115727.4	27.33	1	246
A354V	MRPL45	NP_115727.4	12.33	1	111
Y172C	MRPL45	NP_115727.4	12.6	1	113.4
WT	MRPL46	NP_071446.2	17.17	1	171.67
A354V	MRPL46	NP_071446.2	10.83	1	108.33
Y172C	MRPL46	NP_071446.2	7.2	1	72
WT	MRPL47	NP_065142.2	15.67	1	156.67
A354V	MRPL47	NP_065142.2	8.5	1	85
Y172C	MRPL47	NP_065142.2	8.4	1	84
WT	MRPL48	NP_057139.1	13.83	1	138.33
A354V	MRPL48	NP_057139.1	8.17	1	81.67
Y172C	MRPL48	NP_057139.1	9.8	1	98
WT	MRPL49	NP_004918.1	15.67	1	156.67
A354V	MRPL49	NP_004918.1	9.17	1	91.67
Y172C	MRPL49	NP_004918.1	8.6	1	86
WT	MRPL50	NP_061924.1	20.17	1	201.67
A354V	MRPL50	NP_061924.1	10.67	1	106.67
Y172C	MRPL50	NP_061924.1	13.8	1	138
WT	MRPL51	NP_057581.2	2.83	1	28.33
WT	MRPL52	NP_848026.1	4.5	1	45
A354V	MRPL52	NP_848026.1	2.67	0.99	26.67
WT	MRPL53	NP_444278.1	7.5	1	75
A354V	MRPL53	NP_444278.1	3.5	1	35
Y172C	MRPL53	NP_444278.1	5.4	1	54
A354V	MRPL55	NP_852127.2	2.5	0.99	25
Y172C	MRPL55	NP_852127.2	3.8	0.98	38
WT	MRPL57	NP_076931.1	2.5	0.97	25
A354V	MRPL57	NP_076931.1	2	0.97	20

Y172C	MRPL57	NP_076931.1	1.6	0.96	16
WT	MRPL58	NP_001536.1	5.83	1	58.33
A354V	MRPL58	NP_001536.1	4.17	1	41.67
Y172C	MRPL58	NP_001536.1	4.4	0.99	44
WT	MRPL9	NP_113608.1	9.83	1	98.33
A354V	MRPL9	NP_113608.1	7.33	1	73.33
Y172C	MRPL9	NP_113608.1	11.2	1	112
WT	MRPS10	NP_060611.2	72.67	1	726.67
A354V	MRPS10	NP_060611.2	35.83	1	358.33
Y172C	MRPS10	NP_060611.2	32.4	1	324
WT	MRPS11	NP_073750.2	12	1	10.29
A354V	MRPS11	NP_073750.2	12.17	1	10.43
Y172C	MRPS11	NP_073750.2	10.4	1	8.91
A354V	MRPS12	NP_066930.1	3.17	1	28.5
WT	MRPS14	NP_071383.1	27.17	1	271.67
A354V	MRPS14	NP_071383.1	22.83	1	228.33
Y172C	MRPS14	NP_071383.1	30.4	1	304
A354V	MRPS15	NP_112570.2	5.83	1	58.33
Y172C	MRPS15	NP_112570.2	4.8	1	48
WT	MRPS16	NP_057149.1	36	1	360
A354V	MRPS16	NP_057149.1	30.67	1	306.67
Y172C	MRPS16	NP_057149.1	32.4	1	324
WT	MRPS17	NP_057053.1	25.83	1	258.33
A354V	MRPS17	NP_057053.1	17.33	1	173.33
Y172C	MRPS17	NP_057053.1	16.8	1	168
WT	MRPS18A	NP_060605.1	6.17	1	61.67
WT	MRPS18B	NP_054765.1	75	1	750
A354V	MRPS18B	NP_054765.1	51.83	1	518.33
Y172C	MRPS18B	NP_054765.1	56.2	1	562
WT	MRPS18C	NP_057151.1	11	1	110
A354V	MRPS18C	NP_057151.1	8.17	1	81.67
Y172C	MRPS18C	NP_057151.1	9.6	1	96
WT	MRPS2	NP_057118.1	158.33	1	1583.33
A354V	MRPS2	NP_057118.1	84.5	1	845
Y172C	MRPS2	NP_057118.1	109.4	1	1094
WT	MRPS21	NP_114107.1	10.83	1	8.48
A354V	MRPS21	NP_114107.1	11.67	1	9.13
WT	MRPS22	NP_064576.1	147.17	1	1471.67
A354V	MRPS22	NP_064576.1	111.33	1	1113.33
Y172C	MRPS22	NP_064576.1	113.6	1	1136
WT	MRPS23	NP_057154.2	115	1	1150

A354V	MRPS23	NP_057154.2	65.67	1	656.67
Y172C	MRPS23	NP_057154.2	69.6	1	696
WT	MRPS24	NP_114403.1	58.17	1	581.67
A354V	MRPS24	NP_114403.1	37.83	1	378.33
Y172C	MRPS24	NP_114403.1	44.6	1	446
WT	MRPS25	NP_071942.1	193.17	1	347.7
A354V	MRPS25	NP_071942.1	104.83	1	188.7
Y172C	MRPS25	NP_071942.1	102.4	1	184.32
WT	MRPS26	NP_110438.1	77.67	1	776.67
A354V	MRPS26	NP_110438.1	62.83	1	628.33
Y172C	MRPS26	NP_110438.1	67.8	1	678
WT	MRPS27	NP_055899.2	113	1	1130
A354V	MRPS27	NP_055899.2	81.17	1	811.67
Y172C	MRPS27	NP_055899.2	89.6	1	896
WT	MRPS28	NP_054737.1	179.67	1	1617
A354V	MRPS28	NP_054737.1	82	1	738
Y172C	MRPS28	NP_054737.1	72	1	648
WT	MRPS30	NP_057724.2	11.67	1	116.67
A354V	MRPS30	NP_057724.2	4.5	1	45
Y172C	MRPS30	NP_057724.2	4.8	1	48
WT	MRPS31	NP_005821.2	147.33	1	1473.33
A354V	MRPS31	NP_005821.2	94.67	1	946.67
Y172C	MRPS31	NP_005821.2	106	1	1060
WT	MRPS33	NP_444263.1	18.67	1	186.67
A354V	MRPS33	NP_444263.1	10.83	1	108.33
Y172C	MRPS33	NP_444263.1	13	1	130
WT	MRPS34	NP_076425.1	86.33	1	863.33
A354V	MRPS34	NP_076425.1	61.5	1	615
Y172C	MRPS34	NP_076425.1	80.2	1	802
WT	MRPS35	NP_068593.2	115	1	1150
A354V	MRPS35	NP_068593.2	83.5	1	835
Y172C	MRPS35	NP_068593.2	92.4	1	924
WT	MRPS36	NP_150597.1	22.83	1	228.33
A354V	MRPS36	NP_150597.1	16.33	1	163.33
Y172C	MRPS36	NP_150597.1	12	1	120
WT	MRPS5	NP_114108.1	115.5	1	1155
A354V	MRPS5	NP_114108.1	83.5	1	835
Y172C	MRPS5	NP_114108.1	122.6	1	1226
WT	MRPS6	NP_115865.1	50.5	1	505
A354V	MRPS6	NP_115865.1	34.83	1	348.33
Y172C	MRPS6	NP_115865.1	33.8	1	338

WT	MRPS7	NP_057055.2	98.33	1	983.33
A354V	MRPS7	NP_057055.2	70.5	1	705
Y172C	MRPS7	NP_057055.2	75.6	1	756
WT	MRPS9	NP_872578.1	150.83	1	1508.33
A354V	MRPS9	NP_872578.1	90.67	1	906.67
Y172C	MRPS9	NP_872578.1	99.8	1	998
WT	MTERF3	NP_057026.3	19.17	1	191.67
A354V	MTERF3	NP_057026.3	18.83	1	188.33
Y172C	MTERF3	NP_057026.3	17.8	1	178
A354V	MTG1	NP_612393.2	4	1	40
Y172C	MTG1	NP_612393.2	4.4	0.99	44
WT	MTHFD1L	NP_001229696.1	44.17	1	20.38
A354V	MTHFD1L	NP_001229696.1	22.67	0.99	10.46
Y172C	MTHFD1L	NP_001229696.1	22.8	0.97	10.52
WT	MTIF2	NP_002444.2	24.17	1	241.67
A354V	MTIF2	NP_002444.2	18	1	180
Y172C	MTIF2	NP_002444.2	17.4	1	174
WT	MTPAP	NP_060579.3	26.83	1	43.91
A354V	MTPAP	NP_060579.3	24.17	1	39.55
Y172C	MTPAP	NP_060579.3	32.6	1	53.35
Y172C	MTRF1	NP_004285.2	3.4	1	34
WT	MUT	NP_000246.2	1.83	0.98	18.33
WT	NDUFA12	NP_061326.1	53.33	1	533.33
A354V	NDUFA12	NP_061326.1	26	1	260
Y172C	NDUFA12	NP_061326.1	29	1	290
WT	NDUFA13	NP_057049.5	3	1	30
Y172C	NDUFA13	NP_057049.5	4.4	1	44
WT	NDUFA2	NP_002479.1	18.83	1	188.33
A354V	NDUFA2	NP_002479.1	12.83	1	128.33
Y172C	NDUFA2	NP_002479.1	11.6	1	116
WT	NDUFA5	NP_004991.1	29.67	1	48.55
A354V	NDUFA5	NP_004991.1	22.17	1	36.27
Y172C	NDUFA5	NP_004991.1	23.4	1	38.29
WT	NDUFA6	NP_002481.2	25.17	1	251.67
A354V	NDUFA6	NP_002481.2	12.67	1	126.67
Y172C	NDUFA6	NP_002481.2	21.6	1	216
WT	NDUFA7	NP_004992.2	40.67	1	406.67
A354V	NDUFA7	NP_004992.2	17	1	170
Y172C	NDUFA7	NP_004992.2	16.8	1	168

WT	NDUFA9	NP_004993.1	123	1	88.56
A354V	NDUFA9	NP_004993.1	65.67	1	47.28
Y172C	NDUFA9	NP_004993.1	59.4	1	42.77
WT	NDUFAF1	NP_057097.2	14.5	1	145
WT	NDUFAF2	NP_777549.1	16.67	1	166.67
A354V	NDUFAF2	NP_777549.1	5.33	1	53.33
Y172C	NDUFAF2	NP_777549.1	8	1	80
WT	NDUFAF3	NP_951032.1	4.67	1	46.67
A354V	NDUFAF3	NP_951032.1	2.5	0.98	25
WT	NDUFAF4	NP_054884.1	11.83	1	118.33
A354V	NDUFAF4	NP_054884.1	7.83	1	78.33
Y172C	NDUFAF4	NP_054884.1	4.8	1	48
WT	NDUFS1	NP_001186913.1	177.67	1	799.5
A354V	NDUFS1	NP_001186913.1	73.67	1	331.5
Y172C	NDUFS1	NP_001186913.1	78	1	351
WT	NDUFS2	NP_004541.1	135.33	1	1218
A354V	NDUFS2	NP_004541.1	65	1	585
Y172C	NDUFS2	NP_004541.1	59.6	1	536.4
WT	NDUFS3	NP_004542.1	75.5	1	339.75
A354V	NDUFS3	NP_004542.1	48.33	1	217.5
Y172C	NDUFS3	NP_004542.1	59.4	1	267.3
WT	NDUFS4	NP_002486.1	21.83	1	218.33
A354V	NDUFS4	NP_002486.1	10.33	1	103.33
Y172C	NDUFS4	NP_002486.1	11	1	110
WT	NDUFS6	NP_004544.1	35.5	1	355
A354V	NDUFS6	NP_004544.1	16.83	1	168.33
Y172C	NDUFS6	NP_004544.1	15.8	1	158
WT	NDUFS7	NP_077718.3	25	1	250
A354V	NDUFS7	NP_077718.3	19.33	1	193.33
Y172C	NDUFS7	NP_077718.3	15.2	1	152
WT	NDUFS8	NP_002487.1	20.5	1	205
A354V	NDUFS8	NP_002487.1	14.67	1	146.67
Y172C	NDUFS8	NP_002487.1	16.6	1	166
WT	NDUFV1	NP_009034.2	69.17	1	691.67
A354V	NDUFV1	NP_009034.2	39	1	390
Y172C	NDUFV1	NP_009034.2	38.4	1	384
WT	NDUFV2	NP_066552.2	27.67	1	276.67
A354V	NDUFV2	NP_066552.2	12.17	1	121.67
Y172C	NDUFV2	NP_066552.2	16.6	1	166

WT	NDUFV3	NP_066553.3	135.67	1	1356.67
A354V	NDUFV3	NP_066553.3	83.17	1	831.67
Y172C	NDUFV3	NP_066553.3	110.8	1	1108
WT	NFS1	NP_066923.3	29	1	290
A354V	NFS1	NP_066923.3	13.83	1	138.33
Y172C	NFS1	NP_066923.3	12.8	1	128
WT	NGRN	NP_001028260.2	4.5	1	45
A354V	NGRN	NP_001028260.2	2.17	0.99	21.67
WT	NIPSNAP1	NP_003625.2	10.67	1	64
A354V	NIPSNAP1	NP_003625.2	6.17	1	37
Y172C	NIPSNAP1	NP_003625.2	10.2	1	61.2
WT	NME4	NP_005000.1	30.17	1	135.75
A354V	NME4	NP_005000.1	19	1	85.5
Y172C	NME4	NP_005000.1	18	1	81
WT	NT5DC2	NP_075059.1	19.67	1	9.83
A354V	NT5DC2	NP_075059.1	20.67	1	10.33
Y172C	NT5DC2	NP_075059.1	20.2	1	10.1
A354V	NUBPL	NP_079428.2	1.83	0.98	18.33
WT	OAT	NP_000265.1	10	0.97	12
A354V	OAT	NP_000265.1	9.17	0.96	11
WT	OGDH	NP_002532.2	137.17	1	1371.67
A354V	OGDH	NP_002532.2	70.67	1	706.67
Y172C	OGDH	NP_002532.2	67	1	670
WT	OXA1L	NP_005006.3	5.17	1	51.67
WT	PAM16	NP_057153.8	6.17	1	61.67
Y172C	PAM16	NP_057153.8	3	0.99	30
WT	PDHA1	NP_001166925.1	8.67	0.97	12
WT	PDHB	NP_000916.2	8.5	0.99	15.3
WT	PDK1	NP_002601.1	3.83	1	38.33
WT	PDK3	NP_001135858.1	9.5	1	95
A354V	PDK3	NP_001135858.1	11.83	1	118.33
Y172C	PDK3	NP_001135858.1	12.4	1	124
WT	PDPR	NP_060460.4	2.17	0.99	21.67
A354V	PDSS1	NP_055132.2	2.33	1	23.33
Y172C	PDSS1	NP_055132.2	4	1	40
WT	PNPT1	NP_149100.2	17.33	1	173.33
A354V	PNPT1	NP_149100.2	11	1	110

Y172C	PNPT1	NP_149100.2	8.4	1	84
WT	POLDIP2	NP_056399.1	11.17	1	33.5
A354V	POLDIP2	NP_056399.1	31.17	1	93.5
Y172C	POLDIP2	NP_056399.1	34.6	1	103.8
WT	POLG	NP_001119603.1	4.5	1	45
WT	POLRMT	NP_005026.3	54.67	1	546.67
A354V	POLRMT	NP_005026.3	36.33	1	363.33
Y172C	POLRMT	NP_005026.3	45.2	1	452
WT	PPA2	NP_789845.1	3.17	1	31.67
A354V	PPA2	NP_789845.1	3.17	1	31.67
WT	PPIF	NP_005720.1	7.33	1	73.33
A354V	PPIF	NP_005720.1	9.33	1	93.33
Y172C	PPIF	NP_005720.1	14.8	1	148
A354V	PREPL	NP_001035844.1	8	1	80
Y172C	PREPL	NP_001035844.1	10	1	100
WT	PTCD3	NP_060422.4	209	1	2090
A354V	PTCD3	NP_060422.4	131.83	1	1318.33
Y172C	PTCD3	NP_060422.4	144.2	1	1442
WT	PUS1	NP_001002019.1	4.17	0.97	15
A354V	PUS1	NP_001002019.1	6.67	1	24
Y172C	PUS1	NP_001002019.1	7.8	1	28.08
WT	PYCR1	NP_008838.2	44.67	1	34.96
A354V	PYCR1	NP_008838.2	29.67	1	23.22
Y172C	PYCR1	NP_008838.2	23.2	0.99	18.16
WT	PYCR2	NP_037460.2	75.33	1	64.57
A354V	PYCR2	NP_037460.2	54.67	1	46.86
Y172C	PYCR2	NP_037460.2	49.6	1	42.51
WT	QRSL1	NP_060762.3	12.17	1	121.67
A354V	RARS2	NP_064716.2	15	1	54
Y172C	RARS2	NP_064716.2	15.8	0.98	56.88
WT	RBMX	NP_002130.2	42.67	0.97	4.31
WT	RCC1L	NP_110425.1	9	1	90
A354V	RCC1L	NP_110425.1	5.5	1	55
WT	RPUSD3	NP_775930.2	2.17	0.98	21.67
A354V	RPUSD3	NP_775930.2	4.83	1	48.33
WT	RPUSD4	NP_116184.2	11.17	1	111.67
A354V	RPUSD4	NP_116184.2	6.5	1	65

Y172C	RPUSD4	NP_116184.2	6.4	1	64
WT	RTN4IP1	NP_116119.2	8.5	1	85
WT	SDHB	NP_002991.2	5.5	1	55
Y172C	SDHB	NP_002991.2	5.4	1	54
WT	SHMT2	NP_005403.2	151	1	93.72
A354V	SHMT2	NP_005403.2	108.33	1	67.24
Y172C	SHMT2	NP_005403.2	98.4	1	61.08
WT	SLC30A9	NP_006336.3	4	1	40
A354V	SLC30A9	NP_006336.3	4.83	1	48.33
Y172C	SLC30A9	NP_006336.3	4.2	1	42
WT	SLIRP	NP_112487.1	287.67	1	2876.67
A354V	SLIRP	NP_112487.1	79.67	1	796.67
Y172C	SLIRP	NP_112487.1	70.6	1	706
WT	SSBP1	NP_001243439.	13	1	78
A354V	SSBP1	NP_001243439.	19.5	1	117
Y172C	SSBP1	NP_001243439.	18	1	108
WT	STOML2	NP_038470.1	10.67	0.97	5.49
A354V	STOML2	NP_038470.1	13.33	1	6.86
Y172C	STOML2	NP_038470.1	13	1	6.69
WT	SUCLA2	NP_003841.1	18.67	1	18.67
A354V	SUCLA2	NP_003841.1	10.67	0.99	10.67
Y172C	SUCLA2	NP_003841.1	8	0.93	8
WT	SUCLG1	NP_003840.2	6.17	0.96	11.1
WT	SUPV3L1	NP_003162.2	6.83	1	68.33
A354V	SUPV3L1	NP_003162.2	4	1	40
Y172C	SUPV3L1	NP_003162.2	3.2	0.99	32
WT	TACO1	NP_057444.2	31	1	279
A354V	TACO1	NP_057444.2	17.33	1	156
Y172C	TACO1	NP_057444.2	18.8	1	169.2
A354V	TBRG4	NP_001248763.	26.83	1	60.38
Y172C	TBRG4	NP_001248763.	30.6	1	68.85
WT	TEFM	NP_078959.3	4	1	40
A354V	TEFM	NP_078959.3	4.5	1	45
Y172C	TFB2M	NP_071761.1	2.2	0.98	22
WT	THEM4	NP_444283.2	8.17	1	81.67
A354V	THEM4	NP_444283.2	4.17	1	41.67
WT	TIMM44	NP_006342.2	35.67	1	321
A354V	TIMM44	NP_006342.2	32.67	1	294
Y172C	TIMM44	NP_006342.2	31	1	279
A354V	TOP3A	NP_004609.1	3.17	0.99	31.67
WT	TRMT10C	NP_060289.2	45	1	67.5

A354V	TRMT10C	NP_060289.2	33	1	49.5
Y172C	TRMT10C	NP_060289.2	29.6	1	44.4
WT	TRMT2B	NP_079193.2	3.67	1	36.67
A354V	TRMT2B	NP_079193.2	2.17	0.97	21.67
Y172C	TRMT2B	NP_079193.2	2.8	0.98	28
WT	TRMT5	NP_065861.2	3	0.99	30
WT	TRMT61B	NP_060380.3	6.67	0.99	66.67
WT	TRUB2	NP_056494.1	11.83	1	118.33
A354V	TRUB2	NP_056494.1	13.33	1	133.33
Y172C	TRUB2	NP_056494.1	8.2	1	82
WT	TSFM	NP_005717.3	3.5	0.95	15.75
A354V	TSFM	NP_005717.3	10.5	1	47.25
Y172C	TSFM	NP_005717.3	12.4	0.99	55.8
WT	UQCC1	NP_060714.3	6	1	60
A354V	UQCC1	NP_060714.3	6.5	1	65
Y172C	UQCC1	NP_060714.3	4	0.99	40
Y172C	UQCRFS1	NP_005994.2	4	0.97	18
WT	VARS2	NP_065175.4	13	1	78
WT	VWA8	NP_055873.1	55.17	1	165.5
A354V	VWA8	NP_055873.1	25.5	1	76.5
Y172C	VWA8	NP_055873.1	41.2	1	123.6
WT	WARS2	NP_056651.1	3.67	1	36.67
A354V	WARS2	NP_056651.1	4.5	1	45
WT	YARS2	NP_001035526.1	16.67	1	30
A354V	YARS2	NP_001035526.1	53.17	1	95.7
Y172C	YARS2	NP_001035526.1	50.4	1	90.72
WT	ZFR	NP_057191.2	29.83	1	6.39
A354V	ZFR	NP_057191.2	17.83	0.99	3.82

Table 5.1. Interacting partners of wild type (WT), A354V LRPPRC, and Y172C LRPPRC identified by BioID.

A)

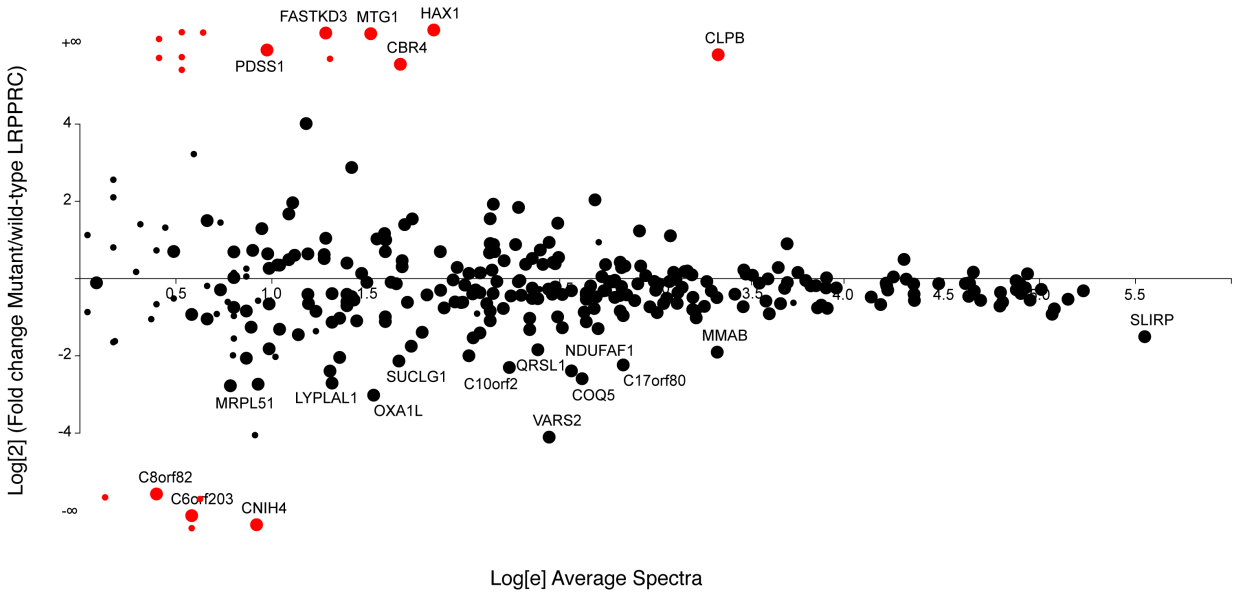
FASTKD3
MTG1
HAX1
CBR4
PDSS1
CLPB
SLIRP
MMAB
NDUFAF1
QRSL1
C17orf80
COQ5
SUCLG1
C10orf2
MRPL51
LYPLAL1
OXA1L
VARS2
C8orf82
C6orf203
CNIH4
+∞
4
2
-2
-4
-∞
0.5
1.0
4.0
4.5
5.5
Log[2] (Fold change Mutant/wild-type LRPPRC)
Log[e] Average Spectra

B)

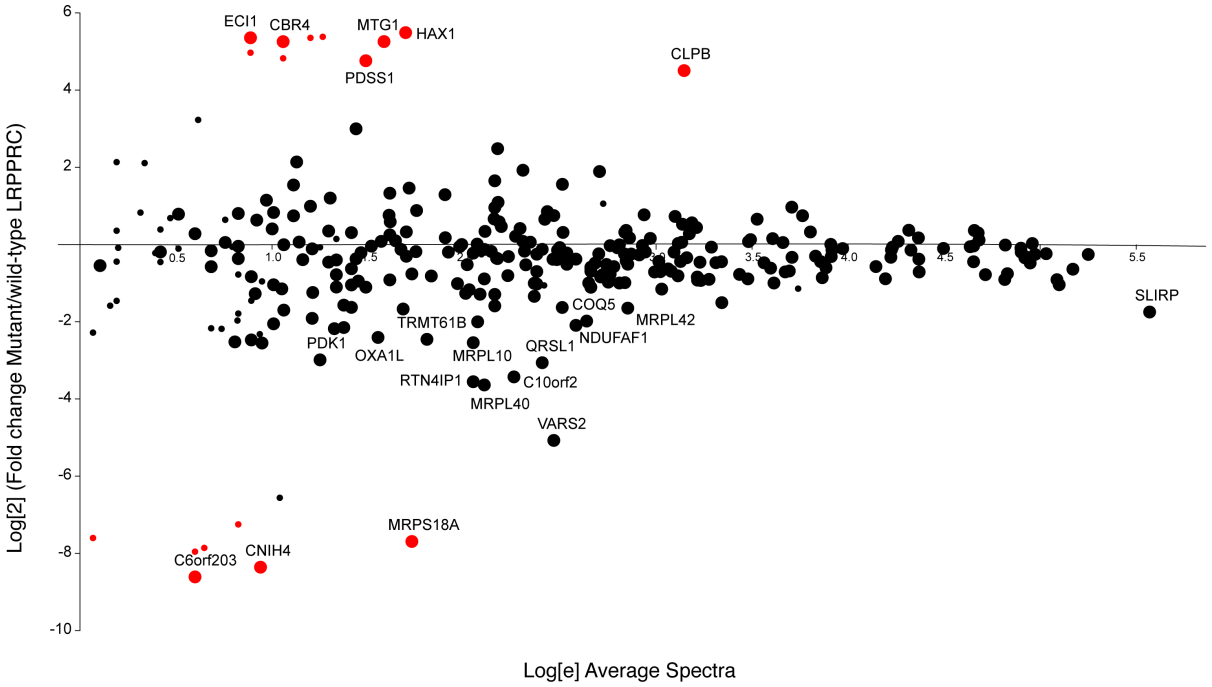
ECI1
CBR4
MTG1
HAX1
PDSS1
CLPB
SLIRP
COQ5
MRPL42
TRMT61B
NDUFAF1
PDK1
OXA1L
MRPL10
QRSL1
RTN4IP1
C10orf2
MRPL40
VARS2
MRPS18A
C6orf203
CNIH4
6
4
2
-2
-4
-6
-8
-10
0.5
1.0
4.0
4.5
5.5
Log[2] (Fold change Mutant/wild-type LRPPRC)
Log[e] Average Spectra

Figure 5.9. Identification of the interacting partners of A354V and Y172C LRPPRC variants using BioID. Panels A and B show the proteins that interact specifically with A354V and Y172C LRPPRC variants, respectively. The preys on the top of the scatter plot indicate proteins to which A354V or Y172C LRPPRC-BirA-FLAG specifically interact, whereas the preys on the bottom correspond to the proteins that only interact with wt LRPPRC-BirA-FLAG. The preys in the middle are found in both. The Y axis indicates the fold change of LRPPRC variant over the wild type, and the X axis represents the average spectra.

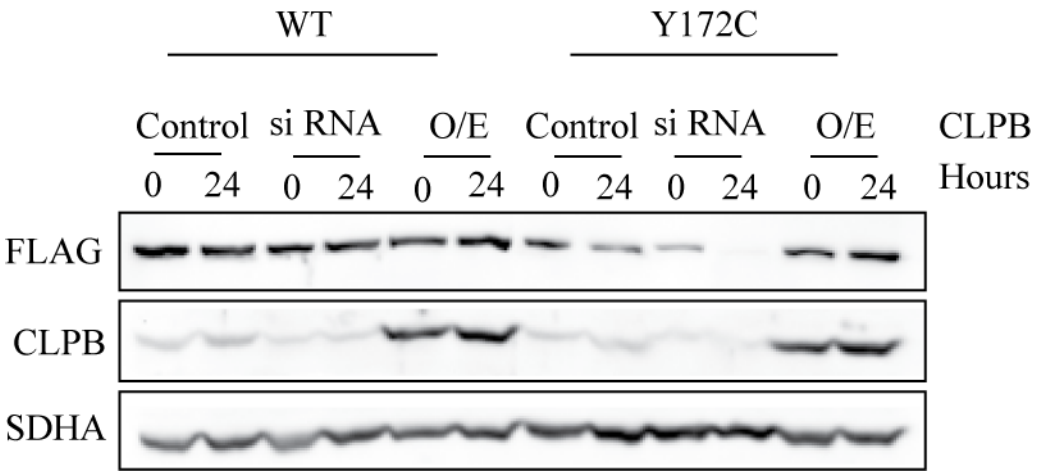
WT
Y172C
Control
si RNA
O/E
Control
si RNA
O/E
CLPB
0 24 0 24 0 24 0 24 0 24 0 24
Hours
FLAG
CLPB
SDHA

Figure 5.10. CLPB expression in 293 cells rescues the low level of Y172C LRPPRC. 293 cells stably expressing wt and Y172C LRPPRC-BirA-FLAG were transiently and stably transfected with siCLPB (- CLPB) and CLPB/pBabe (+ CLPB), respectively. Protein levels were determined from the cell lysates, and the protein stability was monitored at two time points (0 and 24 hours). The proteins were extracted using 1.5% DDM and subjected to 8% SDS-PAGE.

A)

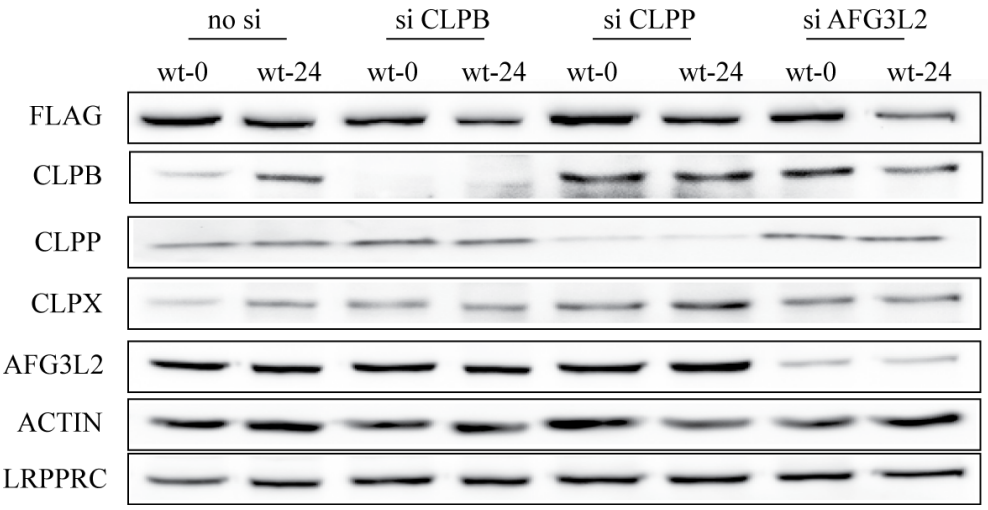
no si
si CLPB
si CLPP
si AFG3L2
wt-0
wt-24
wt-0
wt-24
wt-0
wt-24
wt-0
wt-24
FLAG
CLPB
CLPP
CLPX
AFG3L2
ACTIN
LRPPRC

B)

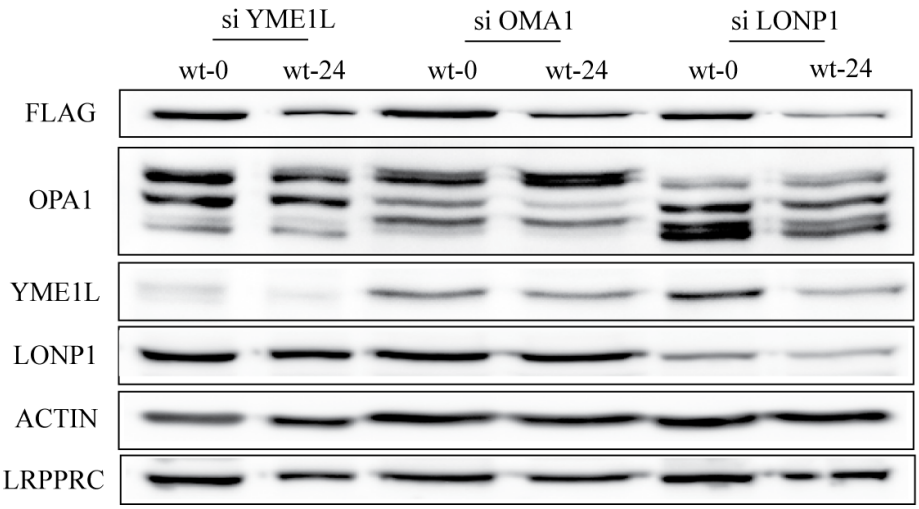
si YME1L
si OMA1
si LONP1
wt-0
wt-24
wt-0
wt-24
wt-0
wt-24
FLAG
OPA1
YME1L
LONP1
ACTIN
LRPPRC

C)

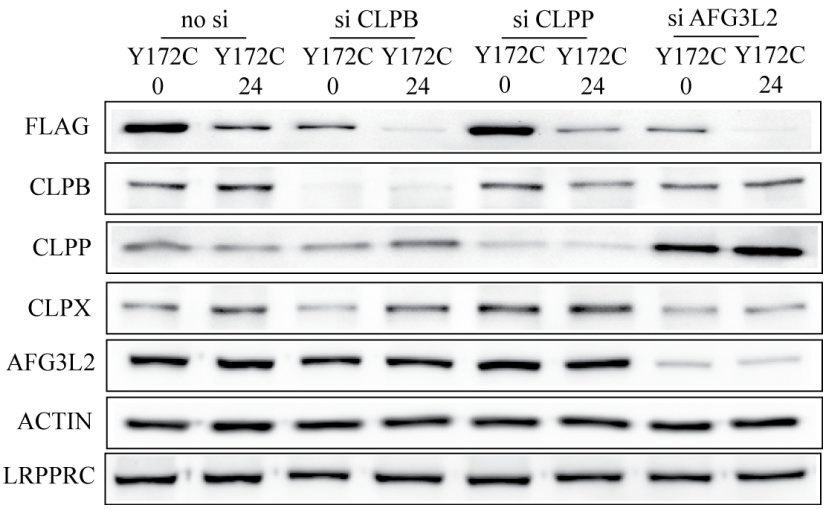
no si
si CLPB
si CLPP
si AFG3L2
Y172C Y172C Y172C Y172C Y172C Y172C Y172C Y172C
0 24 0 24 0 24 0 24
FLAG
CLPB
CLPP
CLPX
AFG3L2
ACTIN
LRPPRC

D)

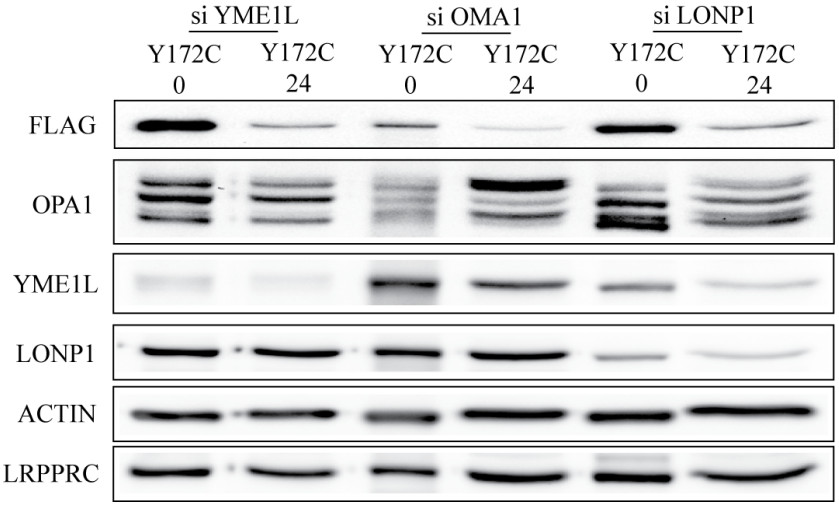
si YME1L
si OMA1
si LONP1
Y172C Y172C Y172C Y172C Y172C Y172C
0 24 0 24 0 24
FLAG
OPA1
YME1L
LONP1
ACTIN
LRPPRC

Figure 5.11. Loss of AFG3L2, OMA1, and CLPB decreases the stability of Y172C LRPPRC. 293 cells expressing wt LRPPRC-BirA-FLAG (A and B) and Y172C LRPPRC-BirA-FLAG (C and D) were transiently transfected with siRNAs for CLPB, CLPP, AFG3L2/SPG7, YME1L, OMA1, and LONP1. And the protein stability was monitored at two time points (0 and 24 hours). The proteins were extracted using 1.5% DDM and subjected to 8% SDS-PAGE. Each blot was probed with corresponding antibodies depending on the knock-down experiment that was carried out.

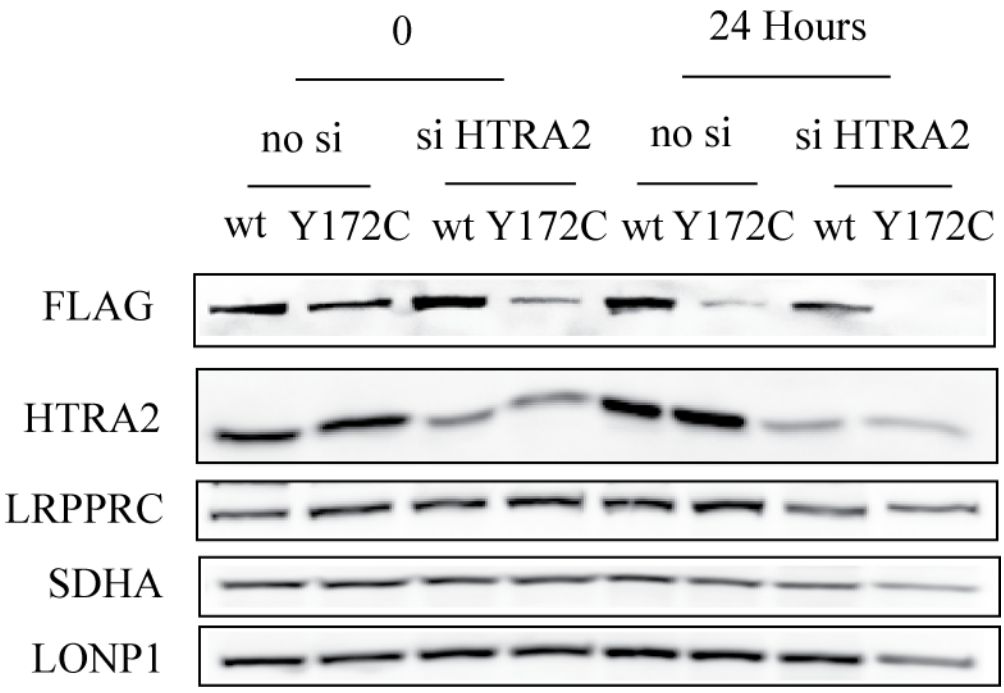
0
24 Hours
no si
si HTRA2
no si
si HTRA2
wt
Y172C
wt
Y172C
wt
Y172C
wt
Y172C
FLAG
HTRA2
LRPPRC
SDHA
LONP1

Figure 5.12. HTRA2, a mitochondrial IMS protease, is not involved in the degradation of Y172C LRPPRC. SDS-PAGE analysis of BirA-FLAG tagged wt and Y172C LRPPRC in the absence of HTRA2 (si HTRA2). Protein levels were determined from the cell lysates, and the protein stability was measured at two time points (0 and 24 hours). The proteins were extracted using 1.5% DDM and subjected to 8% SDS-PAGE.

A)

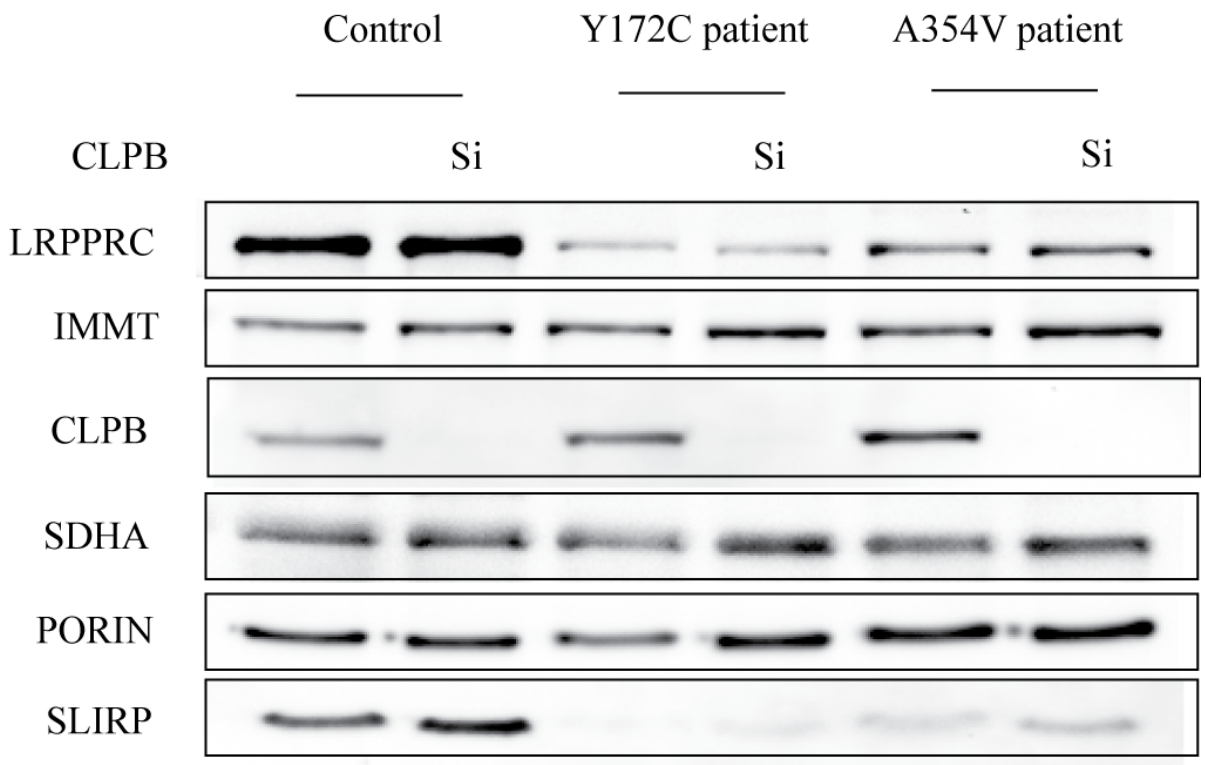
Control
Y172C patient
A354V patient
CLPB
Si
Si
Si
LRPPRC
IMMT
CLPB
SDHA
PORIN
SLIRP

B)

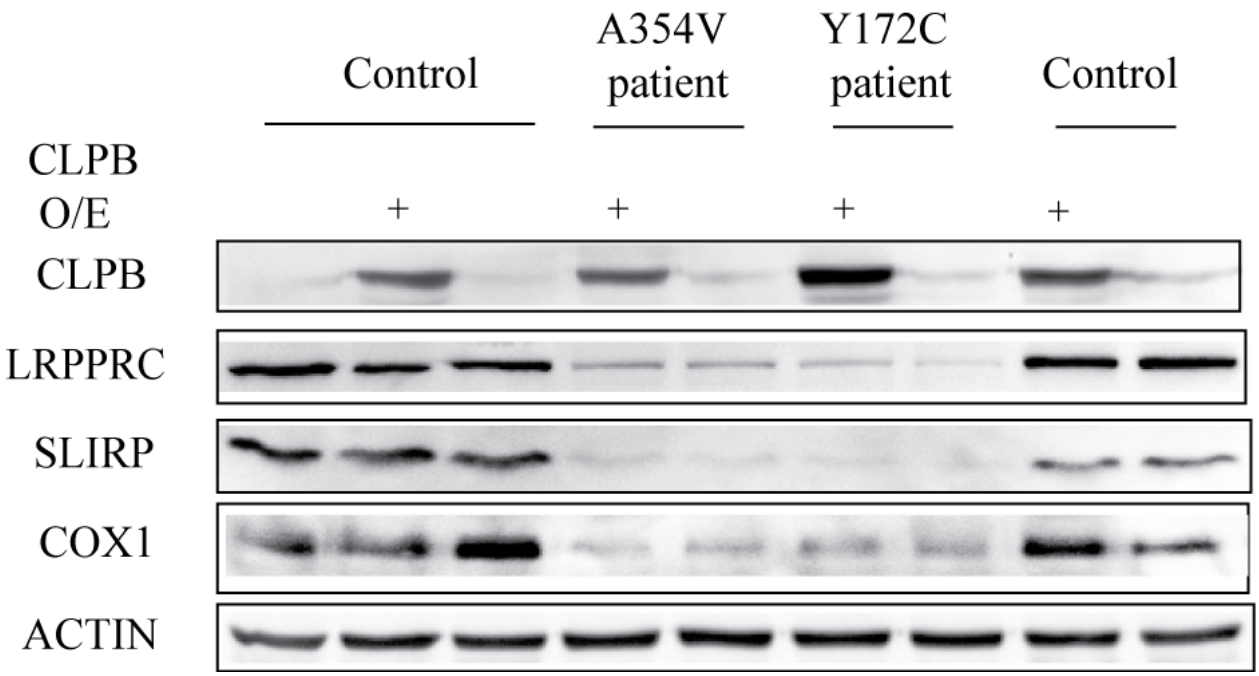
Control
A354V patient
Y172C patient
Control
CLPB O/E
+
+
+
+
CLPB
LRPPRC
SLIRP
COX1
ACTIN

C)

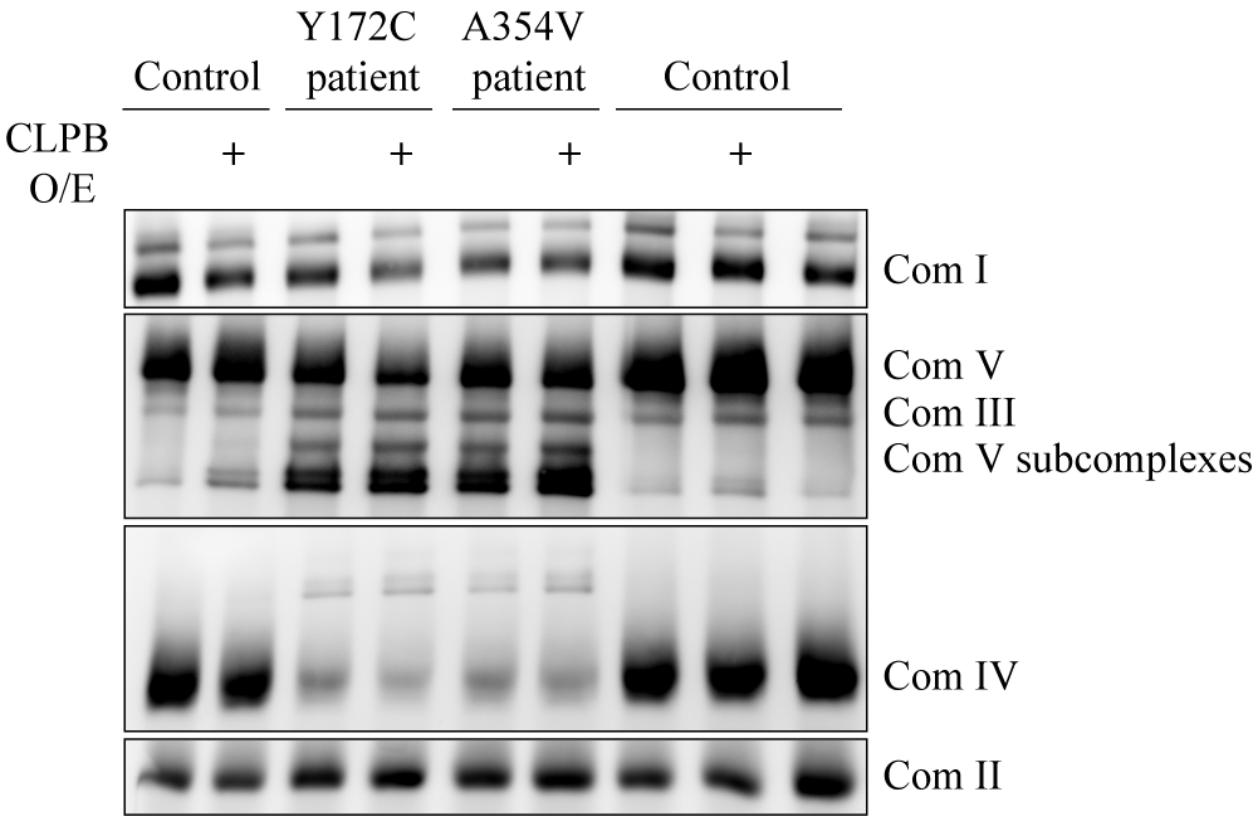
Control
Y172C patient
A354V patient
Control
CLPB O/E
+
+
+
+
Com I
Com V
Com III
Com V subcomplexes
Com IV
Com II

Figure 5.13. The biochemical defects of LRPPRC deficiency remains unaltered in LSFC fibroblasts expressing CLPB. Immunoblot analysis of LRPPRC, SLIRP, and COX I steady-state levels in control and LSFC subject fibroblasts (A) transiently transfected with si CLPB (- CLPB), (B) with CLPB expression (+ CLPB). Porin, Actin, and the complex II 70-KDa subunit were used as loading controls. (C) BN-PAGE analysis of the assembly of individual OXPHOS complexes in control and LSFC subject fibroblasts expressing CLPB (+ CLPB).

A)

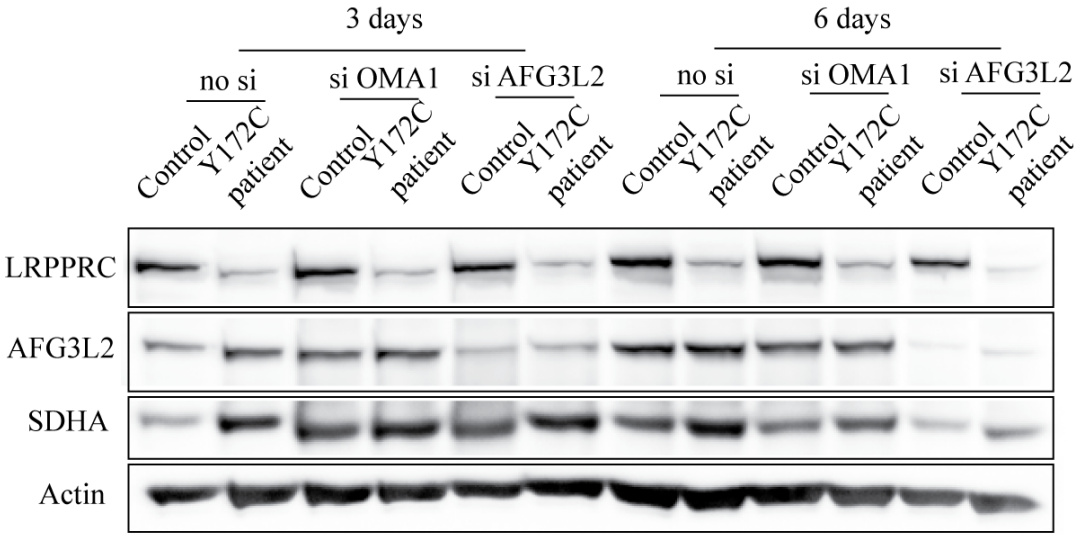
3 days
6 days
no si
si OMA1
si AFG3L2
no si
si OMA1
si AFG3L2
Control
Y172C patient
LRPPRC
AFG3L2
SDHA
Actin

B)

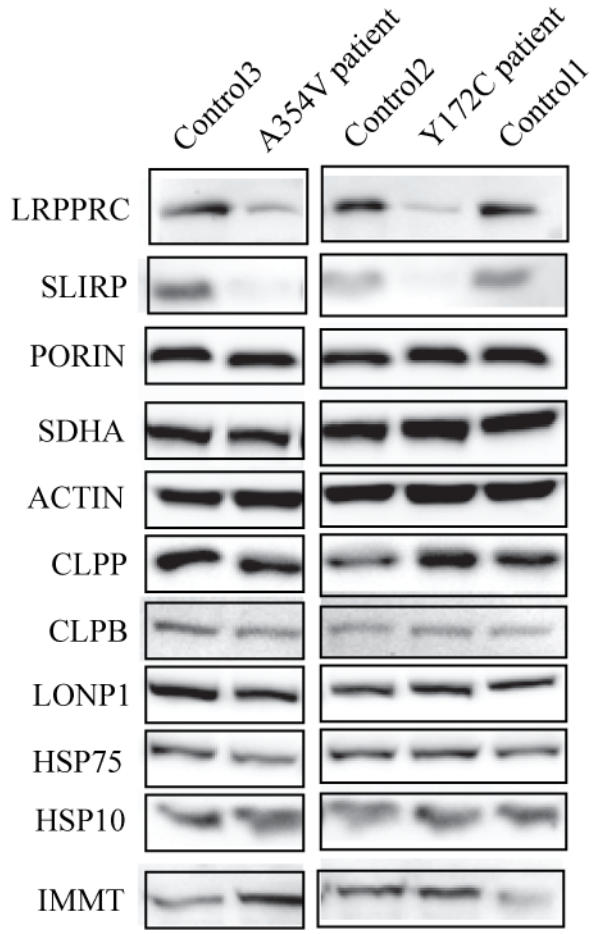
Control3
A354V patient
Control2
Y172C patient
Control1
LRPPRC
SLIRP
PORIN
SDHA
ACTIN
CLPP
CLPB
LONP1
HSP75
HSP10
IMMT

Figure 5.14. Monitoring the steady-state levels of a number of mitochondrial proteases in LSFC subject fibroblasts. (A) Immunoblot analysis of LRPPRC steady-state level in control and LSFC subject fibroblasts transiently transfected with si OMA1 and AFG3L2, (B) Immunoblot analysis of LRPPRC, SLIRP, CLPP, CLPB, LONP1, HSP75, and HSP10 steady-state levels in controls (1, 2, and 3) and LSFC subjects' fibroblasts (A354V and Y172C patients).

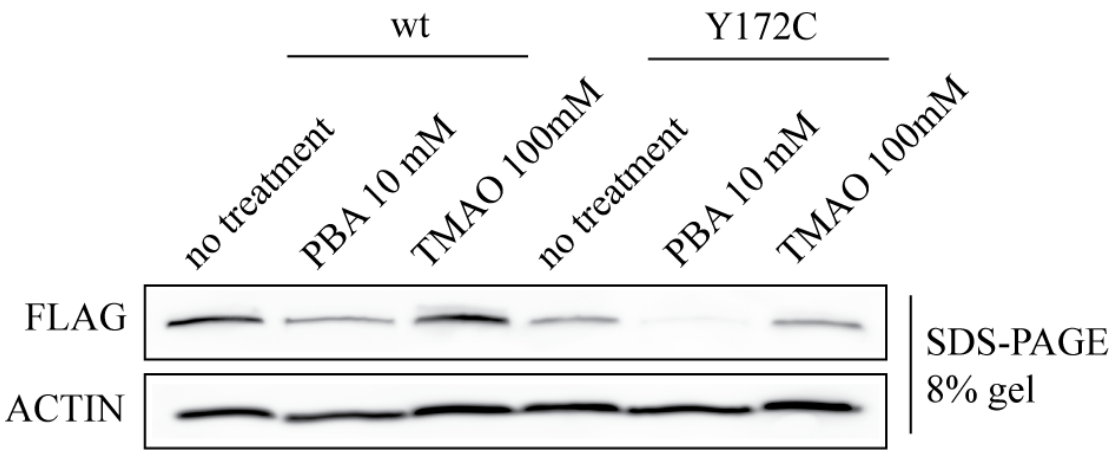
wt
Y172C
no treatment
PBA 10 mM
TMAO 100mM
no treatment
PBA 10 mM
TMAO 100mM
FLAG
ACTIN
SDS-PAGE
8% gel

Figure 5.15. Treating 293 cell line models with molecular chaperons fails to stabilize LRPPRC variant (Y172C). 293 cell lines (wt- and Y172C-LRPPRC-BirA-FLAG) were treated with two molecular chaperons, PBA and TMAO, and the whole cell extracts were subjected to 8% SDS-PAGE followed by immunoblotting with indicated antibodies. ACTIN is shown as a loading control.

Chapter 6 Discussion

6.1. Multifaceted mitochondrial phenotypes in liver-specific *Lrpprc* knock-out mice

We demonstrate a number of new insights into the function of LRPPRC, and our results reveal that specific loss of LRPPRC in the liver induces a generalized growth delay, macroscopic liver abnormalities, reduced levels of polyadenylated mitochondrial mRNAs, and CIV and CV assembly defects. LRPPRC deficiency in knock-out mice also leads to impairment of long-chain fatty acid oxidation, dysregulation of the mitochondrial permeability transition pore, and an alteration of trans-membrane H_2O_2 diffusion.

Complex V assembly defect observed in our conditional knock-out model is similar to that of published by [75], which demonstrated an assembly defect of CV in heart-specific *Lrpprc* knock-out mice. However, to date, no studies on LSFC subjects have reported complex V assembly defects. Indeed, the only observed deficiency is a severe or moderate reduction in CIV assembly in the liver and heart, and combined defects of CIV and CI in skeletal muscles [71] with no evidence of other OXPHOS complexes being affected. This difference could be explained by the presence of greater residual amounts of LRPPRC in patient tissues compared to knock-out mouse tissues, which would be sufficient to allow proper assembly of CV. However, we consider this possibility to be unlikely since upon knock-down of LRPPRC in patient fibroblasts, there was a globalized defect of all OXPHOS complexes, and not particularly CV [69]. Therefore, the CV assembly defect reported in the liver and heart likely represents a species-specific response to LRPPRC deficiency. We also show here that LRPPRC/SLIRP complex is detectable in all mouse tissues including liver, heart, and skeletal muscles, but in the human tissues investigated, this complex is only observed in the liver and skeletal muscles [71], which could indicate species-specific difference. Our results demonstrate the importance of LRPPRC in regulating the stability of some mt-mRNAs through polyadenylation. There is no

correlation between reduced steady-state levels of mt-mRNAs and the presence of poly A tail in Lrpprc$^{-/-}$ samples. For instance, the RNA level of COX1 and COX2 is significantly reduced and that the level remains constant for ND3, although all three transcripts lose their poly A tail in these mice.

The significant reduction of O_2 consumption observed in Lrpprc$^{-/-}$ mice could be due to disassembled CV rather than defects in CIV activity as the respiration was not altered in the presence of the uncoupling agent CCCP. However, BN-PAGE analysis of OXPHOS complexes suggests a very severe defect in CIV assembly. It is unlikely that low level of assembled CIV is due to the detergent extraction step as the results from immunohistochemistry of liver sections suggests a pronounced decrease in CIV activity in Lrpprc$^{-/-}$ mice.

In addition, we also demonstrated that the loss of LRPPRC induces a marked resistance to PTP opening that could be explained by complex V deficiency in Lrpprc$^{-/-}$ mice. The PTP located in the mitochondrial inner membrane plays an important role in the physiological regulation of ROS production, mitochondrial Ca^{2+} release, and cellular differentiation, as well as pathological activation of cell death [118], but the molecular components of PTP remain to be unequivocally determined. Perhaps CV acts as the core constituent of the PTP as suggested by recent studies in yeast and mammalian cell models [142-144]. A striking dysregulation of the PTP in a mouse model of primary complex V defect provides support for this model. Yet, it is unclear how CV shifts from an ATP synthetizing unit to a high conductance non-specific pore [122, 123]. One model proposes that the PTP forms at the interface of complex V dimers [122, 124]. At this level, several subunits of the F0 sector (a, e, f, g, and A6L) bind together, and stabilize the central c-ring of the F0 sector and the lateral stalk of the F-ATPase [125-128], which contributes to the formation of 86°-angled CV dimers that define areas of high membrane curvature at the level of cristae ridges [129-131]. In the presence of increased Ca^{2+}

concentrations, Ca^{2+} is suggested to displace Mg^{2+} from catalytic sites on the F1 sector. Under this condition, CV would adopt a conformation that induces pore formation at the interface between the two CV monomers [122, 124]. The exact mechanism of pore formation currently remains unclear. The c-ring was initially proposed as the pore-forming channel [132], but recent studies strongly argue against this possibility [133]. Subunits of the Fo sector that are required for the stabilization of CV dimers [134] could be the candidates [122] as recent studies suggest that knock-out of subunits e and g induces a strong resistance to PTP opening [135]. It is hypothesized that binding of CypD to CV induces a conformational change that facilitates pore formation [136, 137]. However, in our mouse model the steady-state levels of CypD were increased. It is possible that loss of mitochondrially-encoded subunits ATP6 and ATP8 (Fig. 3.4 and [138]) and potentially other associated Fo subunits may lead to alterations in the assembly between the Fo sector, and the peripheral stalk which prevents CypD binding from exerting its pore-promoting conformational changes. More detailed structure-function studies are required to elucidate the precise mechanisms involved.

Oxidative stress is considered a significant contributor to the pathogenesis of OXPHOS defects [139, 140]. Mitochondrial ROS production, and its consequences on signalling pathways, and mitochondrial/cellular injury is generally viewed as the result of a disequilibrium between the production of ROS by dysfunctional ETC complexes, and their elimination by various mitochondrial antioxidant systems. However, our results show the importance of considering mitochondrial membranes as potential diffusion barriers that can affect mito-cellular ROS dynamics in pathological states. Furthermore, loss of LRPPRC in the liver reduced the capacity of mitochondria to release and take-up H_2O_2. This effect occurred in the absence of major remodelling of key antioxidant enzymes (Catalase and SOD2) and was abolished by progressive permeabilization with small amounts of digitonin.

In fact, mitochondrial $O^{-\bullet}_2$ and H_2O_2 production was higher in LRPPRC-deficient mice when measured in inside-out sub-mitochondrial particles, suggesting that reduced membrane permeability to H_2O_2 in LRPPRC-deficient livers confined ROS to the mitochondrial compartment. It seems that changes in the lipid composition of membranes in LRPPRC-deficient mitochondria is the main factor responsible for the impaired diffusion of H_2O_2. Although the precise mechanism remains unclear, one possibility is that loss of membrane cholesterol, which is already present at low levels in mitochondrial membranes [141], contributes to the H_2O_2 diffusion impairment. It should however be noted that under normal healthy conditions, mitochondrial membranes may not constitute a major diffusion barrier, since in our experiments progressive permeabilization of mitochondrial membranes with digitonin did not reveal evidence of H_2O_2 trapping in wild-type mitochondria. Pathological loss of cholesterol and specific changes in the lipid composition of mitochondrial membranes may be required to observe a diffusion limitation.

In summary, our mouse model of hepatic LRPPRC deficiency reveals that genetic OXPHOS defects can be accompanied by broad phenotypic alterations. From a clinical perspective, our results also indicate that the investigation of PTP dysregulation is warranted in patients harbouring CV assembly defects. Furthermore, the substantial remodeling of the lipid composition of mitochondrial membranes in our mouse model suggests that membrane lipidomics should be performed in patients with genetic OXPHOS defects as this might assist diagnostic and have significant impact on mitochondrial functions and the disease phenotype.

6.2. Impact of LRPPRC deficiency on mt-mRNAs poly A tail in LSFC tissues

Post transcriptional regulation plays a key role in the expression of the mitochondrial genome. However, the mitochondrial genome encodes a small number of genes that are transcribed polycistronically. In this system, there are several RNA binding proteins (RBPs) that play a key role in stabilizing, degrading, or processing the corresponding RNAs. LRPPRC is one of the RBPs that is essential for the stability of several mt-mRNAs, and mutations in this protein lead to LSFC. In this view, LRPPRC has a high affinity with some mt-mRNAs and regulates their stability through promoting polyadenylation, but this is very tissue-specific as in our hands, the defect in polyadenylation was more severe in certain tissues. To date, despite all the efforts have been made in mitochondrial RNA processing, the precise role of LRPPRC still remains to be elucidated [69, 71, 74, 75, 145].

Mitochondrial polycistronic RNA gets processed in RNA granules, which are juxtaposed to mitochondrial nucleoids right after the transcription of mt-DNA [146]. In this paradigm, transcripts punctuated by tRNAs are immediately released by the activity of the processing enzymes RNase P and Z that cleave tRNAs at the 5′ and 3′ ends, respectively. Other RNAs such as ATP8/6, COX1, COX3, cytb, and ND5 are processed by FASTKD5 in RNA granules localized in the proximity to the nucleoid [147]. Mitochondrial RNA granules (MRGs) contain many protein components involved in RNA metabolism and ribosomal biogenesis [27, 148]. Several of the FAST proteins including FASTK, FASTKD1, FASTKD2, and FASTKD5 are found to be localized in mitochondrial MRGs as well as other RNA binding proteins such as RNase P, RNase Z, GRSF1, and hSuv3p-PNPase complex [146-151]. Our group characterized the proteome of the MRGs and showed several RNA binding proteins [147]. Of the list, two

RNA helicases DDX28 and DDX30 were demonstrated to be localized in MRGs and are shown to be required for mitochondrial ribosomal biogenesis [147].

As LRPPRC is not shown to be localized in MRGs, it seems evident that LRPPRC is involved in stabilizing a number of mature mitochondrial transcripts after they are processed in MRGs. However, the mRNA stabilization process could be either through promoting mt-mRNA polyadenylation or inhibiting the degradation of mt-mRNA, which occurs by SUV3-PNPase degradosome machinery [74]. What is perplexing is the fact that polyadenylation in human mitochondria has a different role compared to plant mitochondria, chloroplasts, and bacteria where mRNAs with elongated poly A tail are degraded by endonucleases [155]. Interestingly, polyadenylation in the nucleus is required for the stabilization and translation of the majority of the transcripts and occurs through a two-step process by which a *cis*-acting motif upstream of the polyadenylation site leads RNA binding proteins to cleave the site and polyadenylate the 3′ terminus [156]. However, human mitochondrial transcripts lack the *cis*-acting motif and the precise mechanism of polyadenylation needs to be investigated. It seems reasonable to suggest that LRPPRC binds to mitochondrial mRNA coding sequence [74] and stimulates the polyadenylation.

The results presented in this chapter demonstrate striking differences in the mt-mRNA poly A tail length in human tissues. The amplified products of MPAT assay for selected mt-mRNAs (COX1, COX2, and ND3) vary in size. Interestingly, in case of COX1 and COX2 mRNAs, the PCR amplifications resulted in smear in liver and heart and a single sharp band in skeletal muscles. Measuring the percentage of polyadenylated mRNAs, we show that COX1 and COX2 are always polyadenylated in skeletal muscles while the length of poly A tail is reduced to variable degrees in other tissues. This results further suggest the complex nature of post-transcriptional handling of mitochondrial mRNAs both amongst mRNAs and between tissues.

This could be due to a fact that tissues have alternative strategies to regulate the stability and substantially the expression of mitochondrial mRNAs depending on their need for OXPHOS subunits and the energy-demand.

Knowing that the addition of poly A is essential to complete the stop codon of several mitochondrial mRNAs, it needs to be elucidated whether polyadenylation is a signal for stability or degradation of mitochondrial mRNAs [157-160]. It seems reasonable to speculate that polyadenylation is a signal for stabilizing some transcripts, while oligoadenylation could trigger the degradation of other mt-mRNAs. When subjected to poly A tail length assay, the majority of COX1 mRNAs were shown to have truncated poly A tails in the liver without the presence of a single polyadenylated transcript. While in the heart, a significant percentage of transcripts were oligo or polyadenylated. In this model, if polyadenylation is the signal for stabilization, it seems evident that the steady-state level of COX1 mRNA is higher in heart compared to liver, and this was previously established by our group [71]. What is unexpected, however, is that in skeletal muscles, COX1 mRNA is all polyadenylated, but with an extremely low steady-state level. This could be due to the fact that in this particular case, polyadenylation is a signal for degradation.

The polyadenylation profile of COX2 in human tissues is very similar to COX1 with some minor differences. As such, COX2 is all polyadenylated in skeletal muscles, while in the heart the majority of the transcript is oligoadenylated with a small percentage lacking poly A tails. Interestingly, there is an equal distribution of poly or oligoadenylated COX2 mRNAs in the liver without the presence of a single nonadenylated transcript. Similar to COX1, the steady-state levels of COX2 was very low in skeletal muscles. Therefore, it is possible that mitochondrial mRNAs with long half-life are less abundant in skeletal muscles and more present in the liver. It is probably because in skeletal muscles the COX1 and COX2 translation products have longer half-lives that there is less need to generate mRNAs.

Moreover, we show that all three mitochondrial mRNAs tested in our experiments lose their poly A tails in LSFC subject tissues, further emphasizing the role of LRPPRC in maintaining mitochondrial mRNA poly A tail length. About 10% of COX1 mRNAs remain polyadenylated in LSFC heart, which could be explained by the presence of residual LRPPRC in this tissue. Interestingly, almost half of COX2 mRNAs are polyadenylated in LSFC skeletal muscles and heart, but the majority of the transcripts lack a poly A tail in the liver. For ND3, it is evident that loss of LRPPRC has very little impact on the polyadenylation as the population of nonadenylated ND3 mRNAs are not even increased in the skeletal muscles or heart.

In conclusion, loss of LRPPRC in LSFC subject tissues has a very different impact on polyadenylation profile of each mt-mRNA, which further complicates our understanding of the role of LRPPRC in mt-mRNA stability and polyadenylation. In addition, there are some populations of COX1, COX2, ND3 mRNAs with short and variable chain length terminated before the stop codon, which we labeled short fragments. If the short fragments are the products of mt-mRNA degradation, then in case of COX1, a small percentage of short fragments are only present in control liver and heart and absent in skeletal muscles, but this percentage is increased in all tissues of the LSFC subject. This suggests that LRPPRC may play a role in inhibiting the degradation of COX1 mRNA. However, this hypothesis is not true for COX2 and ND3 as the population of short fragments are only moderately increased in the liver but not in other tissues of the LSFC subject.

As shown by Temperley *et al* [121], COX1 and COX2 mRNAs are flanked by a 71- and 25-nucleotide 3′UTRs, respectively. Here, we show that the length of 3′UTR of COX1 and COX2 transcripts slightly varies in the tissues of LSFC subject. This suggests that loss of LRPPRC could have an impact on the chain length of the COX1 and COX2 3′ UTRs, but the exact mechanism remains to be discovered, as little is known about the role of mitochondrial

mRNA 3′UTRs. The features of mt-mRNAs 3′end including 3′ UTR and poly A tail length in human liver is inconsistent between mt-mRNAs. ND6, encoded by L-strand, is the only mt-mRNA lacking poly A tail, and probably its stability is regulated through other mechanisms. The reason why some mitochondrial mRNAs are flanked by 3′UTRs remains unclear. One possibility is that COX1 and COX2 require 3′ UTRs in addition to poly A tail to protect their ends from degradation. This may possibly be the reason why ND6 contains a large 3′UTR, since the ND6 3′end is not protected by poly A tail.

In conclusion, the work in this chapter leads us to two main conclusions. First, our data show that the way mt-mRNAs are polyadenylated is variable and tissue-specific. Second, the LRPPRC mutation leads to defect in polyadenylation of mitochondrial mRNAs.

6.3. Pathogenetic mechanisms of LRPPRC mutations in LSFC disease

Sasarman *et al* [71] demonstrated that siRNA mediated knock down of LRPPRC in control fibroblasts phenocopies the biochemical defects of LSFC. Therefore, we attempted to express *LRPPRC* cDNA in LSFC subject fibroblasts using retroviral expression vectors to correct the defects. What was unexpected, and remains to be elucidated, is that despite using various expression vectors (Figure 5.2 C), constructs (Figure 5.2 A-B), cell lines (Figure 5.3 D), or co-expressing both LRPPRC/SLIRP (Figure 5.3 A), the steady-state levels of LRPPRC, SLIRP, and COX1 proteins remained unchanged or barely increased in both control or LSFC subject fibroblasts. Even testing 293 cells in which the construct is flipped into the chromosome, we showed that BirA-FLAG tagged LRPPRC is expressed about 50% of the endogenous LRPPRC (Figure 5.5 A); however, longer treatment of the cells with tetracycline was not able to increase the levels more than 50% (Figure 5.5 B). We thus propose a model in which suggests that the levels of LRPPRC are tightly regulated at the post-transcriptional level. One possibility is that LRPPRC acts as an autoregulator of translation of its own mRNA as co-expressing LRPPRC/SLIRP in control fibroblasts leads to 3.5-fold increase at the mRNA level, but the protein level at its maximum is only enhanced by 1.4-fold. However, this model fails to explain why the levels of both LRPPRC mRNA and protein remains unchanged in LSFC fibroblasts co-expressing LRPPRC/SLIRP. It is also possible that other factors regulate the expression of LRPPRC by interacting to the untranslated regions of the mRNA and modulating the protein translation, but this remains to be investigated.

Our data demonstrate the importance of using human cell lines to understand the pathogenesis of LRPPRC variants in LSFC disease. Interestingly, using 293 cells, we show that the level of BirA- FLAG tagged LRPPRC variants is low compared to the wild-type protein, which happens due to the rapid turnover of the proteins carrying a pathogenic variant. As such, the half-life for wild type LRPPRC is about 26 hours compared to significantly lower number of 11 hours for Y172C LRPPRC. What is most extraordinary, is the fact that the BirA-FLAG tagged LRPPRC either wild-type or mutant localizes in mitochondria (Figure 5.4 C) and forms a stable complex with SLIRP (Figure 5.7 A-B). Thus, fusing 35 KDa BirA and 1 KDa FLAG tag to the c-terminus of LRPPRC does not interfere with the proper localization or the function of LRPPRC. Moreover, we show that the BirA-FLAG tagged A354V and Y172C LRPPRC is present in higher molecular weight bands in SDS-PAGE and forms small foci in mitochondria that could be because of the fact that the LRPPRC variants are incorporated into protein aggregates. A very low percentage of wt-LRPPRC-BirA-FLAG presents the same features including being incorporated into a higher molecular weight band and the formation of concentrated foci that requires to be further investigated.

wt-LRPPRC similar to LRPPRC variants is localized to the mitochondrial matrix and was shown to be associated with mitochondrial inner membrane (Figure 5.6 and 5.7 A-B). Interestingly, our BioID results show the interaction of the two IMS proteins, CLPB and HAX1, and several mitochondrial matrix proteins with A354V and Y172C LRPPRC, but wt-LRPPRC is only found to interact with matrix proteins. Amongst all the preys, CLPB was selected as an interacting partner of mutant LRPPRC for two reasons: a) the fold change is high, and the interaction is specific to LRPPRC variants compared to other preys, b) CLPB is involved in degradation or reactivation of misfolded proteins in bacteria [162, 163].

In addition to CLPB, we also found several other proteins that weakly interact with LRPPRC variants. Of the list, there are some heat shock proteins such as DnaJ Heat Shock Protein Family (HSP40) Member A3 (DNAJA3), Heat Shock Protein Family (HSP10) member 1 (HSPE1), several RNA binding proteins such as Fas Activated Serine-Threonine Kinase domain contain protein (FASTKD3), a mitochondrial RNA binding protein involved in post-transcriptional regulation of mitochondrial mRNAs [164], and DEAD box protein (DDX28), a mitochondrial RNA helicase [147]. Moreover, we found some enzymes and release factors involved in mitochondrial translation interacting with LRPPRC variants.

Significantly, reducing CLPB to the levels undetectable by immunoblotting further destabilized the Y172C LRPPRC while expressing CLPB increased the stability of the protein. The mechanism through which CLPB plays a role in the stability of Y172C LRPPRC remains to be investigated, but it appears that CLPB reactivates misfolded LRPPRC through its chaperone activity. We were, however, not able to convincingly demonstrate that Y172C LRPPRC is misfolded as treating cell lines with molecular chaperones failed to stabilize mutant LRPPRC (Figure 5.15). To our surprise, the defects in the level of LRPPRC or the assembly of the OXPHOS complexes in LSFC subject fibroblasts were not rescued in cell lines expressing CLPB. This could be due to the fact that we uncovered the effect of CLPB in 293 cells transiently expressing the LRPPRC, and the protein in LSFC subject fibroblasts has reached steady-state levels that may not be changed by increasing CLPB levels.

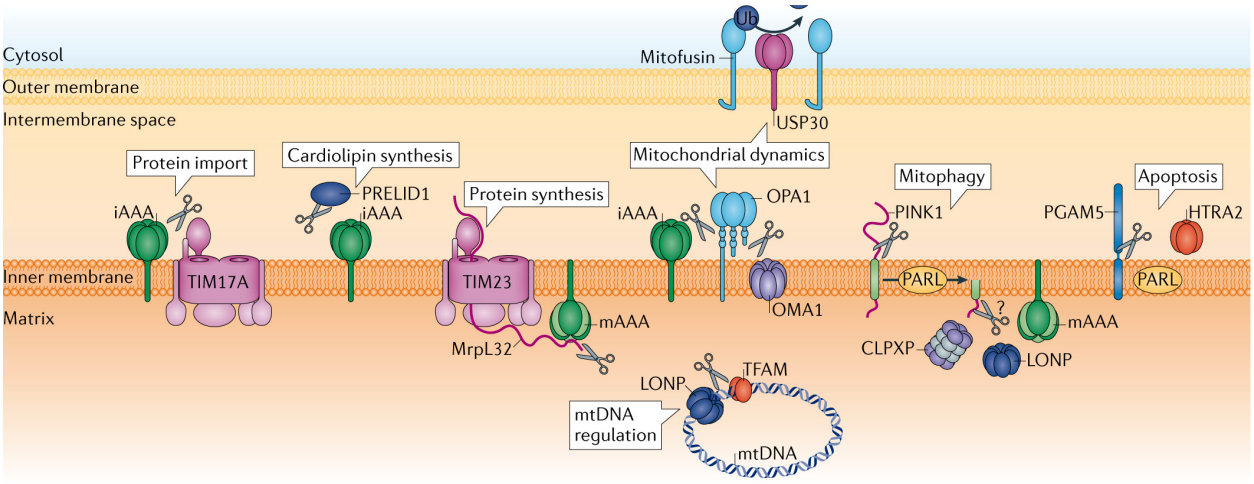
Cytosol
Outer membrane
Intermembrane space
Inner membrane
Matrix
Ub
Mitofusin
USP30
Protein import
iAAA
TIM17A
Cardiolipin synthesis
PRELID1
iAAA
Protein synthesis
TIM23
mAAA
MrpL32
Mitochondrial dynamics
iAAA
OPA1
OMA1
Mitophagy
PINK1
PARL
?
CLPXP
mAAA
LONP
Apoptosis
PGAM5
HTRA2
PARL
LONP
TFAM
mtDNA regulation
mtDNA

Figure 6.1. Schematic view of mitochondrial proteases regulating several mitochondrial functions. The proteases are localized in different mitochondrial compartment depending on their function. The inter membrane proteases CLPB and HTRA2 along with some of the matrix proteases LONP and CLPXP are indicated in black circles. The inner membrane proteases YME1L and OMA1 regulate mitochondrial dynamics by processing OPA1. The figure is from Quiros *et al* [165].

Knowing that LRPPRC variants are instable, it seemed reasonable to screen for some major components of mitochondrial quality control (Figure 6.1) to identify a protease that degrades Y172C LRPPRC. In fact, we demonstrate that CLPB is not the only mitochondrial protease affecting the stability of LRPPRC variant (Y172C). We show that Y172C LRPPRC-BirA FLAG almost completely disappears after being expressed for 24 hours in the absence of AFG3L2 and OMA1. In this condition, it is likely that the membrane potential is decreased as described by other groups [166], which could affect the stability of LRPPRC variants. Thus, it is possible that LRPPRC variants disappear from mitochondria through a mechanistic pathway rather than direct proteolytic activity of a single mitochondrial protease.

The work described here lays the foundation for the following studies: a) determining the regulatory mechanisms of LRPPRC expression, b) determining exactly how CLPB affects the stability of LRPPRC variants, c) determining the nature of the foci in 293 cells expressing LRPPRC variants.

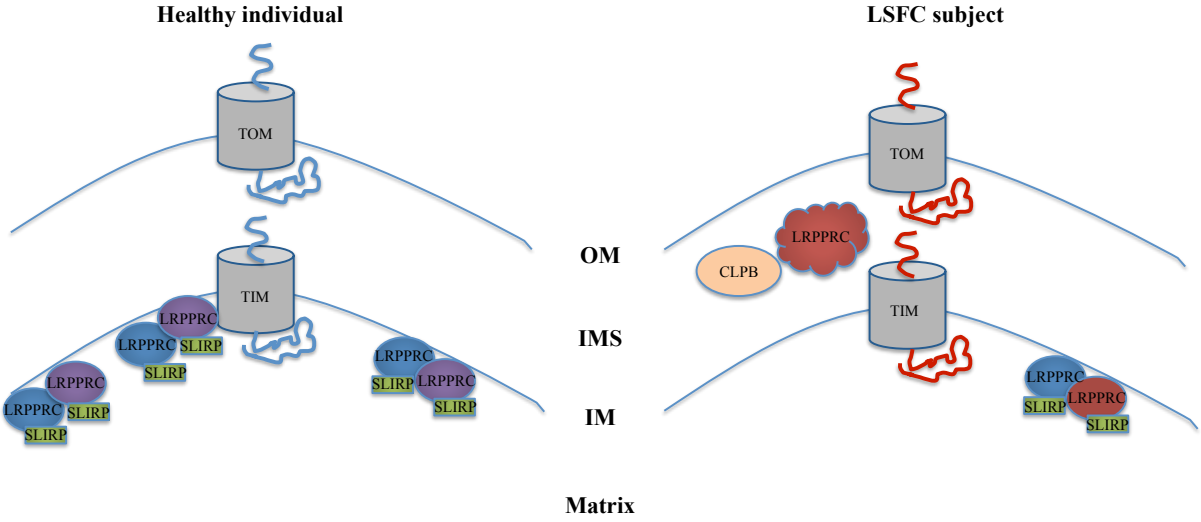
Healthy individual
LSFC subject
TOM
TIM
LRPPRC
SLIRP
CLPB
OM
IMS
IM
Matrix

24

Figure 6.2. Schematic view of a hypothetical model for the pathogenesis of LRPPRC variants. In healthy individual, LRPPRC is synthesized with N-terminal mitochondrial targeting sequence in cytoplasm. LRPPRC is then imported by translocase of the outer membrane (TOM) and translocase of the inner membrane (TIM) into the mitochondrial matrix where the N-terminal targeting sequence is cleaved and the mature protein forms a complex with SLIRP. In LSFC subject, LRPPRC carrying the pathogenic amino acid substitution is synthesized with N-terminal mitochondrial targeting sequence in cytoplasm, and it is imported by TOM; however, it gets stuck into the mitochondrial inter membrane space (IMS) due to potential folding problem. While the majority of the LRPPRC variant is degraded by the mitochondrial quality control system, CLPB refolds some proportion, and TIM imports the refolded LRPPRC carrying the pathogenic amino acid substitution into the mitochondrial matrix where the N-terminal targeting sequence is cleaved and the mature protein forms a complex with SLIRP.
Abbreviations: OM, outer membrane; IMS, inter membrane space; IM, inner membrane.

Chapter 7 Conclusions and future directions

The work in this thesis describes a) the role of LRPPRC in post-transcriptional handling of a subset of mitochondrial mRNAs as well as other mitochondrial pathways such as oxidation of long chain fatty acids, regulation of PTP, and ROS diffusion and b) the impact of amino acid substitutions on LRPPRC stability and function. These studies provide the molecular basis for the pathogenesis of LRPPRC variants in LSFC that could further help us to understand mitochondrial diseases using cell culture.

How LRPPRC impacts the stability of some mitochondrial mRNAs and how it is involved in polyadenylation of the majority of mitochondrial transcripts is less obvious. A recent study found that LRPPRC in complex with SLIRP impacts the RNA folding of mitochondrial transcriptome. Additionally, the same study found that LRPPRC/SLIRP complex acts as an RNA chaperon that binds to mitochondrial transcriptome with a preference to mt-mRNAs, and exposes the sites essential for translation, polyadenylation, and stabilization [145]. Thus, the role of LRPPRC in polyadenylation may be linked to RNA chaperone activity of this protein that makes the 3′ end sites of mitochondrial mRNAs recognizable by RNA binding proteins and mitochondrial poly A polymerase (MTPAP). This could potentially point out the function of LRPPRC in regulating the stability of mitochondrially encoded COX subunits mRNAs as LRPPRC defects in LSFC patients mainly leads to cytochrome *c* oxidase deficiency. How LRPPRC deficiency in the skeletal muscles of LSFC subjects affects the assembly of complex I in addition to complex IV is unclear and needs to be investigated.

Finally, the mechanisms underlying the pathogenesis of LSFC have not yet been fully elucidated. The chapter five of this thesis elaborates why the steady-state level of LRPPRC variants is low in LSFC patient fibroblasts, and more specifically, identifies the interacting partners of these variants. In fact, we demonstrate that the protein carrying pathogenic amino acid substitution has a significantly shorter half-life in 293 cells due to a putative folding

problem that could be rescued by CLPB expression. How CLPB stabilizes LRPPRC variants remains to be explained. CLPB has chaperone activity, and previous studies in *E. coli* suggests the involvement of CLPB in unfolding, disassembly and disaggregation. It is thus likely that the pathogenic amino acid substitution in LRPPRC introduces an unstable structure that is corrected by the chaperone activity of CLPB. But, this phenomenon is only observed when LRPPRC variants get expressed transiently in 293 cell lines expressing CLPB. Thus, it seems evident that mitochondrial quality control system actively degrades LRPPRC variants in LSFC fibroblasts, but the protease by which these proteins are targeted remains to be discovered. It should be noted that LRPPRC protein with tyrosine to cysteine substitution at position 172 is less stable compared to the founder effect pathogenic LRPPRC mutation (p. A354V) in the Quebec population. Both alanine and valine amino acids have hydrophobic side chain with similar properties, but cysteine is a small amino acid containing a sulfur hydride (SH) group and lacks the aromatic chain present in tyrosine. Thus, the p. Y172C substitution could distort the 3-dimensional structure of the protein to a severe degree and consequently get degraded faster.

In summary, understanding the function of LRPPRC and the interacting partners of the protein variants will likely improve our understanding of the disease pathogenesis and suggest a therapeutic intervention. In addition, BioID is a reliable technique that could be a key to understanding other neurodegenerative or rare disorders by discovering how protein interactomes in mitochondria are altered in disease states. I believe, the work in this thesis has a small but significant contribution in the understanding of LSFC disease pathogenesis.

Chapter 8 References

1. Mimaki M, Wang X, McKenzie M, Thorburn DR, Ryan MT. Understanding mitochondrial complex I assembly in health and disease. Biochim Biophys Acta. 2012 Jun;1817(6):851-62.
2. Hahn, Parey K, Bublitz M, Mills DJ, Zickermann V, Vonck J, Kühlbrandt W, Meier T. A. Structure of a Complete ATP Synthase Dimer Reveals the Molecular Basis of Inner Mitochondrial Membrane Morphology. Mol Cell, 2016. 63(3): p. 445-56.
3. Shmookler Reis, R.J. and S. Goldstein, Mitochondrial DNA in mortal and immortal human cells. Genome number, integrity, and methylation. J Biol Chem, 1983. 258(15): p. 9078-85.
4. Ylikallio, E. and A. Suomalainen, Mechanisms of mitochondrial diseases. Ann Med, 2012. 44(1): p. 41-59.
5. Grossman LI, Shoubridge EA (1996) Mitochondrial genetics and human disease. Bioessays 18: 983-91.
6. Satoh, M. and T. Kuroiwa, Organization of multiple nucleoids and DNA molecules in mitochondria of a human cell. Exp Cell Res, 1991. 196(1): p. 137-40.
7. Kukat C, Wurm CA, Spahr H, Falkenberg M, Larsson NG, Jakobs S. Super-resolution microscopy reveals that mammalian mitochondrial nucleoids have a uniform size and frequently contain a single copy of mtDNA. Proc Natl Acad Sci U S A. 2011;108(33):13534-9.
8. Bogenhagen DF, Rousseau D, Burke S. The layered structure of human mitochondrial DNA nucleoids. J Biol Chem. 2008;283(6):3665-75.
9. Arnberg, A., E.F. van Bruggen, and P. Borst, The presence of DNA molecules with a displacement loop in standard mitochondrial DNA preparations. Biochim Biophys Acta, 1971. 246(2): p. 353-7.

10. Hance, N., M.I. Ekstrand, and A. Trifunovic, Mitochondrial DNA polymerase gamma is essential for mammalian embryogenesis. Hum Mol Genet, 2005. 14(13): p. 1775-83.

11. Tyynismaa, H., Sembongi H, Bokori-Brown M, Granycome C, Ashley N, Poulton J, Jalanko A, Spelbrink JN, Holt IJ, Suomalainen A. Twinkle helicase is essential for mtDNA maintenance and regulates mtDNA copy number. Hum Mol Genet, 2004. 13(24): p. 3219-27.

12. Cerritelli, S.M., et al., Failure to produce mitochondrial DNA results in embryonic lethality in Rnaseh1 null mice. Mol Cell, 2003. 11(3): p. 807-15.

13. Simsek, D., et al., Crucial role for DNA ligase III in mitochondria but not in Xrcc1-dependent repair. Nature, 2011. 471(7337): p. 245-8.

14. Kasamatsu H, Vinograd J. Unidirectionality of replication in mouse mitochondrial DNA. Nat New Biol. 1973;241(108):103-5.

15. Yang MY, Bowmaker M, Reyes A, Vergani L, Angeli P, Gringeri E, Jacobs HT, Holt IJ. 2002. Biased incorporation of ribonucleotides on the mitochondrial L-strand accounts for apparent strand-asymmetric DNA replica- tion. Cell 111: 495–505.

16. Yasukawa T, Reyes A, Cluett TJ, Yang MY, Bowmaker M, Jacobs HT, Holt IJ. 2006. Replication of vertebrate mitochondrial DNA entails transient ribonucleotide incorporation throughout the lagging strand. EMBO J 25: 5358 – 5371

17 Holt, I.J., H.E. Lorimer, and H.T. Jacobs, Coupled leading- and lagging-strand synthesis of mammalian mitochondrial DNA. Cell, 2000. 100(5): p. 515-24.

18. Litonin D, Sologub M, Shi Y, Savkina M, Anikin M, Falkenberg M, et al. Human mitochondrial transcription revisited: only TFAM and TFB2M are required for transcription of the mitochondrial genes in vitro. J Biol Chem. 2010;285(24):18129-33.

19. Spelbrink, J.N., Functional organization of mammalian mitochondrial DNA in nucleoids: history, recent developments, and future challenges. IUBMB Life, 2010. 62(1): p. 19-32.

20. Ngo HB, Lovely GA, Phillips R, Chan DC. Distinct structural features of TFAM drive mitochondrial DNA packaging versus transcriptional activation. Nat Commun. 2014;5: 3077.

21. Fukuoh A, Ohgaki K, Hatae H, Kuraoka I, Aoki Y, Uchiumi T, Jacobs HT, Kang D. DNA conformation-dependent activities of human mitochondrial RNA polymerase. Genes Cells. 2009 Aug;14(8):1029-42.

22. Sologub M, Litonin D, Anikin M, Mustaev A, Temiakov D. TFB2 is a transient component of the catalytic site of the human mitochondrial RNA polymerase. Cell. 2009 Nov 25;139(5):934-44. doi: 10.1016/j.cell.2009.10.031.

23. Morozov YI, Parshin AV, Agaronyan K, Cheung AC, Anikin M, Cramer P, Temiakov D. A model for transcription initiation in human mitochondria. Nucleic Acids Res. 2015 Apr 20;43(7):3726-35.

24. Barshad G, Marom S, Cohen T, Mishmar D. Mitochondrial DNA Transcription and Its Regulation: An Evolutionary Perspective. Trends Genet. 2018.

25. Gustafsson, C.M., M. Falkenberg, and N.G. Larsson, Maintenance and Expression of Mammalian Mitochondrial DNA. Annu Rev Biochem, 2016. 85: p. 133-60.

26. Ojala, D., J. Montoya, and G. Attardi, tRNA punctuation model of RNA processing in human mitochondria. Nature, 1981. 290(5806): p. 470-4.

27. Antonicka, H., Sasarman F, Nishimura T, Paupe V, Shoubridge EA., The mitochondrial RNA-binding protein GRSF1 localizes to RNA granules and is required for posttranscriptional mitochondrial gene expression. Cell Metab, 2013. 17(3): p. 386-98.

28. Nagaike T, Suzuki T, Tomari Y, Takemoto-Hori C, Negayama F, Watanabe K, Ueda T. Identification and characterization of mammalian mitochondrial tRNA nucleotidyltransferases. J Biol Chem. 2001 Oct 26;276(43):40041-9.

29. Rose KM, Morris HP, Jacob ST. Mitochondrial poly(A) polymerase from a poorly differentiated hepatoma: purification and characteristics. Biochemistry. 1975;14(5):1025-32.

30. Mai, N., Z.M. Chrzanowska-Lightowlers, and R.N. Lightowlers, The process of mammalian mitochondrial protein synthesis. Cell Tissue Res, 2017. 367(1): p. 5-20.

31. O'Brien, T.W., The general occurrence of 55 S ribosomes in mammalian liver mitochondria. J Biol Chem, 1971. 246(10): p. 3409-17.

32. Amunts A, Brown A, Toots J, Scheres SHW, Ramakrishnan V. Ribosome. The structure of the human mitochondrial ribosome. Science. 2015;348(6230):95-8.

33. Greber BJ, Bieri P, Leibundgut M, Leitner A, Aebersold R, Boehringer D, Ban N. Ribosome. The complete structure of the 55S mammalian mitochondrial ribosome. Science. 2015 Apr 17;348(6232):303-8.

34. Benit, P., S. Lebon, and P. Rustin, Respiratory-chain diseases related to complex III deficiency. Biochim Biophys Acta, 2009. 1793(1): p. 181-5.

35. Koopman WJ, Distelmaier F, Smeitink JA, Willems PH. OXPHOS mutations and neurodegeneration. EMBO J. 2013 Jan 9;32(1):9-29.

36. Calvo, S.E., K.R. Clauser, and V.K. Mootha, MitoCarta2.0: an updated inventory of mammalian mitochondrial proteins. Nucleic Acids Res, 2016. 44(D1): p. D1251-7.

37. Lightowlers, R.N., R.W. Taylor, and D.M. Turnbull, Mutations causing mitochondrial disease: What is new and what challenges remain? Science, 2015. 349(6255): p. 1494-9.

38. Koopman, W.J., et al., Mitochondrial disorders in children: toward development of small-molecule treatment strategies. EMBO Mol Med, 2016. 8(4): p. 311-27.

39. Craven, L., et al., Recent Advances in Mitochondrial Disease. Annu Rev Genomics Hum Genet, 2017. 18: p. 257-275.28.

40. Wallace, D.C., Mitochondrial diseases in man and mouse. Science, 1999. 283(5407): p. 1482-8.

41. Sato, A., et al., Gene therapy for progeny of mito-mice carrying pathogenic mtDNA by nuclear transplantation. Proc Natl Acad Sci U S A, 2005. 102(46): p. 16765-70.

42. Tachibana M, Sparman M, Sritanaudomchai H, Ma H, Clepper L, Woodward J, Li Y, Ramsey C, Kolotushkina O, Mitalipov S. Mitochondrial gene replacement in primate offspring and embryonic stem cells. Nature. 2009 Sep 17;461(7262):367-72.

43. Slone, J., J. Zhang, and T. Huang, Experience from the First Live-Birth Derived From Oocyte Nuclear Transfer as a Treatment Strategy for Mitochondrial Diseases. J Mol Genet Med, 2017. 11(2).

44. Li Y, Huang TT, Carlson EJ, Melov S, Ursell PC, Olson JL, Noble LJ, Yoshimura MP, Berger C, Chan PH, Wallace DC, Epstein CJ. Dilated cardiomyopathy and neonatal lethality in mutant mice lacking manganese superoxide dismutase. Nat Genet. 1995 Dec;11(4):376-81.

45. Ruzzenente, B., A. Rotig, and M.D. Metodiev, Mouse models for mitochondrial diseases. Hum Mol Genet, 2016. 25(R2): p. R115-R122.

46. Dogan, S.A., et al., Tissue-specific loss of DARS2 activates stress responses independently of respiratory chain deficiency in the heart. Cell Metab, 2014. 19(3): p. 458-69.

47. Cerritelli, S.M., et al., Failure to produce mitochondrial DNA results in embryonic lethality in Rnaseh1 null mice. Mol Cell, 2003. 11(3): p. 807-15.

48. Lima, W.F., et al., Viable RNaseH1 knockout mice show RNaseH1 is essential for R loop processing, mitochondrial and liver function. Nucleic Acids Res, 2016. 44(11): p. 5299-312.

49. Leigh, D., Subacute necrotizing encephalomyelopathy in an infant. J Neurol Neurosurg Psychiatry, 1951. 14(3): p. 216-21.

50. Lake, N.J., et al., Leigh syndrome: neuropathology and pathogenesis. J Neuropathol Exp Neurol, 2015. 74(6): p. 482-92.

51. Shoubridge, E.A., Cytochrome c oxidase deficiency. American Journal of Medical Genetics, 2001. 106: p. 46-52.

52. Lake, N.J., et al., Leigh syndrome: One disorder, more than 75 monogenic causes. Ann Neurol, 2016. 79(2): p. 190-203.

53. Morin, C., et al., Clinical, metabolic, and genetic aspects of cytochrome C oxidase deficiency in Saguenay-Lac-Saint-Jean. Am J Hum Genet, 1993. 53(2): p. 488-96.

54. Merante, F., et al., A biochemically distinct form of cytochrome oxidase (COX) deficiency in the Saguenay-Lac-Saint-Jean region of Quebec. Am J Hum Genet, 1993. 53(2): p. 481-7.

55. Mootha, V.K., et al., Identification of a gene causing human cytochrome c oxidase deficiency by integrative genomics. Proc Natl Acad Sci U S A, 2003. 100(2): p. 605-10.

56. Debray, F.G., et al., LRPPRC mutations cause a phenotypically distinct form of Leigh syndrome with cytochrome c oxidase deficiency. J Med Genet, 2011. 48(3): p. 183-9.

57. Olahova, M., et al., LRPPRC mutations cause early-onset multisystem mitochondrial disease outside of the French-Canadian population. Brain, 2015. 138(Pt 12): p. 3503-19.

58. Han, V.X., et al., Novel LRPPRC Mutation in a Boy With Mild Leigh Syndrome, French-Canadian Type Outside of Quebec. Child Neurol Open, 2017. 4: p. 2329048X17737638.

59. Rackham, O. and A. Filipovska, The role of mammalian PPR domain proteins in the regulation of mitochondrial gene expression. Biochim Biophys Acta, 2012. 1819(9-10): p. 1008-16.

60. Rubinson, E.H. and B.F. Eichman, Nucleic acid recognition by tandem helical repeats. Curr Opin Struct Biol, 2012. 22(1): p. 101-9.

61. Barkan, A., et al., A combinatorial amino acid code for RNA recognition by pentatricopeptide repeat proteins. PLoS Genet, 2012. 8(8): p. e1002910.

62. Small, I.D. and N. Peeters, The PPR motif - a TPR-related motif prevalent in plant organellar proteins. Trends Biochem Sci, 2000. 25(2): p. 46-7.

63. Yin, P., et al., Structural basis for the modular recognition of single-stranded RNA by PPR proteins. Nature, 2013. 504(7478): p. 168-71.

64. Barkan, A. and I. Small, Pentatricopeptide repeat proteins in plants. Annu Rev Plant Biol, 2014. 65: p. 415-42.

65. Fujii, S. and I. Small, The evolution of RNA editing and pentatricopeptide repeat genes. New Phytol, 2011. 191(1): p. 37-47.

66. Schild, C., et al., Mitochondrial leucine tRNA level and PTCD1 are regulated in response to leucine starvation. Amino Acids, 2014. 46(7): p. 1775-83.

67. Perks, K.L., et al., PTCD1 Is Required for 16S rRNA Maturation Complex Stability and Mitochondrial Ribosome Assembly. Cell Rep, 2018. 23(1): p. 127-142.

68. Mili, S. and S. Pinol-Roma, LRP130, a pentatricopeptide motif protein with a noncanonical RNA-binding domain, is bound in vivo to mitochondrial and nuclear RNAs. Mol Cell Biol, 2003. 23(14): p. 4972-82.

69. Sasarman, F., et al., LRPPRC and SLIRP interact in a ribonucleoprotein complex that regulates posttranscriptional gene expression in mitochondria. Mol Biol Cell, 2010. 21(8): p. 1315-23.

70. Colley, S.M. and P.J. Leedman, SRA and its binding partners: an expanding role for RNA-binding coregulators in nuclear receptor-mediated gene regulation. Crit Rev Biochem Mol Biol, 2009. 44(1): p. 25-33.

71. Sasarman, F., et al., Tissue-specific responses to the LRPPRC founder mutation in French Canadian Leigh Syndrome. Hum Mol Genet, 2015. 24(2): p. 480-91.

72. Lagouge, M., et al., SLIRP Regulates the Rate of Mitochondrial Protein Synthesis and Protects LRPPRC from Degradation. PLoS Genet, 2015. 11(8): p. e1005423.

73. Gohil, V.M., et al., Mitochondrial and nuclear genomic responses to loss of LRPPRC expression. J Biol Chem, 2010. 285(18): p. 13742-7.

74. Chujo, T., et al., LRPPRC/SLIRP suppresses PNPase-mediated mRNA decay and promotes polyadenylation in human mitochondria. Nucleic Acids Res, 2012.

75. Ruzzenente, B., et al., LRPPRC is necessary for polyadenylation and coordination of translation of mitochondrial mRNAs. EMBO J, 2012. 31(2): p. 443-56.

76. Roux, K.J., et al., A promiscuous biotin ligase fusion protein identifies proximal and interacting proteins in mammalian cells. J Cell Biol, 2012. 196(6): p. 801-10.

77. Hance N, Ekstrand MI, Trifunovic A. Mitochondrial DNA polymerase gamma is essential for mammalian embryogenesis. Hum Mol Genet. 2005 Jul 1;14(13):1775-83.

78. Williams RS. Mitochondrial gene expression in mammalian striated muscle. Evidence that variation in gene dosage is the major regulatory event. J Biol Chem. 1986 Sep 15;261(26):12390-4.

79. Taylor RW, Turnbull DM. Mitochondrial DNA mutations in human disease. Nat Rev Genet. 2005 May;6(5):389-402.80

80. Tiranti V, Rossi E, Ruiz-Carrillo A, Rossi G, Rocchi M, DiDonato S, Zuffardi O, Zeviani M. Chromosomal localization of mitochondrial transcription factor A (TCF6), single-stranded DNA-binding protein (SSBP), and endonuclease G (ENDOG), three human housekeeping genes involved in mitochondrial biogenesis. Genomics. 1995 Jan 20;25(2):559-64.

81. Shokolenko IN, Alexeyev MF. Mitochondrial transcription in mammalian cells. Front Biosci (Landmark Ed). 2017 Jan 1;22: 835-853.

82. Morozov YI, Temiakov D. Human Mitochondrial Transcription Initiation Complexes Have Similar Topology on the Light and Heavy Strand Promoters. J Biol Chem. 2016 Jun 24;291(26):13432-5.

83. Posse V, Hoberg E, Dierckx A, Shahzad S, Koolmeister C, Larsson NG, Wilhelmsson LM, Hällberg BM, Gustafsson CM. The amino terminal extension of mammalian mitochondrial RNA polymerase ensures promoter specific transcription initiation. Nucleic Acids Res. 2014 Apr;42(6):3638-47.

84. Koenig MK. Presentation and diagnosis of mitochondrial disorders in children. Pediatr Neurol. 2008 May;38(5):305-13.

85. Hart PC, Mao M, de Abreu AL, Ansenberger-Fricano K, Ekoue DN, Ganini D, Kajdacsy-Balla A, Diamond AM, Minshall RD, Consolaro ME, Santos JH, Bonini MG. MnSOD

upregulation sustains the Warburg effect via mitochondrial ROS and AMPK-dependent signalling in cancer. Nat Commun. 2015 Feb 5; 6:6053.

86. Dogan SA, Pujol C, Maiti P, Kukat A, Wang S, Hermans S, Senft K, Wibom R, Rugarli EI, Trifunovic A. Tissue-specific loss of DARS2 activates stress responses independently of respiratory chain deficiency in the heart. Cell Metab. 2014 Mar 4;19(3):458-69.

87. Larsson NG, Wang J, Wilhelmsson H, Oldfors A, Rustin P, Lewandoski M, Barsh GS, Clayton DA. Mitochondrial transcription factor A is necessary for mtDNA maintenance and embryogenesis in mice. Nat Genet. 1998 Mar;18(3):231-6.

88. Kühl I, Kukat C, Ruzzenente B, Milenkovic D, Mourier A, Miranda M, Koolmeister C, Falkenberg M, Larsson NG. POLRMT does not transcribe nuclear genes. Nature. 2014 Oct 9;514(7521): E7-11.

89. Xu F, Ackerley C, Maj MC, Addis JB, Levandovskiy V, Lee J, Mackay N, Cameron JM, Robinson BH. Disruption of a mitochondrial RNA-binding protein gene results in decreased cytochrome b expression and a marked reduction in ubiquinol-cytochrome c reductase activity in mouse heart mitochondria. Biochem J. 2008 Nov 15;416(1):15-26.

90. Metodiev MD, Lesko N, Park CB, Cámara Y, Shi Y, Wibom R, Hultenby K, Gustafsson CM, Larsson NG. Methylation of 12S rRNA is necessary for in vivo stability of the small subunit of the mammalian mitochondrial ribosome. Cell Metab. 2009 Apr;9(4):386-97.

91. Paul E, Cronan R, Weston PJ, Boekelheide K, Sedivy JM, Lee SY, Wiest DL, Resnick MB, Klysik JE. Disruption of Supv3L1 damages the skin and causes sarcopenia, loss of fat, and death. Mamm Genome. 2009 Feb;20(2):92-108.

92. Metodiev MD, Spåhr H, Loguercio Polosa P, Meharg C, Becker C, Altmueller J, Habermann B, Larsson NG, Ruzzenente B. NSUN4 is a dual function mitochondrial

protein required for both methylation of 12S rRNA and coordination of mitoribosomal assembly. PLoS Genet. 2014 Feb 6;10(2): e100411.

93. Shoubridge EA (2001) Cytochrome c oxidase deficiency. Am J Med Genet 106: 46-52.

94. Robinson BH (2000) Human cytochrome oxidase deficiency. Pediatr Res 48: 581-5.

95. Burelle Y, Bemeur C, Rivard ME, Thompson Legault J, Boucher G; LSFC Consortium, Morin C, Coderre L, Des Rosiers C. Mitochondrial vulnerability and increased susceptibility to nutrient-induced cytotoxicity in fibroblasts from leigh syndrome French canadian patients. PLoS One. 2015 Apr 2;10(3): e0120767.

96. Thompson Legault J, Strittmatter L, Tardif J, Sharma R, Tremblay-Vaillancourt V, Aubut C, Boucher G, Clish CB, Cyr D, Daneault C, Waters PJ; LSFC Consortium, Vachon L, Morin C, Laprise C, Rioux JD, Mootha VK, Des Rosiers C. A Metabolic Signature of Mitochondrial Dysfunction Revealed through a Monogenic Form of Leigh Syndrome. Cell Rep. 2015 Nov 3;13(5):981-9.

97. Cuillerier A, Honarmand S, Cadete VJJ, Ruiz M, Forest A, Deschênes S, Beauchamp C; LSFC Consortium, Charron G, Rioux JD, Des Rosiers C, Shoubridge EA, Burelle Y. Loss of hepatic LRPPRC alters mitochondrial bioenergetics, regulation of permeability transition and trans-membrane ROS diffusion. Hum Mol Genet. 2017 Aug 15;26(16): 3186-3201.

98. Bradford MM. A rapid and sensitive method for the quantitation of microgram quantities of protein utilizing the principle of protein-dye binding. Anal Biochem. 1976;72:248-54.

99. Schagger H, von Jagow G. Blue native electrophoresis for isolation of membrane protein complexes in enzymatically active form. Anal Biochem. 1991;199(2):223-31.

100. Schagger H, von Jagow G. Tricine-sodium dodecyl sulfate-polyacrylamide gel electrophoresis for the separation of proteins in the range from 1 to 100 kDa. Anal Biochem. 1987;166(2):368-79.

101. Temperley RJ, Seneca SH, Tonska K, Bartnik E, Bindoff LA, Lightowlers RN, et al. Investigation of a pathogenic mtDNA microdeletion reveals a translation-dependent deadenylation decay pathway in human mitochondria. Hum Mol Genet. 2003;12(18):2341-8.

102. Picard M, Azuelos I, Jung B, Giordano C, Matecki S, Hussain S, White K, Li T, Liang F, Benedetti A, Gentil BJ, Burelle Y, Petrof BJ. Mechanical ventilation triggers abnormal mitochondrial dynamics and morphology in the diaphragm. J Appl Physiol (1985). 2015 May 1;118(9):1161-71.

103. Cadete VJ, Deschênes S, Cuillerier A, Brisebois F, Sugiura A, Vincent A,Turnbull D, Picard M, McBride HM, Burelle Y. Formation of mitochondrial-derived vesicles is an active and physiologically relevant mitochondrial quality control process in the cardiac system. J Physiol. 2016 Sep 15;594(18):5343-62. doi:10.1113/JP272703. Epub 2016 Jul 24.

104. DiMauro S, Schon EA. Mitochondrial disorders in the nervous system. Annu Rev Neurosci. 2008; 31:91-123.

105. Rahman S, Blok RB, Dahl HH, Danks DM, Kirby DM, Chow CW, Christodoulou J, Thorburn DR. Leigh syndrome: clinical features and biochemical and DNA abnormalities. Ann Neurol. 1996 Mar;39(3):343-51.

106. Zhu Z, Yao J, Johns T, Fu K, De Bie I, Macmillan C, Cuthbert AP, Newbold RF, Wang J, Chevrette M, Brown GK, Brown RM, Shoubridge EA. SURF1, encoding a factor involved in the biogenesis of cytochrome c oxidase, is mutated in Leigh syndrome. Nat Genet. 1998 Dec;20(4):337-43.

107. Marcil M, Ascah A, Matas J, Bélanger S, Deschepper CF, Burelle Y. Compensated volume overload increases the vulnerability of heart mitochondria without affecting their functions in the absence of stress. J Mol Cell Cardiol. 2006 Dec;41(6):998-1009.

108. Matas J, Young NT, Bourcier-Lucas C, Ascah A, Marcil M, Deschepper CF, Burelle Y. Increased expression and intramitochondrial translocation of cyclophilin-D associates with increased vulnerability of the permeability transition pore to stress-induced opening during compensated ventricular hypertrophy. J Mol Cell Cardiol. 2009 Mar;46(3):420-30.

109. Emaus RK, Grunwald R, Lemasters JJ. Rhodamine 123 as a probe of transmembrane potential in isolated rat-liver mitochondria: spectral and metabolic properties. Biochim Biophys Acta. 1986 Jul 23;850(3):436-48.

110. Godin R, Daussin F, Matecki S, Li T, Petrof BJ, Burelle Y. Peroxisome proliferator-activated receptor γ coactivator1- gene α transfer restores mitochondrial biomass and improves mitochondrial calcium handling in post-necrotic mdx mouse skeletal muscle. J Physiol. 2012 Nov 1;590(21):5487-502.

111. Pon L.A., Schon E.A. (2017) Mitochondria 2nd edn. Academic Press, 944 p, ISBN-13: 978-0125441735.

112. Matyash V, Liebisch G, Kurzchalia TV, Shevchenko A, Schwudke D. Lipid extraction by methyl-tert-butyl ether for high-throughput lipidomics. J Lipid Res. 2008 May;49(5):1137-46.

113. Sandra K, Pereira Ados S, Vanhoenacker G, David F, Sandra P. Comprehensive blood plasma lipidomics by liquid chromatography/quadrupole time-of-flight mass spectrometry. J Chromatogr A. 2010 Jun 18;1217(25):4087-99

114. Couzens AL, Knight JD, Kean MJ, Teo G, Weiss A, Dunham WH, Lin ZY, Bagshaw RD, Sicheri F, Pawson T, Wrana JL, Choi H, Gingras AC. Protein interaction network of the mammalian Hippo pathway reveals mechanisms of kinase-phosphatase interactions. Sci Signal. 2013 Nov 19;6(302):rs15.

115. Leary SC, Sasarman F, Nishimura T, Shoubridge EA. Human SCO2 is required for the synthesis of CO II and as a thiol-disulphide oxidoreductase for SCO1. Hum Mol Genet. 2009 Jun 15;18(12):2230-40.

116. Schindelin J, Arganda-Carreras I, Frise E, Kaynig V, Longair M, Pietzsch T, Preibisch S, Rueden C, Saalfeld S, Schmid B et al (2012) Fiji: an open-source platform for biological-image analysis. Nat Methods 9: 676–682.

117. Diaz F, Garcia S, Hernandez D, Regev A, Rebelo A, Oca-Cossio J, et al. Pathophysiology and fate of hepatocytes in a mouse model of mitochondrial hepatopathies. Gut. 2008;57(2):232-42.

118. Kwong JQ, Molkentin JD. Physiological and pathological roles of the mitochondrial permeability transition pore in the heart. Cell Metab. 2015 Feb 3;21(2):206-214.

119. Dreyfus M, Régnier P. The poly(A) tail of mRNAs: bodyguard in eukaryotes, scavenger in bacteria. Cell. 2002 Nov 27;111(5):611-3.

120. Gagliardi D, Stepien PP, Temperley RJ, Lightowlers RN, Chrzanowska-Lightowlers ZM. Messenger RNA stability in mitochondria: different means to an end. Trends Genet. 2004 Jun;20(6):260-7. Review. Erratum in: Trends Genet. 2005 Jan;21(1):36.

121. Temperley RJ, Wydro M, Lightowlers RN, Chrzanowska-Lightowlers ZM. Human mitochondrial mRNAs-like members of all families, similar but different. Biochim Biophys Acta. 2010;1797(6-7):1081-5.

122. Bernardi P, Di Lisa F, Fogolari F, Lippe G. From ATP to PTP and Back: A Dual Function for the Mitochondrial ATP Synthase. Circ Res. 2015 May 22;116(11):1850-62.

123. Solesio ME, Elustondo PA, Zakharian E, Pavlov EV. Inorganic polyphosphate (poly P) as an activator and structural component of the mitochondrial permeability transition pore. Biochem Soc Trans. 2016 Feb; 44(1):7-12.

124. Bernardi P. The mitochondrial permeability transition pore: a mystery solved? Front Physiol. 2013 May 10; 4:95.

125. Spannagel C., Vaillier J., Arselin G., Graves P.V., Grandier-Vazeille X., Velours J. (1998) Evidence of a subunit 4 (subunit b) dimer in favor of the proximity of ATP synthase complexes in yeast inner mitochondrial membrane. Biochim. Biophys. Acta, 1414, 260–264.

126. Everard-Gigot V., Dunn C.D., Dolan B.M., Brunner S., Jensen R.E., Stuart R.A. (2005) Functional analysis of subunit e of the F1Fo-ATP synthase of the yeast *Saccharomyces cerevisiae*: importance of the N-terminal membrane anchor region. Eukaryotic Cell, 4, 346–355.

127. Bisetto E., Picotti P., Giorgio V., Alverdi V., Mavelli I., Lippe G. (2008) Functional and stoichiometric analysis of subunit e in bovine heart mitochondrial F0F1ATP synthase. J. Bioenerg. Biomembr., 40, 257–267.

128. Bustos D.M. (2005) The modification of the conserved GXXXG motif of the membrane-spanning segment of subunit g destabilizes the supramolecular species of yeast ATP synthase. J. Biol. Chem., 280, 29004–29010.

129. Davies K.M., Strauss M., Daum B., Kief J.H., Osiewacz H.D., Rycovska A., Zickermann V., Kühlbrandt W. (2011) Macromolecular organization of ATP synthase and complex I in whole mitochondria. Proc. Natl Acad. Sci. U S A, 108, 14121–14126.

130. Davies K.M., Anselmi C., Wittig I., Faraldo-Gómez J.D., Kühlbrandt W. (2012) Structure of the yeast F1Fo-ATP synthase dimer and its role in shaping the mitochondrial cristae. Proc Natl Acad Sci U S A, 109, 13602–13607.

131. Strauss M., Hofhaus G., Schröder R.R., Kühlbrandt W. (2008) Dimer ribbons of ATP synthase shape the inner mitochondrial membrane. embo J., 27, 1154–1160.

132. Alavian K.N., Beutner G., Lazrove E., Sacchetti S., Park H.A., Licznerski P., Li H., Nabili P., Hockensmith K., Graham M. et al. (2014) An uncoupling channel within the c-subunit ring of the F1FO ATP synthase is the mitochondrial permeability transition pore. Proc. Natl Acad. Sci. U S A, 111, 10580–10585.

133. He J., Ford H.C., Carroll J., Ding S., Fearnley I.M., Walker J.E. (2017) Persistence of the mitochondrial permeability transition in the absence of subunit c of human ATP synthase. Proc. Natl Acad. Sci. U S A, 114, 3409–3414.

134. Wittig I., Meyer B., Heide H., Steger M., Bleier L., Wumaier Z., Karas M., Schägger H. (2010) Assembly and oligomerization of human ATP synthase lacking mitochondrial subunits a and A6L. Biochim. Biophys. Acta., 1797, 1004–1011.

135. Carraro M., Giorgio V., Šileikytė J., Sartori G., Forte M., Lippe G., Zoratti M., Szabò I., Bernardi P. (2014) Channel formation by yeast F-ATP synthase and the role of dimerization in the mitochondrial permeability transition. J. Biol. Chem., 289, 15980–15985.

136. Giorgio V., von Stockum S., Antoniel M., Fabbro A., Fogolari F., Forte M., Glick G.D., Petronilli V., Zoratti M., Szabò I. et al. (2013) Dimers of mitochondrial ATP synthase form the permeability transition pore. Proc. Natl Acad. Sci. U S A, 110, 5887–5892.

137. Giorgio V., Bisetto E., Soriano M.E., Dabbeni-Sala F., Basso E., Petronilli V., Forte M.A., Bernardi P., Lippe G. (2009) Cyclophilin D modulates mitochondrial F0F1-ATP synthase by interacting with the lateral stalk of the complex. J. Biol. Chem., 284, 33982–33988.

138. Böttinger L., Horvath S.E., Kleinschroth T., Hunte C., Daum G., Pfanner N., Becker T. (2012) Phosphatidylethanolamine and cardiolipin differentially affect the stability of mitochondrial respiratorychain supercomplexes. J. Mol. Biol., 423, 677–686.

139. Verkaart S., Koopman W.J.H., van Emst-de Vries S.E., Nijtmans L.G.J., van den Heuvel L.W.P.J., Smeitink J.A.M., Willems P.H.G.M. (2007) Superoxide production is inversely related to complex I activity in inherited complex I deficiency. Biochim. Biophys. Acta, 1772, 373–381.

140. Distelmaier F., Visch H.-J., Smeitink J.A.M., Mayatepek E., Koopman W.J.H., Willems P.H.G.M. (2009) The antioxidant Trolox restores mitochondrial membrane potential and Ca2+-stimulated ATP production in human complex I deficiency. J. Mol. Med., 87, 515–522.

141. Fritzen A.J., Grunnet N., Quistorff B. (2007) Flux control analysis of mitochondrial oxidative phosphorylation in rat skeletal muscle: pyruvate and palmitoyl-carnitine as substrates give different control patterns. Eur. J. Appl. Physiol., 101, 679–689.

142. Baker C.D., Basu Ball W., Pryce E.N., Gohil V.M. (2016) Specific requirements of nonbilayer phospholipids in mitochondrial respiratory chain function and formation. Mol. Biol. Cell, 27, 2161–2171.

143. Shinzawa-Itoh K., Aoyama H., Muramoto K., Terada H., Kurauchi T., Tadehara Y., Yamasaki A., Sugimura T., Kurono S., Tsujimoto K. et al. (2007) Structures and physiological roles of 13 integral lipids of bovine heart cytochrome c oxidase. embo J., 26, 1713–1725.

144. Mourier A., Ruzzenente B., Brandt T., Kuhlbrandt W., Larsson N.G. (2014) Loss of LRPPRC causes ATP synthase deficiency. Hum. Mol. Genet., 10.1093/hmg/ddt652.

145. Siira SJ, Spåhr H, Shearwood AJ, Ruzzenente B, Larsson NG, Rackham O, Filipovska A. LRPPRC-mediated folding of the mitochondrial transcriptome. Nat Commun. 2017 Nov 16;8(1):1532.

146. Jourdain AA, Boehm E, Maundrell K, Martinou JC. Mitochondrial RNA granules: Compartmentalizing mitochondrial gene expression. J Cell Biol. 2016 Mar 14; 212(6):611-4.

147. Antonicka H, Shoubridge EA. Mitochondrial RNA Granules Are Centers for Posttranscriptional RNA Processing and Ribosome Biogenesis. Cell Rep. 2015 Feb 12. pii: S2211-1247 (15) 00055-8.

148. Jourdain AA, Koppen M, Wydro M, Rodley CD, Lightowlers RN, Chrzanowska-Lightowlers ZM, Martinou JC. GRSF1 regulates RNA processing in mitochondrial RNA granules. Cell Metab. 2013 Mar 5; 17(3): 399-410.

149. Sirey TM, Ponting CP. Insights into the post-transcriptional regulation of the mitochondrial electron transport chain. Biochem Soc Trans. 2016 Oct 15;44(5):1491-1498.

150. Ramaswami M, Taylor JP, Parker R. Altered ribostasis: RNA-protein granules in degenerative disorders. Cell. 2013 Aug 15;154(4):727-36.

151. Jourdain AA, Popow J, de la Fuente MA, Martinou JC, Anderson P, Simarro M. The FASTK family of proteins: emerging regulators of mitochondrial RNA biology. Nucleic Acids Res. 2017 Nov 2;45(19):10941-10947.

152. Tian Q, Taupin J, Elledge S, Robertson M, Anderson P. Fas-activated serine/threonine kinase (FAST) phosphorylates TIA-1 during Fas-mediated apoptosis. J Exp Med. 1995 Sep 1;182(3):865-74.

153. Boehm E, Zaganelli S, Maundrell K, Jourdain AA, Thore S, Martinou JC. FASTKD1 and FASTKD4 have opposite effects on expression of specific mitochondrial RNAs, depending upon their endonuclease-like RAP domain. Nucleic Acids Res. 2017 Jun 2;45 (10): 6135-6146.

154. Popow J, Alleaume AM, Curk T, Schwarzl T, Sauer S, Hentze MW. FASTKD2 is an RNA-binding protein required for mitochondrial RNA processing and translation. RNA. 2015 Nov; 21(11): 1873-84.

155. Slomovic S, Laufer D, Geiger D, Schuster G. Polyadenylation and degradation of human mitochondrial RNA: the prokaryotic past leaves its mark. Mol Cell Biol. 2005 Aug; 25(15):6427-35.

156. Jenal M, Elkon R, Loayza-Puch F, van Haaften G, Kühn U, Menzies FM, Oude Vrielink JA, Bos AJ, Drost J, Rooijers K, Rubinsztein DC, Agami R. The poly(A)-binding protein nuclear 1 suppresses alternative cleavage and polyadenylation sites. Cell. 2012 Apr 27;149(3):538-53.

157. Tomecki R, Dmochowska A, Gewartowski K, Dziembowski A, Stepien PP. Identification of a novel human nuclear-encoded mitochondrial poly(A) polymerase. Nucleic Acids Res. 2004 Nov 16;32(20):6001-14. Print 2004.

158. Nagaike T, Suzuki T, Katoh T, Ueda T. Human mitochondrial mRNAs are stabilized with polyadenylation regulated by mitochondria-specific poly(A) polymerase and polynucleotide phosphorylase. J Biol Chem. 2005 May 20;280(20):19721-7.

159. Wilson WC, Hornig-Do HT, Bruni F, Chang JH, Jourdain AA, Martinou JC, Falkenberg M, Spåhr H, Larsson NG, Lewis RJ, Hewitt L, Baslé A, Cross HE, Tong L, Lebel RR, Crosby AH, Chrzanowska-Lightowlers ZM, Lightowlers RN. A human mitochondrial poly(A) polymerase mutation reveals the complexities of post-transcriptional mitochondrial gene expression. Hum Mol Genet. 2014 Dec 1;23(23):6345-55.

160. Bratic A, Clemente P, Calvo-Garrido J, Maffezzini C, Felser A, Wibom R, Wedell A, Freyer C, Wredenberg A. Mitochondrial Polyadenylation Is a One-Step Process Required for mRNA Integrity and tRNA Maturation. PLoS Genet. 2016 May 13;12(5): e1006028.

161. Weraarpachai W, Sasarman F, Nishimura T, Antonicka H, Auré K, Rötig A, Lombès A, Shoubridge EA. Mutations in C12orf62, a factor that couples COX I synthesis with cytochrome c oxidase assembly, cause fatal neonatal lactic acidosis. Am J Hum Genet. 2012 Jan 13;90(1):142-51.

162. Acebrón SP, Martín I, del Castillo U, Moro F, Muga A. DnaK-mediated association of ClpB to protein aggregates. A bichaperone network at the aggregate surface. FEBS Lett. 2009 Sep 17;583(18):2991-6.

163. Haslberger T, Zdanowicz A, Brand I, Kirstein J, Turgay K, Mogk A, Bukau B. Protein disaggregation by the AAA+ chaperone ClpB involves partial threading of looped polypeptide segments. Nat Struct Mol Biol. 2008 Jun;15(6):641-50.

164. Boehm E, Zornoza M, Jourdain AA, Delmiro Magdalena A, García-Consuegra I, Torres Merino R, Orduña A, Martín MA, Martinou JC, De la Fuente MA, Simarro M. Role of FAST Kinase Domains 3 (FASTKD3) in Post-transcriptional Regulation of Mitochondrial Gene Expression. J Biol Chem. 2016 Dec 9;291(50):25877-25887.

165. Quirós PM, Langer T, López-Otín C. New roles for mitochondrial proteases in health, ageing and disease. Nat Rev Mol Cell Biol. 2015 Jun;16(6):345-59.

166. König T, Tröder SE, Bakka K, Korwitz A, Richter-Dennerlein R, Lampe PA, Patron M, Mühlmeister M, Guerrero-Castillo S, Brandt U, Decker T, Lauria I, Paggio A, Rizzuto R, Rugarli EI, De Stefani D, Langer T. The m-AAA Protease Associated with Neurodegeneration Limits MCU Activity in Mitochondria. Mol Cell. 2016 Oct 6;64(1):148-162.

167. Castandet B, Araya A. 2012. The nucleocytoplasmic conflict, a driving force for the emergence of plant organellar RNA editing. IUBMB Life 64:120–25.

168. Maier UG, Bozarth A, Funk HT, Zauner S, Rensing SA, Schmitz-Linneweber C, Börner T, Tillich M. Complex chloroplast RNA metabolism: just debugging the genetic programme? BMC Biol. 2008 Aug 28; 6:36.

169. Schmitz-Linneweber C, Small I. 2008. Pentatricopeptide repeat proteins: a socket set for organelle gene expression. Trends Plant Sci. 13:663–70.

Appendix

SPRINGER NATURE LICENSE
TERMS AND CONDITIONS

Oct 30, 2018

This Agreement between Mrs. Shamisa Honarmand ("You") and Springer Nature ("Springer Nature") consists of your license details and the terms and conditions provided by Springer Nature and Copyright Clearance Center.

License Number	4458820436208
License date	Oct 30, 2018
Licensed Content Publisher	Springer Nature
Licensed Content Publication	Nature Reviews Genetics
Licensed Content Title	Mitochondrial DNA mutations in human disease
Licensed Content Author	Robert W. Taylor, Doug M. Turnbull
Licensed Content Date	May 1, 2005
Licensed Content Volume	6
Licensed Content Issue	5
Type of Use	Thesis/Dissertation
Requestor type	academic/university or research institute
Format	electronic
Portion	figures/tables/illustrations
Number of figures/tables/illustrations	1
High-res required	no
Will you be translating?	no
Circulation/distribution	<501
Author of this Springer Nature content	no
Title	Molecular Mechanisms Underlying the Pathogenesis of Leigh Syndrome French Canadian
Institution name	McGill University
Expected presentation date	Oct 2018
Portions	Figure 1

JOHN WILEY AND SONS LICENSE TERMS AND CONDITIONS

Oct 30, 2018

This Agreement between Mrs. Shamisa Honarmand ("You") and John Wiley and Sons ("John Wiley and Sons") consists of your license details and the terms and conditions provided by John Wiley and Sons and Copyright Clearance Center.

License Number	4458361182729
License date	Oct 29, 2018
Licensed Content Publisher	John Wiley and Sons
Licensed Content Publication	Annals of Neurology
Licensed Content Title	Leigh syndrome: One disorder, more than 75 monogenic causes
Licensed Content Author	Nicole J. Lake, Alison G. Compton, Shamima Rahman, et al
Licensed Content Date	Dec 15, 2015
Licensed Content Volume	79
Licensed Content Issue	2
Licensed Content Pages	14
Type of use	Dissertation/Thesis
Requestor type	University/Academic
Format	Electronic
Portion	Figure/table
Number of figures/tables	1
Original Wiley figure/table number(s)	Table 1
Will you be translating?	No
Title of your thesis / dissertation	Molecular Mechanisms Underlying the Pathogenesis of Leigh Syndrome French Canadian
Expected completion date	Oct 2018

ANNUAL REVIEWS, INC ORDER DETAILS

Oct 30, 2018

Order Number	501440263
Order date	Oct 30, 2018
Licensed content publisher	Annual Reviews, Inc
Licensed content title	Annual review of plant biology
Licensed content date	Jan 1, 2002
Type of Use	Thesis/Dissertation
Requestor type	Academic institution
Format	Electronic
Portion	image/photo
Number of images/photos requested	1
The requesting person/organization is:	Shamisa Honarmand/McGill University
Title or numeric reference of the portion(s)	Pentatrichopeptide repeat proteins in plants, Figure 1.
Title of the article or chapter the portion is from	Pentatrichopeptide repeat proteins in plants
Editor of portion(s)	N/A
Author of portion(s)	Barkan Alice
Volume of serial or monograph.	65
Page range of the portion	415-42
Publication date of portion	January 27, 2014
Rights for	Main product
Duration of use	Life of current edition

OXFORD UNIVERSITY PRESS LICENSE
TERMS AND CONDITIONS

Oct 30, 2018

This Agreement between Mrs. Shamisa Honarmand ("You") and Oxford University Press ("Oxford University Press") consists of your license details and the terms and conditions provided by Oxford University Press and Copyright Clearance Center.

License Number	4458911307706
License date	Oct 30, 2018
Licensed content publisher	Oxford University Press
Licensed content publication	Human Molecular Genetics
Licensed content title	Loss of hepatic LRPPRC alters mitochondrial bioenergetics, regulation of permeability transition and trans-membrane ROS diffusion
Licensed content author	Cuillerier, Alexanne; Honarmand, Shamisa
Licensed content date	May 31, 2017
Type of Use	Thesis/Dissertation
Institution name	
Title of your work	Molecular Mechanisms Underlying the Pathogenesis of Leigh Syndrome French Canadian
Publisher of your work	McGill University
Expected publication date	Oct 2018
Permissions cost	0.00 CAD
Value added tax	0.00 CAD
Total	0.00 CAD
Title	Molecular Mechanisms Underlying the Pathogenesis of Leigh Syndrome French Canadian
Institution name	McGill University
Expected presentation date	Oct 2018
Portions	Figure 1, Figure 2, Figure 3, Figure 4, Figure 5, Figure 6, Figure 7.

SPRINGER NATURE LICENSE
TERMS AND CONDITIONS

Oct 30, 2018

This Agreement between Mrs. Shamisa Honarmand ("You") and Springer Nature ("Springer Nature") consists of your license details and the terms and conditions provided by Springer Nature and Copyright Clearance Center.

License Number	4458381188096
License date	Oct 29, 2018
Licensed Content Publisher	Springer Nature
Licensed Content Publication	Nature Reviews Molecular Cell Biology
Licensed Content Title	New roles for mitochondrial proteases in health, ageing and disease
Licensed Content Author	Pedro M. Quirós, Thomas Langer, Carlos López-Otín
Licensed Content Date	May 13, 2015
Licensed Content Volume	16
Licensed Content Issue	6
Type of Use	Thesis/Dissertation
Requestor type	academic/university or research institute
Format	electronic
Portion	figures/tables/illustrations
Number of figures/tables/illustrations	1
High-res required	no
Will you be translating?	no
Circulation/distribution	<501
Author of this Springer Nature content	no
Title	Molecular Mechanisms Underlying the Pathogenesis of Leigh Syndrome French Canadian
Institution name	McGill University
Expected presentation date	Oct 2018
Portions	Figure 4